Sm-Nd Isotopic Composition of Mantle-Derived Rocks from the Saglek-Hebron Gneiss Complex, Northern Labrador

Janick Flageole

Thesis submitted in partial fulfillment of the requirements for the

Master's degree in Earth Sciences

Department of Earth and Environmental Sciences
Faculty of Science
University of Ottawa

Preface

The work presented here takes part of the larger Saglek-Hebron research project lead by Jonathan O'Neil (University of Ottawa) and Hanika Rizo (Carleton University), funded by NSERC. Fieldwork was conducted by a team of researchers lead by Jonathan O'Neil and Hanika Rizo, providing samples for this project. Under their supervision, I was the lead investigator of this project, responsible for data collection, analysis and interpretation. Petrological and geochemical data of the mafic and ultramafic samples were obtained and interpreted by Benjamin Wasilewski as part of his PhD project. I have performed all petrological and geochemical analyses and interpretations related to the two generations of mafic dikes. My contribution to this project, therefore, includes sample preparation, major and trace element geochemical analyses of the mafic dikes, as well as acquisition of isotopic data acquisition (TIMS analyses) of all 83 samples, including mafic and ultramafic samples and two generations of mafic dikes.

Abstract

The Saglek-Hebron Gneiss Complex (SHC) is located in Northern Labrador within the Nain Province. It has recorded multiple magmatic events over more than 1 billion years, making it ideal to study the evolution of mantle-derived rocks through time. Here we present a ^{147}Sm-^{143}Nd isotopic study focussing on the different generations of mantle-derived rocks in the SHC. A total of 83 samples have been analysed, including: 1) mafic metavolcanic rocks; 2) ultramafic rocks divided into two distinct groups (a Fe-rich group enriched in incompatible elements and more depleted ultramafic rocks with lower Fe contents); 3) mafic metamorphosed dikes called the Saglek dikes; and 4) undeformed mafic dikes. Some samples exhibit evidence of post-magmatic geochemical and isotopic disturbance but only the least disturbed samples have been considered to constrain the timing of formation of the different lithologies and the isotopic composition of their mantle source. The mafic metavolcanic rocks combined with the co-genetic low-Fe ultramafic rocks yield an isochron age of 3819 ± 190 Ma (MSWD=34, n=25) with an initial εNd value of +2.3 ± 0.6. The high-Fe enriched ultramafic rocks yield a younger age of 3433 ± 220 Ma (MSWD=10.4, n=10) with an initial εNd= +1.8 ± 0.5. The two generations of mafic dikes appear to have been emplaced in the Mesoarchean and the Neoarchean. The Saglek dikes yield an isochron age of 3565 ±120 Ma (MSWD=1.17, n=10) with an initial εNd value of +1.7 ± 0.1, while the Sm-Nd isochron age for the undeformed mafic dikes is 2694 ±79 Ma (MSWD=3.2, n=21) with an initial εNd value of +1.7 ± 0.1. All generations of mantle-derived rocks yield positive initial εNd values, where only the Eoarchean rocks display an initial Nd isotopic composition similar to the depleted mantle. The Mesoarchean ultramafic rocks, Saglek dikes and Neoarchean mafic dikes display almost identical initial εNd values, despite an age difference of ~800 Ma. This could suggest the contribution of distinct mantle sources or, if all generations of mantle-derived rocks in

the SHC were produced from the same mantle source, it implies that this source evolved with a nearly chondritic Sm/Nd ratio for almost the whole Archean Eon. The fact that the initial isotopic compositions of the mantle-derived rocks appear to deviate from the depleted mantle with time, could also suggest an increasing interaction with older evolved crust.

Résumé

Le complexe gneissique de Saglek-Hebron (SHC) est situé dans le Nord du Labrador, dans la province de Nain. Ce complexe a enregistré plusieurs événements magmatiques sur plus d'un milliard d'années, ce qui en fait un terrain idéal pour étudier l'évolution du manteau au fil du temps. Nous présentons ici une étude isotopique ^{147}Sm-^{143}Nd centrée sur les différentes générations de roches dérivées du manteau qui forment le SHC. Un total de 83 échantillons ont été analysés, notamment: 1) des roches métavolcaniques mafiques; 2) les roches ultramafiques divisées en deux groupes distincts (un groupe riche en Fe et enrichi en éléments incompatibles, et les roches ultramafiques appauvries avec une teneur plus faible en Fe); 3) les dikes mafiques métamorphisés, nommés dikes de Saglek; et 4) les dikes mafiques non déformés. Certains échantillons présentent des évidences de perturbations géochimiques et isotopiques post-magmatiques, mais seuls les échantillons les moins perturbés ont été considéré pour la datation des différentes lithologies ainsi que pour la composition isotopique de leur source mantellique. Les roches co-génétiques métavolcaniques mafiques et ultramafiques appauvries, donnent un âge isochrone de 3819 ± 190 Ma (MSWD = 34; n = 25) et une valeur εNd initiale de +2,3 ± 0,6. L'isochrone des roches ultramafiques enrichies donne un âge plus jeune de 3433 ± 220 Ma (MSWD = 10,4; n = 10) avec un εNd initial = +1,8 ± 0,5. Les deux générations de dikes mafiques semblent avoir été mises en place durant le Mésoarchéen et le Néoarchéen. Les dikes de Saglek donnent un âge isochrone de 3565 ± 120 Ma (MSWD = 1,17; n = 10) et une valeur εNd initiale de +1,7 ± 0,1, tandis que l'âge

isochrone Sm-Nd pour les dikes mafiques non déformés est de 2694 ± 79 Ma (MSWD = 3,2; n = 21) avec une valeur εNd initiale de +1,7 ± 0,1. Toutes les générations de roches mafiques/ultramafiques ont des valeurs εNd initiales positives, où seules les roches éoarchéennes ont une composition isotopique de Nd similaire à celle du manteau appauvri. Les roches ultramafiques mésoarchéennes, les dikes de Saglek et les dikes mafiques néoarchéens ont des valeurs εNd initiales presque identiques, malgré une différence d'âge d'environ 800 Ma. Cela peut suggérer la contribution de sources mantelliques distinctes ou, si toutes les générations de roches mafiques et ultramafiques, dans le SHC, sont dérivées d'une même source mantellique, cela impliquerait que cette source aurait évolué avec un rapport Sm/Nd presque chondritique. Le fait que les compositions isotopiques initiales des roches dérivées du manteau semblent s'éloignées progressivement du manteau appauvri avec le temps, pourrait également suggérer une interaction avec une croûte évoluée plus ancienne.

Acknowledgments

I would first like to thank my supervisor Jonathan O'Neil, for taking me as an undergraduate student and again as a Master's student; giving me the opportunity to pursue my interests in igneous petrology and geochemistry. Thank you for your guidance, helpful advice, encouragement and your endless patience, for believing in me and allowing this project to be my own work. I would also like to thank my co-supervisor Hanika Rizo, for all the help provided over the course of this project, this includes assistance in the lab, scientific discussions, feedback and your constant encouragement.

Analyses on the TIMS would not have been possible without the assistance of André Poirier and Shuangquan Zhang, at the GEOTOP and IGGRC laboratories, respectively. Both allowed me to use their instruments and laboratories, thank you. I would also like to thank Evelyn Tennant for her assistance with filaments preparation and cleaning.

To my fellow graduate students in the Ottawa-Carleton Early Earth Research group: Benjamin Wasilewski, Christian Sole, Ayesha Landon-Browne, Alexandre Rouleau and Andréane Dupuis-Mitchell, I am grateful for your constant support, assistance in the lab, scientific discussions, and providing me with feedback.

I would also like to extend my acknowledgments to everyone at the University of Ottawa, staff, faculty members and fellow graduate students, to whom contributed to this project.

Finally, I would like to thank my family and my friends. Thank you to my parents, for constantly believing in me and encouraging my interest in science. My siblings and friends for their constant support and patience throughout my studies.

Table of Contents

Preface ... II
Abstract ... III
Résumé ... IV
Acknowledgments ... VI
List of Figures ... VIII
List of Tables ... X
1. Introduction ... 1
2. Geological Setting ... 2
3. ^{147}Sm-^{143}Nd Isotopic System ... 8
4. Methods ... 11
4.1 Sample preparation ... 11
4.2 Major and trace elements ... 12
4.3 Sm-Nd analytical procedure ... 14
5. Results ... 18
5.1 Petrography and geochemistry ... 18
5.1.1 Basaltic metavolcanic and ultramafic rocks ... 18
5.1.2 Saglek dikes and undeformed mafic dikes ... 26
5.2 ^{147}Sm-^{143}Nd isotope results ... 33
5.2.1 Basaltic metavolcanic and ultramafic rocks ... 33
5.2.2 Saglek dikes and undeformed mafic dikes ... 36
6. Discussion ... 39
6.1 Assessment of igneous primary character of the SHC mantle-derived rocks composition ... 39
6.1.1 Element mobility ... 40
6.1.2 Igneous differentiation ... 43
6.2 Chronology of the SHC mafic magmatism ... 52
6.2.1 Age of the SHC metavolcanic and ultramafic rocks ... 53
6.2.2 Age of the Saglek dikes and undeformed mafic dikes ... 62
6.3 Are the Saglek dikes related to the Southwest Greenland Ameralik dikes? ... 67
6.4 Evolution of the SHC mantle source ... 69
7. Conclusion ... 72
References ... 74
Appendix ... 80

List of Figures

Figure 1 Location map of the Saglek-Hebron Gneiss Complex……..……3

Figure 2 Geological map of the Saglek-Hebron Gneiss Complex……...……4

Figure 3 Example of an isochron digram.....9

Figure 4 Example through time of εNd……...……..……..…….....11

Figure 5 Results of duplicate analyses of rare earth element concentrations…….…….....14

Figure 6 Field photographs of the different lithologies relevant to this study….....20

Figure 7 Microphotographs of the mafic metavolcanic and ultramafic rocks……..….21

Figure 8 Rock classification diagram of the ultramafic samples…….....22

Figure 9 TAS and AFM diagrams of the mafic metavolcanic rocks……..…….……23

Figure 10 Zr vs TiO_2 of the mafic metavolcanic rocks…….…….……24

Figure 11 Rare earth element profiles of the mafic metavolcanic rocks……..……24

Figure 12 Al_2O_3 vs TiO_2 diagram of the ultramafic rocks…….…….…..……25

Figure 13 Rare earth element profiles of the ultramafic rocks……..…...26

Figure 14 Microphotographs of the Saglek dikes and the undeformed mafic dikes……..…..28

Figure 15 Rock classification diagram of the Saglek dikes and the undeformed mafic dikes.….....…...29

Figure 16 TAS and AFM diagrams of the Saglek dikes and the undeformed mafic dikes.....…….....31

Figure 17 Major and trace element diagrams of the Saglek dikes and the undeformed mafic dikes……...32

Figure 18 Rare earth element profiles of the Saglek dikes and the undeformed mafic dikes……..…....33

Figure 19 $^{147}Sm/^{144}Nd$ vs $^{143}Nd/^{144}Nd$ isochron diagram of the mafic metavolcanic samples and ultramafic samples…….36

Figure 20 $^{147}Sm/^{144}Nd$ vs $^{143}Nd/^{144}Nd$ isochron diagram of the Saglek dikes samples……...38

Figure 21 $^{147}Sm/^{144}Nd$ vs $^{143}Nd/^{144}Nd$ isochron diagram of the undeformed mafic dikes samples……39

Figure 22 La/Sm vs K_2O diagram for the mafic metavolcanic rocks and ultramafic rocks…….41

Figure 23 Geochemical diagrams of the Saglek dikes and undeformed mafic dikes…….....43

Figure 24 Al_2O_3 vs TiO_2 diagram of the mafic metavolcanic rocks and the ultramafic rocks……...….45

Figure 25 Fractional crystallisation model and mixing model of the Saglek dikes……..….48

Figure 26 Initial εNd values of the Saglek dikes vs La/Sm…….……..….49

Figure 27 Fractional crystallisation model and mixing model of the undeformed mafic dikes…….……51

Figure 28 Initial εNd values of the undeformed mafic dikes vs La/Sm…….……....52

Figure 29 $^{147}Sm/^{144}Nd$ vs $^{143}Nd/^{144}Nd$ isochron diagram of the mafic metavolcanic samples.....…….….56

Figure 30 $^{147}Sm/^{144}Nd$ vs $^{143}Nd/^{144}Nd$ isochron diagram of the mafic metavolcanic samples and low-Fe ultramafic samples…….....58

Figure 31 Histogram of the initial εNd values of the mafic metavolcanic samples and the low-Fe ultramafic samples…….……59

Figure 32 $^{147}Sm/^{144}Nd$ vs $^{143}Nd/^{144}Nd$ isochron diagram of the high-Fe ultramafic samples.....…….60

Figure 33 $^{147}Sm/^{144}Nd$ vs $^{143}Nd/^{144}Nd$ isochron diagram of the Saglek dikes.....…….…..64

Figure 34 $^{147}Sm/^{144}Nd$ vs $^{143}Nd/^{144}Nd$ isochron diagram of the undeformed mafic dikes...……..…66

Figure 35 $^{147}Sm/^{144}Nd$ vs $^{143}Nd/^{144}Nd$ isochron diagram of the Saglek dikes and the Ameralik dikes…...…68

Figure 36 Initial calculated εNd values for each unit at their time of crystallisation…….……72

List of Tables

Table 1 Weight of powdered sample dissolved, dissolution technique and analytical session…….....15

Table 2 Average JNdi-1 standard values for each analytical session……18

Table 3 Sm-Nd isotopic data of the mafic metavolcanic samples and the ultramafic samples…….35

Table 4 Sm-Nd isotopic data of the Saglek dikes and the undeformed mafic dikes samples…….37

Table 5 Summary of the calculated age and initial εNd values for each unit.....……66

Table A1 Sample locations and coordinates……...……..80

Table A2 Detection limits of the major elements concentrations measured on the XRF...…..……82

Table A3 Columns chemistry protocol…….……...….83

Table A4 Whole rock chemistry of the ultramafic and mafic samples analysed for this study……..…85

Table A5 Petrological descriptions of the Saglek dikes……90

Table A6 Petrological descriptions of the undeformed mafic dikes…….93

Table A7 Whole rock chemistry of the Saglek dikes and the undeformed mafic dikes……..…98

1. Introduction

Our knowledge of the geological processes that shaped the early Earth is limited due to the lack of preservation of ancient geological terranes. Therefore, it is crucial to study these rare terranes, as they provide valuable insights on the composition and processes that formed the Earth's early crust and mantle. The oldest mineral found on Earth is the 4.4 Ga Jack Hill detrital zircons of Western Australia, which provide prominent information on the early Earth; however, the host rock has not been preserved (Wilde et al., 2001). The few terranes that host rocks that are Hadean-Eoarchean in age include: the Nuvvuagittuq greenstone belt, Canada (3.8 to 4.28 Ga) (Cates and Mojzsis, 2007; Darling et al., 2013; O'Neil et al., 2008, 2012), the Acasta Gneiss complex, Canada (4.03 Ga) (Bowring and Williams, 1999; Reimink et al., 2016), the Saglek-Hebron Gneiss Complex, Canada (3.92 Ga) (Bridgwater et al., 1975; Schiøtte et al., 1989a; Shimojo et al., 2016), the Anshan area, China (3.89 Ga) (Song et al., 1996; Wu et al., 2008), the Napier Complex, Antarctica (3.85 Ga) (Black et al., 1986; Kusiak et al., 2014), the Itsaq Gneiss Complex, Greenland (3.85 Ga) (Baadsgaard et al.,1984; Nutman et al., 1996; Nutman and Friend, 2009), the Narryer Terrane in Australia (3.73 Ga) (Nutman et al., 1991; Wilde and Spaggiari, 2007) and the Ancient Gneiss complex, Swaziland (3.66 Ga) (Compston and Kröner, 1988; Kröner, 2007). Most of these terranes host felsic rocks that provide helpful information on the formation of the early felsic crust. However, these felsic rocks are thought to be derived from the melting of mafic precursors, and thus, do not provide direct information on the evolution of the mafic crust or the mantle. Therefore terranes that host mantle-derived rocks are important in our understanding of the processes that formed Earth's early mafic crust and mantle, and their evolution over time.

The Nuvvuagittuq greenstone belt (NGB) and the Isua supracrustal belt (ISB) contain some of the oldest mafic metavolcanic rocks on Earth. These mantle-derived rocks have provided valuable

insights on the composition and petrogenesis of the primitive crust. For example, some of these mafic volcanic rocks are very similar, in terms of composition, to boninites, whose characteristics suggest their formation in a subduction environment (O'Neil et al., 2016; Furnes et al., 2009). It was also shown that the ISB rocks have similar $^{142}Nd/^{144}Nd$ ratios to the NGB rocks at the time of their formation (~4.3 Ga), suggesting that the ISB and the NGB may derive from a common early depleted mantle source (O'Neil et al., 2016). Similarly to the Nuvvuagittuq greenstone belt and the Isua supracrustal belt, the Saglek-Hebron Gneiss Complex is one of the rare terranes that hosts mantle-derived rocks that are Archean in age, it is thus important to conduct studies on this terrane as it will also provide further insights on the formation of the primitive crust. The Saglek-Hebron Gneiss Complex is a typical granite-greenstone belt comprising metavolcanic rocks and granitoids as old as 3.9 Ga. It was suggested that an assemblage of volcano-sedimentary rocks, the Nulliak unit, have been intruded by the 3.9 Ga old granitoids, making the Nulliak suite one of the oldest supracrustal suites on Earth (Komiya et al., 2015; Shimojo et al., 2016). The mafic and ultramafic rocks along with the multiple generations of mafic dikes present in this complex, make it an interesting study area. Here we present new ^{147}Sm-^{143}Nd isotopic data as well as petrological and geochemical data on the different generations of mafic rocks present in the Saglek-Hebron Gneiss Complex. We use this data set to study the petrogenesis of each lithology, constrain their ages and mantle source(s).

2. Geological Setting

The Saglek-Hebron Gneiss Complex (SHC) is located in north-eastern Labrador in the Nain Province, and consists of the western most part of the North Atlantic Craton (NAC), which extends all the way to Scotland, and through southern Greenland (Figure 1). It is a typical granite-greenstone belt, metamorphosed up to amphibolite and granulite facies. The complex is dominated

by supracrustal units and rocks from a tonalite-trondjemite-granodiorite suite (TTG) (Figure 2). It comprises four major granitoid units, with the oldest being the Iqualuk unit, described as a banded grey gneiss, recently dated at ~3.9 Ga (Shimojo et al., 2016; Wasilewski et al., in prep). The Uivak Gneiss, the most dominant unit in the complex, has been described as an orthogneiss with a tonalitic to trondjemitic composition, and has been dated between 3.85 and 3.73 Ga (Collerson et al., 1983; Schiøtte et al., 1989a; Komiya et al., 2015; Shimojo et al., 2016). These units have been intruded by a younger generation of granitic rocks around 3.24 Ga, the Lister Gneiss, as well as younger Neoarchean granites (Schiøtte et al., 1989b).

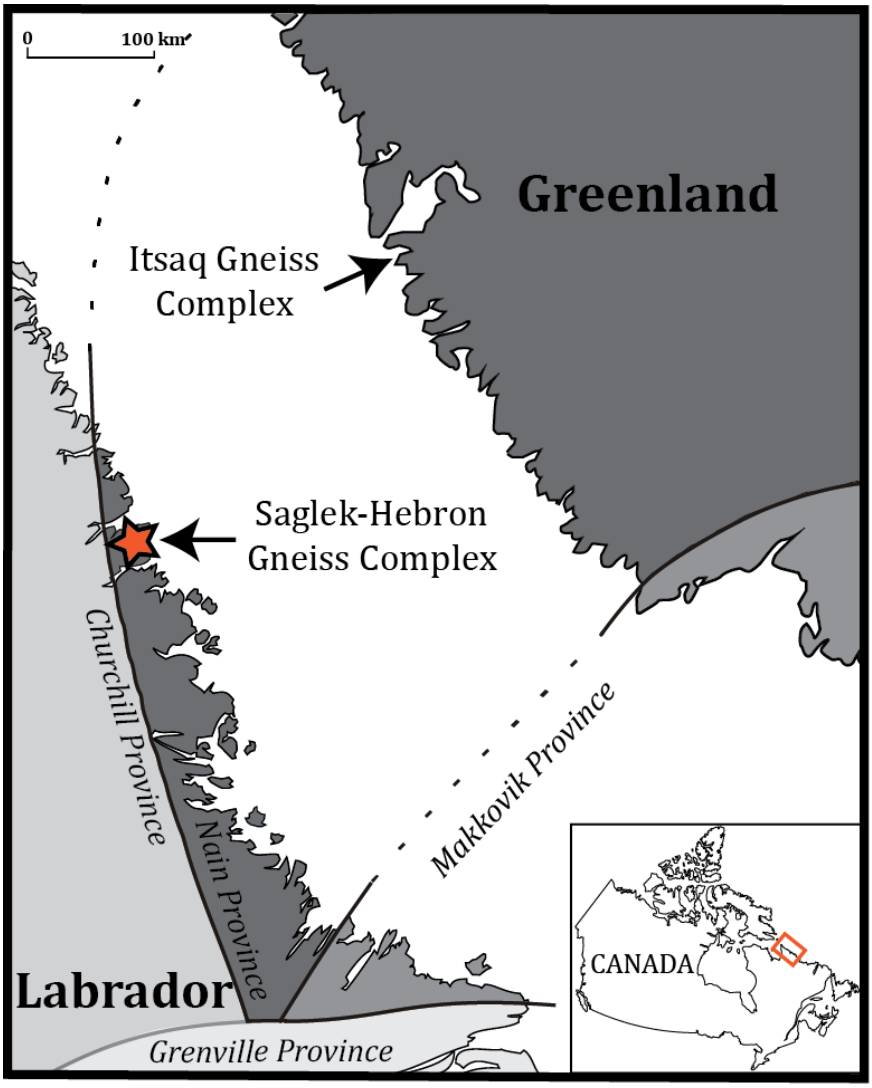

Figure 1 Location map of the Saglek-Hebron Gneiss Complex (Modified from Ryan et al., 2012 & Wasilewski et al., 2019)

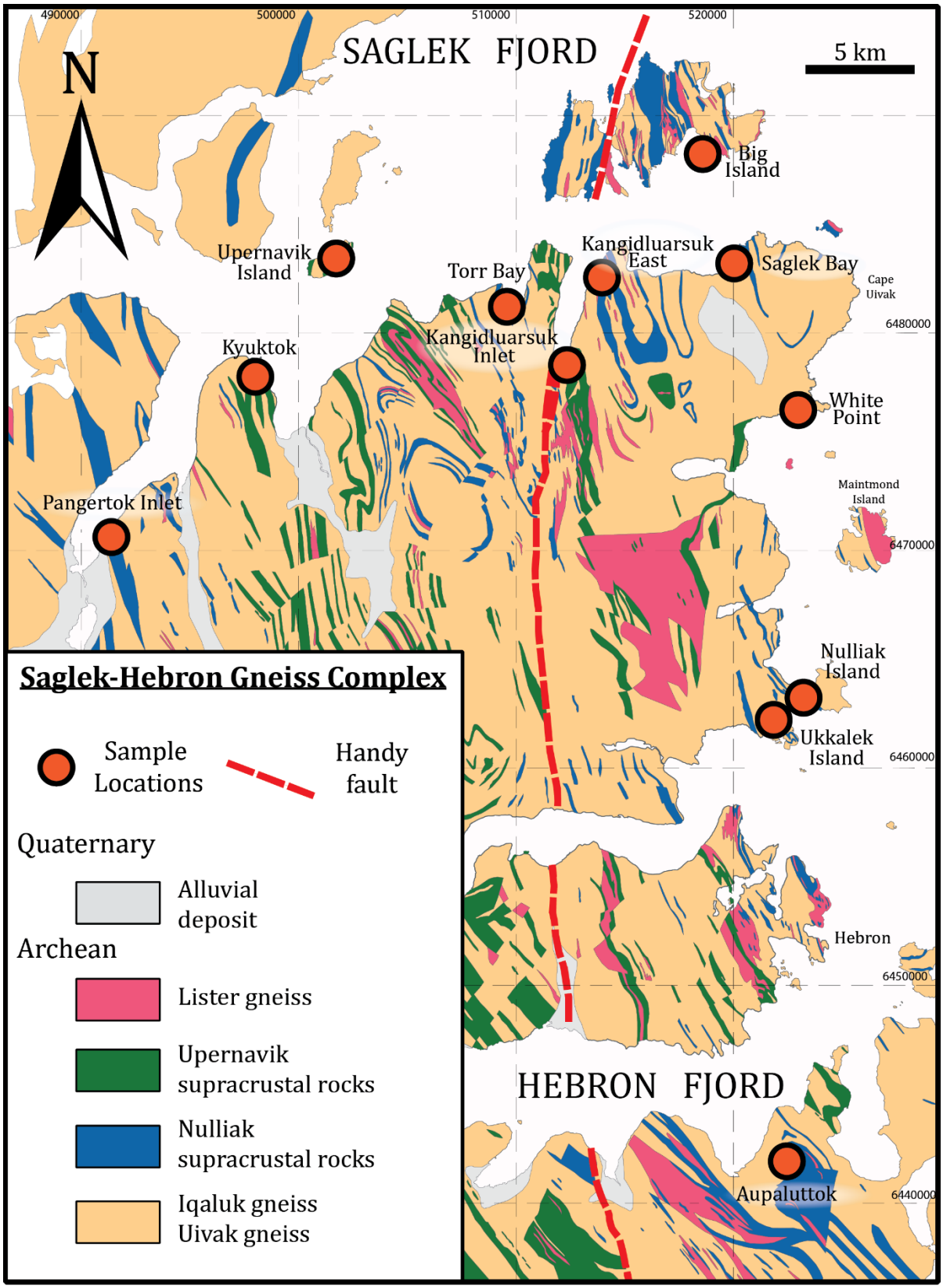

Figure 2 Geological map of the Saglek-Hebron Gneiss Complex (SHC), modified from Ryan et al. (2012), Komiya et al. (2015) & Wasilewski et al. (2019). Includes general sample locations; specific coordinates for each samples are presented in Table A1 in the Appendix. Coordinates are in UTM NAD 27 zone 20.

The SHC comprises volcano-sedimentary rocks, such as the Nulliak suite, occurring as km-scale enclaves within the Uivak gneiss (Bridgwater et al., 1991). The Nulliak suite consists mainly of mafic metavolcanic rocks and ultramafic rocks associated with chemical and clastic sediments. Wasilewski et al. (2019) have described the mafic metavolcanic rocks as medium grained amphibolites that are tholeiitic basalt in composition. These mafic rocks are interpreted to represent differentiated flows with more evolved liquids and rocks consistent with pyroxene-rich cumulate/liquid mixtures. Furthermore, Komiya et al. (2015) and Shimojo et al. (2016) proposed that the Nulliak suite contains the oldest supracrustal rocks on Earth. Based on field interpretations, they suggested an intruding relation of the 3.9 Ga Iqualuk unit into the Nulliak suite. However, recent studies by Whitehouse et al. (2019) questioned their interpretations due to the lack of field and geochronological evidence supporting their observations.

Collerson et al. (1991) first observed two distinct ultramafic suites based on field relations and geochemical data. They described these rocks as metamorphosed peridotites occurring as slivers of residual mantle that were tectonically emplaced, and metakomatiites associated with the Nulliak supracrustal suite. Ishikawa et al. (2017) conducted a Re-Os study in order to constrain the age and sources of these distinct suites of ultramafic rocks. They reported ages of 3096 ± 170 Ma and 3612 ± 130 Ma for the metaperidotite and metakomatiites, respectively. Wasilewski et al. (2019) have conducted a petrological study on these rocks, and identified two distinct suites of ultramafic rocks, as previously identified by Collerson et al. (1991) and Ishikawa et al. (2017). However, Wasilewski et al., (2019) report a distinction between the two suites based on their Fe contents: the *low-Fe ultramafic rocks* have higher Al/Ti ratios and are more depleted in incompatible trace elements compared to the *high-Fe ultramafic rocks* exhibiting relatively higher concentrations in incompatible trace elements with lower Al/Ti ratios. The low-Fe ultramafic rocks could be

equivalent to the metaperidotites and the high-Fe ultramafic rocks could be equivalent to the metakomatiites identified by Collerson et al. (1991). Wasilewski et al., (2019) however interpreted the low-Fe depleted ultramafic rocks as olivine-rich cumulates rather than enclaves of lithospheric mantle.

The possibility of a second group of supracrustal rocks, called the Upernavik unit, younger than the Nulliak unit, was suggested by numerous studies (Hurst et al., 1975; Baadsgaard et al., 1979; Collerson et al., 1979). It was described as km-scale horizons of sedimentary sequences associated with metavolcanic rocks and pods of ultramafic rocks (Baadsgaard et al., 1979; Nutman., 1989). As this suite is indistinguishable in the field from the Nulliak suite, the Nulliak and the Upernavik suites were differentiated based on the occurrence of the mafic dikes, known as the Saglek dikes, intruding into the Nulliak suite only. Using U-Pb on zircon in quartzite and whole-rock Sm-Nd analyses on ultramafic rocks from the Nulliak suite, studies yielded Eoarchean ages of 3.8 Ga and 4.0 Ga, respectively (Schiøtte et al., 1989; Nutman et al., 1991; Collerson et al., 1991). Moreover, U-Pb analyses on detrital zircons from metasediments from the Upernavik suite yielded ages between 3.4 and 3.1 Ga (Schiøtte et al., 1992). Morino et al., (2017, 2018) conducted Sm-Nd and Lu-Hf analyses on the mafic and ultramafic rocks from the Nulliak suite and obtained 3782 ± 93 Ma and 3794 ± 130 Ma, respectively. For the Upernavik suite, the same authors obtained a Sm-Nd age of 3362 ± 100 Ma and a Lu-Hf age of 3023 ± 390 Ma. The proposed Sm-Nd and Lu-Hf isochron ages, however, combine all types of ultramafic samples, despite previous studies (e.g. Collerson et al., 1991) suggesting the presence of two distinct ultramafic suites. Morino et al. (2017) also suggested that the samples forming the older suite exhibit a positive ^{142}Nd anomaly in relation to the terrestrial standard, whereas the younger suite lacks this anomaly. Nonetheless,

previous studies have generally reported Eoarchean ages for the Nulliak suite and Mesoarchean ages for the Upernavik suite.

The SHC has been intruded by a few generations of mafic dikes, which are poorly characterized, and their ages have yet to be constrained. The mafic Saglek dikes were first described by Ryan (1977) as inclusions or enclaves of highly deformed porphyritic amphibolites into the Uivak Gneiss. The Saglek dikes represent an important unit in this complex, as previous and recent studies have used the Saglek dikes for relative geochronology (i.e. pre-Saglek dikes vs. post-Saglek dikes) between the different supracrustal suites and generations of gneisses (Hurst et al., 1975; Collerson et al., 1976; Bridgwater et al., 1991; Shimojo et al., 2016). Given that it was suggested that the Saglek dikes have intruded into Nulliak suite whereas they are absent in the Upernavik suite, their age is assumed to be within a broad time frame between 3.8 and 3.0 Ga. Furthermore, a younger generation of undeformed mafic dikes is present in the SHC, and has been described as massive diabase dikes intruding the whole SHC (Bridgwater et al., 1973). The undeformed character of these mafic dikes have lead studies to suggest that the timing of their emplacement occurred during or after the regional metamorphic events, and therefore are referred as Proterozoic dikes in the literature (Collerson et al., 1979; Hurst et al., 1975; Bridgwater et al., 1973).

The SHC has a complex thermal history including Paleoarchean and Neoarchean metamorphic events, migmatization, as well as plutonic activity. The Paleoarchean marks a period of major deformation, metasomatism and metamorphism events in the SHC (Collerson et al., 1983; Bridgwater et al., 1976; Nutman et al., 1989a). Furthermore, the Neoarchean metamorphism event marks the area's peak metamorphism, which reached granulite facies conditions and occurred around 2.7 Ga (Wendt & Collerson, 1999; Kusiak et al., 2018). This metamorphic event occurred

along with migmatization and plutonic activity, which produced the Neoarchean granites. Finally, the Torngat Orogeny caused major deformation in the area during the Proterozoic, which created the north-south trending, sub-vertical, Handy Fault (Figure 2) (Ryan.,1990). The Handy Fault divides the SHC into two areas: the granulite facies to the west and the amphibolite facies to the east.

3. ^{147}Sm-^{143}Nd Isotopic System

Samarium (Sm) and neodymium (Nd) are geochemically very similar as they are both lithophile, incompatible, light rare earth elements (LREE). However, Nd is generally slightly more incompatible than Sm due to its bigger ionic radius. The parent isotope, ^{147}Sm, decays into the daughter isotope, ^{143}Nd, with a half-life of ~106 billion years. As Sm and Nd have high charges and big radii, they are relatively immobile. Combined with its relatively high closing temperature (~600°C), the Sm-Nd system is a useful geochronological tool to date terranes that have been subjected to complex post-magmatic histories or extensive metamorphism. The long-lived Sm-Nd isotopic system is commonly used for geochronology and as a source tracer during silicate differentiation.

Sm-Nd isotopic data can be used to produce isochron diagrams from which a crystallisation or metamorphic age of a series of co-genetic rocks can be determined. Figure 3 illustrates the principle of isochron geochronology. At t=0, a suite of co-genetic differentiated rocks has the same isotopic composition. With time, samples with high Sm/Nd ratios will evolve to produce more radiogenic ^{143}Nd/^{144}Nd compositions than samples with low Sm/Nd ratios, which will evolve to less radiogenic ^{143}Nd/^{144}Nd ratios. The equation of radioactive decay applied to the Sm-Nd system gives $\frac{143Nd}{144Nd} = \left(\frac{143Nd}{144Nd}\right)_0 + \frac{147Sm}{144Nd}\left(e^{\lambda t} - 1\right)$, where the slope of the isochron diagram $m = e^{\lambda t} - 1$ corresponds to the age of the suite of co-genetic rocks (Figure 3). A larger range in Sm/Nd ratios

usually leads to better constrained slopes and thus better precisions on the ages. Therefore differentiated suites of rocks are preferred for whole-rock isochron dating. In addition, each data point has an experimental error, which is considered when calculating the slope regressions. The Mean Square Weighted Deviation (MSWD) is a statistical value of the degree of dispersion of the data points with respect to the best-fit line. Typically, an isochron is considered "true" when the MSWD value is less than 1, however few isochron diagrams have MSWD values lower than 1 due to our modern analytical precisions.

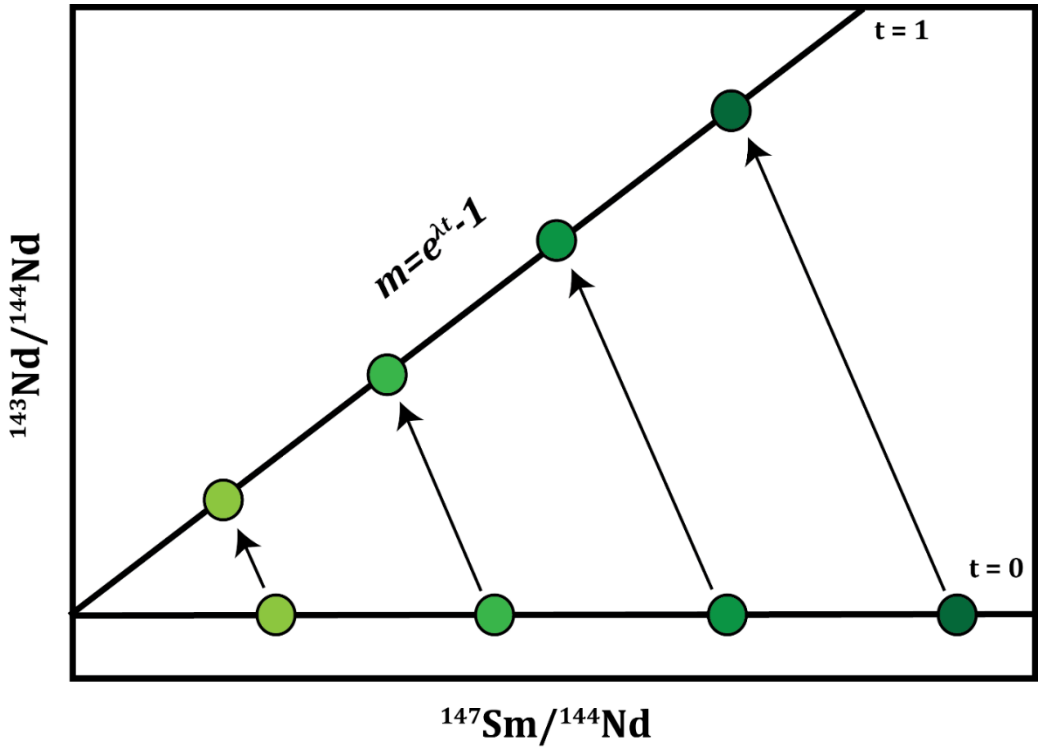

Figure 3 Example of an isochron diagram, illustrating a suite of co-genetic rocks that has fractionated into mafic (lower $^{147}Sm/^{144}Nd$) and ultramafic rocks (higher $^{147}Sm/^{144}Nd$), but still sharing the same initial composition at t=0. Decay and crystallisation commences, and the slope increases until crystallisation is completed (t=1). With the equation of the slope $m = e^{\lambda t} - 1$, which is derived from $\frac{143Nd}{144Nd} = \left(\frac{143Nd}{144Nd}\right)_0 + \frac{147Sm}{144Nd}\left(e^{\lambda t} - 1\right)$, and the known decay constant λ=6.54 x 10^{-12} for ^{147}Sm, the age of crystallisation can be calculated.

The y-intercept of the isochron diagram provides information on the initial isotopic composition of the suite of co-genetic rocks. Since high-temperature igneous processes, such as partial melting or fractional crystallization, do not affect the isotopic compositions of heavy elements, any rock

or reservoir has the same isotopic composition as its source at the time of differentiation. Given that Sm is less incompatible than Nd, reservoirs depleted in incompatible elements will have higher Sm/Nd ratios compared to their source, leading to more radiogenic $^{143}Nd/^{144}Nd$ isotopic composition with time. Similarly, reservoirs enriched in incompatible elements will have lower Sm/Nd ratios evolving to lower $^{143}Nd/^{144}Nd$. The $^{143}Nd/^{144}Nd$ ratios can be expressed as epsilon Nd (εNd) values calculated with the following equation:

$$\varepsilon Nd = \left(\frac{{}^{143Nd}/_{144Nd}\, Sample}{{}^{143Nd}/_{144Nd}\, CHUR} - 1 \right) * 10^4$$

εNd values represent the deviation of $^{143}Nd/^{144}Nd$ ratios of samples (or sources) from CHUR (Chondritic Uniform Reservoir) at a given time. Typically, terrestrial rocks with positive εNd values represent rocks with depleted sources (i.e. with a suprachondritic Sm/Nd), whereas negative εNd values will represent rocks with enriched sources (i.e. with a subchondritic Sm/Nd ratio) (Figure 4).

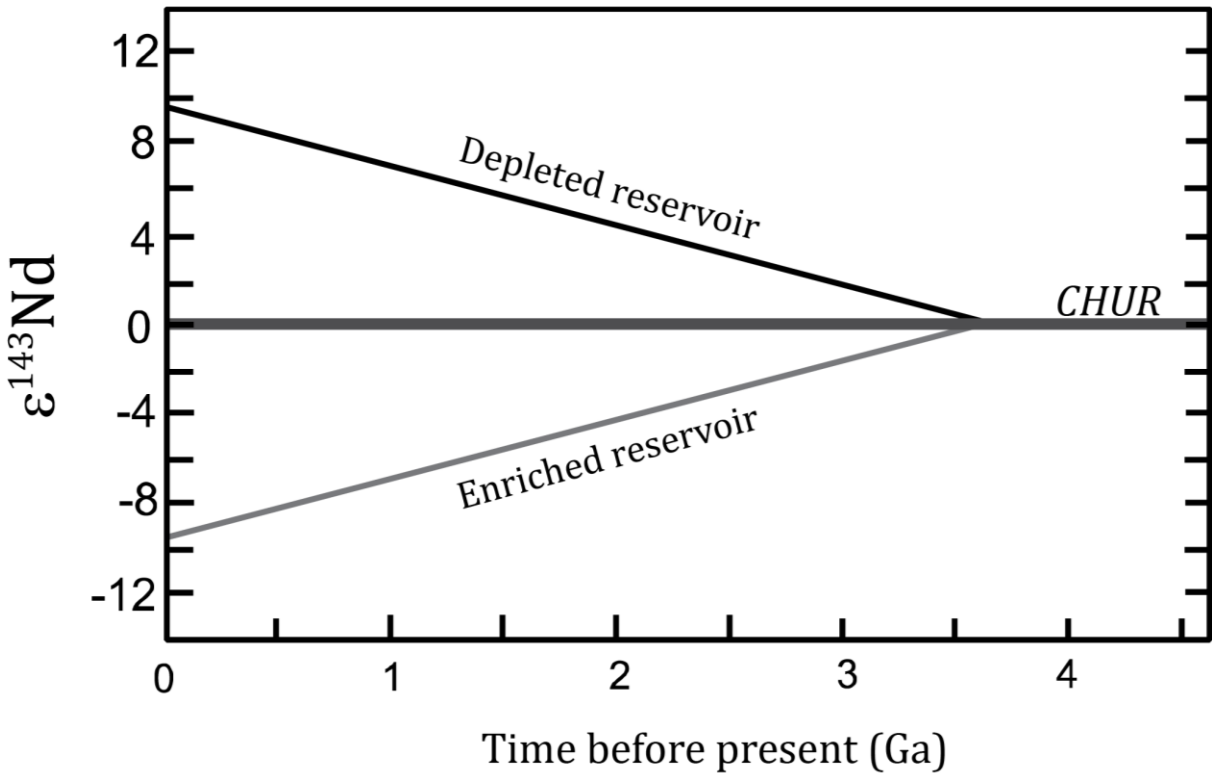

Figure 4 Evolution through time of εNd of a depleted source (positive values) and an enriched source (negative values) as a result of differentiating from CHUR at 3.5 Ga.

4. Methods

4.1 Sample preparation

A total of 83 samples were studied and the main locations of sampling are shown on Figure 2. Locations and rock types for each sample are presented in Table A1 in the Appendix. All 83 samples have been analysed for ^{147}Sm-^{143}Nd isotopic compositions. This includes 24 mafic metavolcanic samples and 19 ultramafic samples from the Nulliak and Upernavik supracrustal suites, 14 Saglek dikes and 26 undeformed mafic dikes. All dikes were analysed for major and trace elements composition during this study and the whole-rock compositions for the mafic metavolcanic and ultramafic rocks were previously analysed and are reported in Wasilewski et al. (2019).

Polished thin sections were done for each sample in order to make observations using a transmitted and reflected light polarized microscope. Weathered surfaces were cut off for all samples prior to crushing. Samples were first crushed in a steel jaw crusher and then grounded to powder in a ceramic pulveriser.

4.2 Major and trace elements

Major elements concentrations for the dikes were analyzed at the laboratories of the department of Earth and Environmental Sciences of the University of Ottawa by X-ray Fluorescence (XRF). These were conducted on a Rigaku Supermini200 WDXRF spectrometer. Powdered sample were fused using a flux made in-house (79/21 $Li_2B_4O_7/LiBO_2$) to produce glass disks (sample/flux ratio of 1:7) with addition of 60-80 mg of LiBr. Reference materials used for mafic and ultramafic sample calibration curves were UB-N, UM-2, MRG-1, PM-s, BCR-2, WS-E, SY-3 BHVO-2, BM, AN-G, BCR-032 and PC-1016. XRF measurements of major element concentrations are reported as oxides in weight percent (wt%) (detection limits are shown in Table A2 in the Appendix).

Trace element analyses for the same samples were also performed in the laboratories of the University of Ottawa. Approximately 100 mg of powdered sample were dissolved in closed Savillex beakers using a 1:5 HNO_3-HF mix, and placed on a hot plate at 125°C for 3 days. Samples were then opened and placed on a hot plate until complete dryness. Samples were then re-dissolved in 6M HCl and placed on a hot plate in closed beakers for two days. Sample were then re-dissolved in concentrated HNO_3 and dried again. Once the dissolution was completed, samples were ready for dilution, where approximately 40ml of 7M HNO_3 was added to the samples and placed overnight on a hotplate. From this solution, an aliquot of 1ml was taken and transferred into a 15ml centrifuge tube, from which we added 11ml of 0.01M HNO_3 with traces of HF. Once the samples were dissolved and diluted, they were ready for analysis. Dilution factors were all calculated by

weight. Trace element concentrations were analysed at the University of Ottawa on an Agilent 8800 QQQ Triple-Quadrupole ICP-MS. BHVO-2, BCR-2 and BIR-1a standards were analysed multiple times for accuracies and precisions. The standard BIR-1a was used to calculate the unknown samples concentrations and standards BCR-2 and BHVO-2 were considered as unknowns to validate the results. Accuracies were <8% for the REE, Sc, V, Cr, Co, Ni, Cu, Zn, Ga, Sr, Y, Zr, Cs, Pb, Th, Hf; between 10-20% for Rb, U; >20% Ba, Nb. Precisions were obtained from repeated measurements of the BIR-1a standard and were between 1-10% on the REE, Sc, Sr, Ba, Hf, Pb, Th, U and between 10-15% for Cr, Ni, V, Zr, Nb, Y, Rb. Trace element concentrations are reported as parts-per-million (ppm). Four samples were sent to Activation Laboratories for duplicate analysis, to ensure the consistency from one laboratory to the other. Samples were analysed by ICP-MS on a Perkin Elmer Sciex ELAN 9000 ICP-MS high-speed quadrupole. Samples were fused using a lithium metaborate flux (LiBO2), using a sample/flux ratio of 1:5. Full analytical techniques and detection limits (Code: research 4B2) are available on the Activation Laboratories website at http://www.actlabs.com/page.aspx?page=555&app=226&cat1=549&tp=12&lk=no&menu=64. Rare earth element compositions for duplicate samples analysed at University of Ottawa and Activation Laboratories are shown on Figure 5. Compositions obtained from both laboratories are consistent with no significant differences.

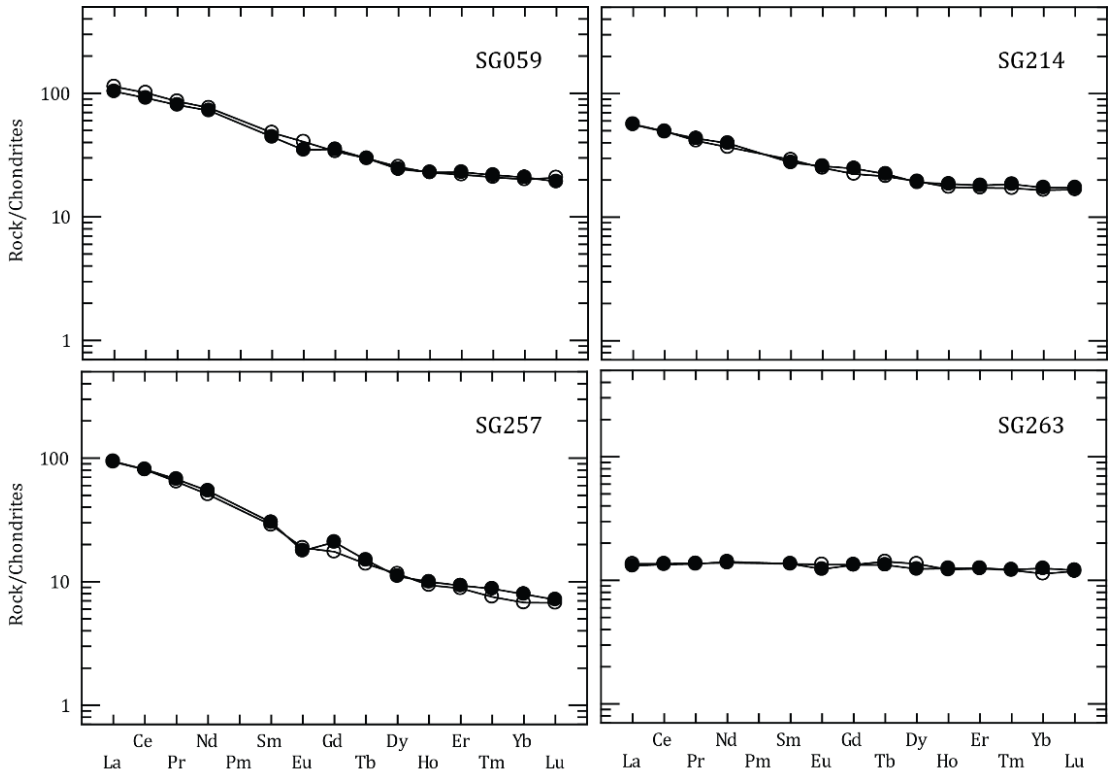

Figure 5 Results of the duplicate analyses of rare earth element concentrations. In black are the samples analysed at the University of Ottawa, and in white are the concentrations from ActLabs for the same samples. Concentrations normalised to chondrite values from Sun & McDonough (1989).

4.3 Sm-Nd analytical procedure

Sample preparation for isotopic analyses was conducted in the clean laboratory of the Department of Earth and Environmental Sciences of the University of Ottawa. Between ~100 and ~350 mg of powdered were dissolved for each sample, depending on their Nd concentrations. A spike enriched with ^{150}Nd and ^{149}Sm tracers was added to the samples prior to dissolution. Sample and spike weights are presented in Table 1. Samples were dissolved in closed Savillex beakers using a 1:5 HNO_3-HF mix and placed on a hot plate at 125°C for 4 days. Samples were then opened and placed on a hot plate until complete dryness. Samples were then re-dissolved in 6M HCl (~5mL) and placed on the hot plate in closed beakers for 48 hours. Samples were then dried after addition of two drops of boric acid to dissolve any fluorides. Samples were re-dissolved in 2.5M HCl and placed to dry. Samples that potentially contained refractory phases such as garnets and/or

chromites, were dissolved in Teflon containers placed in high-pressure steel jacketed Parr bombs. These samples were dissolved using a 1:5 HNO_3-HF mixture in an oven at 140°C for 5 days to reach complete dissolution. After the samples were dried, they were re-dissolved in 6M HCl and placed again in the high-pressure steel jackets for 48 hours. They were then dried after addition of drops of boric acid. Sample SG-006 was dissolved twice for duplicate analyses (SG-006D).

Mafic and Ultramafic Samples					
Sample	**Dissolution Technique**	**Sample weight (g)**	**Spike Weight (g)**	**Spike Number**	**Analytical Session**
SG-006	Teflon bombs	0.36128	0.03909	DTM 16-1-116	5
SG-006-D	Teflon bombs	0.37075	0.04051	DTM 16-1-116	6
SG-009	Teflon bombs	0.11156	0.05558	DTM 16-1-116	5
SG-010	Teflon bombs	0.15335	0.07623	DTM 16-1-116	5
SG-011	Savillex beakers	0.12772	0.13042	DTM 16-1-116	3
SG-013	Savillex beakers	0.10167	0.12711	DTM 16-1-116	3
SG-015	Teflon bombs	0.21195	0.05408	DTM 16-1-116	5
SG-021	Savillex beakers	0.16125	0.07701	DTM 16-1-116	3
SG-022	Savillex beakers	0.31379	0.04989	DTM 16-1-116	3
SG-023	Savillex beakers	0.12788	0.08662	DTM 16-1-116	3
SG-029A	Savillex beakers	0.09212	0.09222	DTM 16-1-116	3
SG-035	Savillex beakers	0.97310	0.09051	DTM 16-1-116	3
SG-044	Teflon bombs	0.12557	0.16638	DTM 16-1-116	2
SG-046	Savillex beakers	0.16558	0.06646	DTM 16-1-116	3
SG-051	Teflon bombs	0.05532	0.03837	DTM 16-1-116	7
SG-063	Teflon bombs	0.09851	0.11438	DTM 16-1-116	5
SG-064	Savillex beakers	0.36287	0.02845	DTM 16-1-116	3
SG-065	Teflon bombs	0.02669	0.10779	DTM 16-1-116	7
SG-066	Teflon bombs	0.36332	0.04115	DTM 16-1-116	5
SG-067	Savillex beakers	0.11360	0.10668	DTM 16-1-116	3
SG-068	Teflon bombs	0.10221	0.10420	DTM 16-1-116	6
SG-069	Teflon bombs	0.09404	0.10131	DTM 16-1-116	6
SG-071	Savillex beakers	0.10105	0.12884	DTM 16-1-116	3
SG-072	Savillex beakers	0.12319	0.13189	DTM 16-1-116	3
SG-075	Savillex beakers	0.14914	0.06676	DTM 16-1-116	3
SG-079	Savillex beakers	0.11395	0.07422	DTM 16-1-116	3
SG-090	Teflon bombs	0.12579	0.16205	DTM 16-1-116	2
SG-092	Teflon bombs	0.14727	0.20179	DTM 16-1-116	2
SG-095	Savillex beakers	0.10175	0.09179	DTM 16-1-116	3
SG-099	Savillex beakers	0.15166	0.07516	DTM 16-1-116	3
SG-100	Savillex beakers	0.12022	0.12127	DTM 16-1-116	3
SG-101	Savillex beakers	0.10969	0.07498	DTM 16-1-116	3
SG-109B	Savillex beakers	0.14760	0.10685	DTM 16-1-116	3
SG-110	Teflon bombs	0.18627	0.12936	DTM 16-1-116	2
SG-112	Savillex beakers	0.10125	0.08108	DTM 16-1-116	3
SG-123	Savillex beakers	0.15615	0.06978	DTM 16-1-116	3
SG-126	Teflon bombs	0.21427	0.17902	DTM 16-1-116	2
SG-128	Savillex beakers	0.10929	0.10361	DTM 16-1-116	3
SG-129	Savillex beakers	0.11188	0.07226	DTM 16-1-116	3
SG-130	Savillex beakers	0.11907	0.08355	DTM 16-1-116	3
SG-205	Teflon bombs	0.09912	0.05415	DTM 16-1-116	7
SG-221A	Teflon bombs	0.36652	0.02011	DTM 16-1-116	7

SG-221B	Teflon bombs	0.35352	0.01964	DTM 16-1-116	7
SG-240	Teflon bombs	0.33855	0.04432	DTM 16-1-116	6
Dike Samples					
Sample	**Dissolution Technique**	**Sample weight (g)**	**Spike Weight (g)**	**Spike Number**	**Analytical Session**
BR-82-119B	Teflon bombs	0.15030	0.03559	GEOTOP	2
BR-83-122	Teflon bombs	0.10518	0.02345	GEOTOP	1
BR-83-46B	Teflon bombs	0.10230	0.02344	GEOTOP	1
SG-001	Teflon bombs	0.10175	0.05061	GEOTOP	7
SG-036	Teflon bombs	0.11756	0.02065	GEOTOP	1
SG-040	Teflon bombs	0.15177	0.02150	GEOTOP	2
SG-050	Teflon bombs	0.15673	0.03846	GEOTOP	2
SG-052	Teflon bombs	0.08392	0.03521	GEOTOP	1
SG-058	Teflon bombs	0.10217	0.02381	GEOTOP	1
SG-059	Teflon bombs	0.07435	0.06180	GEOTOP	1
SG-094	Teflon bombs	0.15403	0.03855	GEOTOP	2
SG-098	Teflon bombs	0.11307	0.04671	GEOTOP	2
SG-118	Teflon bombs	0.14960	0.03545	GEOTOP	7
SG-120	Teflon bombs	0.09448	0.02141	GEOTOP	1
SG-121	Teflon bombs	0.09477	0.03245	GEOTOP	1
SG-211	Savillex beakers	0.12684	0.17078	DTM 16-1-116	4
SG-212	Savillex beakers	0.11086	0.20121	DTM 16-1-116	4
SG-213	Savillex beakers	0.10286	0.25594	DTM 16-1-116	4
SG-214	Savillex beakers	0.10535	0.27122	DTM 16-1-116	4
SG-215	Savillex beakers	0.10446	0.21712	DTM 16-1-116	4
SG-217	Savillex beakers	0.11056	0.16073	DTM 16-1-116	4
SG-218	Savillex beakers	0.09893	0.15705	DTM 16-1-116	4
SG-219	Savillex beakers	0.10556	0.13180	DTM 16-1-116	4
SG-220	Savillex beakers	0.10596	0.16584	DTM 16-1-116	4
SG-222	Savillex beakers	0.12294	0.13266	DTM 16-1-116	4
SG-225	Savillex beakers	0.04880	0.06885	DTM 16-1-116	6
SG-226	Savillex beakers	0.04922	0.07583	DTM 16-1-116	6
SG-231	Savillex beakers	0.05047	0.06435	DTM 16-1-116	6
SG-232	Savillex beakers	0.05108	0.05868	DTM 16-1-116	7
SG-237	Savillex beakers	0.05462	0.06493	DTM 16-1-116	7
SG-249	Savillex beakers	0.05184	0.08402	DTM 16-1-116	7
SG-250	Savillex beakers	0.12041	0.30622	DTM 16-1-116	4
SG-251	Savillex beakers	0.12019	0.24726	DTM 16-1-116	4
SG-253	Savillex beakers	0.10351	0.17186	DTM 16-1-116	4
SG-256	Savillex beakers	0.10482	0.11139	DTM 16-1-116	4
SG-257	Savillex beakers	0.08507	0.29635	DTM 16-1-116	4
SG-261	Savillex beakers	0.05132	0.08248	DTM 16-1-116	7
SG-262	Savillex beakers	0.05124	0.08369	DTM 16-1-116	7
SG-263	Savillex beakers	0.10823	0.09615	DTM 16-1-116	4
SG-268	Savillex beakers	0.05393	0.07912	DTM 16-1-116	6
SG-269	Savillex beakers	0.05188	0.07910	DTM 16-1-116	6
SG-289	Savillex beakers	0.10954	0.05449	DTM 16-1-116	7

Table 1: Weight of powdered sample dissolved, as well as weight and the number of spike added. Including the dissolution technique and analytical session for each sample. Analytical session numbers are detailed in Table 2.

Samples were dissolved in 2ml of 2M HCl for primary column chromatography. Samples were centrifuged prior to sample loading to avoid the introduction any potential residue to the column. The primary columns are filled with 200-400 mesh AG50W-X8 cation exchange resin for the LREE extraction. Samples for which less than 130 mg was dissolved were loaded on columns

containing ~2 ml of resin, whereas larger samples were loaded on columns with ~15 ml of resin to avoid saturation of the cation exchange sites. The Sm and Nd fractions were then separated from the LREE fractions, and purified from other elements potentially creating isobaric interferences, using columns filled with 300 mg of Eichrom Ln-Spec resin 50-100 μm. The complete primary column and Ln-Spec column procedures are shown in Table A3 in the Appendix. Total Nd blanks were <80 pg.

Samarium and Nd isotopic compositions were measured using double rhenium (Re) filaments on the Thermo-Fisher Triton thermal ionisation mass spectrometer (TIMS) at the GEOTOP laboratories of the Université de Québec à Montréal (UQAM) and at the Isotope Geochemistry and Geochronology Research Centre (IGGRC) of the department of Earth Sciences of Carleton University in Ottawa. Sm and Nd fractions were dissolved in 1μl of ~2.5M HCl and loaded onto pre-outgassed Re filaments. Nd runs consisted of measurements of 120 to 140 ratios, and the Sm runs consisted of 100 ratios, both with integration times of 8 seconds. Corrections for instrumental mass bias fractionation were applied using an exponential law of $^{146}Nd/^{144}Nd = 0.7219$ for Nd and $^{147}Sm/^{152}Sm = 0.56081$ for Sm. Isobaric interferences for both Sm and Nd isotopes were monitored and corrected when necessary. The JNdi-1 Nd standard was analysed multiple times during each analytical session and values are reported in Table 2. All $^{143}Nd/^{144}Nd$ results were normalized to JNdi-1 value from Tanaka et al. (2000) of 0.512115 ± 0.000007. JNdi-1 values obtained at the IGGRC during analytical session 3, 4 and 5 are slightly lower than the value of Tanaka et al. (2000), but were obtained before the replacement of all faraday cups on the IGGRC instrument. Note that session 7 took place after all cups were replaced and the JNdi-1 value for that session is higher and overlaps with the value of Tanaka et al. (2000). Sample SG-006 was measured at the IGGRC and was duplicated (SG-006D; separate dissolution) and measured at the GEOTOP. The

$^{143}Nd/^{144}Nd$ ratios for both duplicate samples are overlapping within error. $\varepsilon^{143}Nd$ values are calculated using the CHUR values of $^{143}Nd/^{144}Nd = 0.512630$ and $^{147}Sm/^{144}Nd = 0.1960$ (Bouvier et al., 2008).

Analytical Session	Date	Laboratory	Average of measured JNdi-1	Number of Standard Analysed
Session 1	July, 2016	GEOTOP	0.512094 ± 3	4
Session 2	March, 2017	GEOTOP	0.512099 ± 3	3
Session 3	October, 2017	IGGRC	0.512076 ± 3	6
Session 4	February, 2018	IGGRC	0.512081 ± 2	6
Session 5	April, 2018	IGGRC	0.512077 ± 2	3
Session 6	July, 2018	GEOTOP	0.512099 ± 3	4
Session 7	September, 2018	IGGRC	0.512105 ± 3	4

Table 2: Average values of measured JNdi-1 terrestrial standard for each analytical session, with their respective laboratory and date of analysis. 2σ errors for $^{143}Nd/^{144}Nd$ are in the last decimal place.

5. Results

This section presents the petrography, geochemistry, as well as the Sm-Nd isotope results of the mantle-derived rocks from the SHC. The complex includes four main types of mantle-derived rocks: 1) basaltic metavolcanic rocks; 2) ultramafic rocks, 3) the mafic Saglek dikes; and 4) undeformed mafic dikes. Petrological and geochemical data of the mafic and ultramafic rocks is reported in Wasilewski et al. (2019), and only a brief summary is given here. I have performed the petrological and geochemical analyses of the two generations of mafic dikes, as well as the isotope analyses for all of the different mantle-derived units.

5.1 Petrography and geochemistry

5.1.1 Basaltic metavolcanic and ultramafic rocks

Typically, the mafic metavolcanic rocks occur as amphibolites as part of the supracrustal suites, occasionally displaying pillowed structures (Figure 6A). The ultramafic rocks display the distinguishable feature of a brown weathering surface (Figure 6B), and occur either in the supracrustal suites, commonly found in proximity to the mafic metavolcanic rocks, or they are

found as enclaves of ultramafic rocks in the Uivak gneiss. No petrographic or geochemical differences were observed between the mafic and ultramafic rocks from the Nulliak or the Upernavik supracrustal units (Wasilewski et al., 2019). The mafic metavolcanic rocks are medium grained amphibolites composed of plagioclase + hornblende ± clinopyroxene ± orthopyroxene ± quartz ± phlogopite ± garnet ± ilmenite (Figure 7 A&B). The hornblende occur as stubby euhedral and subeuhedral grains that commonly display 60°/120° cleavage, and have light green to light brown colours in plain polarized light. The plagioclase grains occur as subeuhedral grains that are occasionally weakly sericitized. In addition, weak amphibole mineral alignments as well as alteration rims around the amphibole grains were observed. The ultramafic rocks are mainly composed of olivine + orthopyroxene + clinopyroxene + spinel ± tremolite ± phlogopite (Figure 7 C&D). Some ultramafic samples display equigranular olivine and pyroxene but other ultramafic samples are highly serpentinized. The CIPW normative mineralogy for the ultramafic samples shows variable amounts of olivine, but most samples are harzburgitic and lherzolitic in composition (Figure 8).

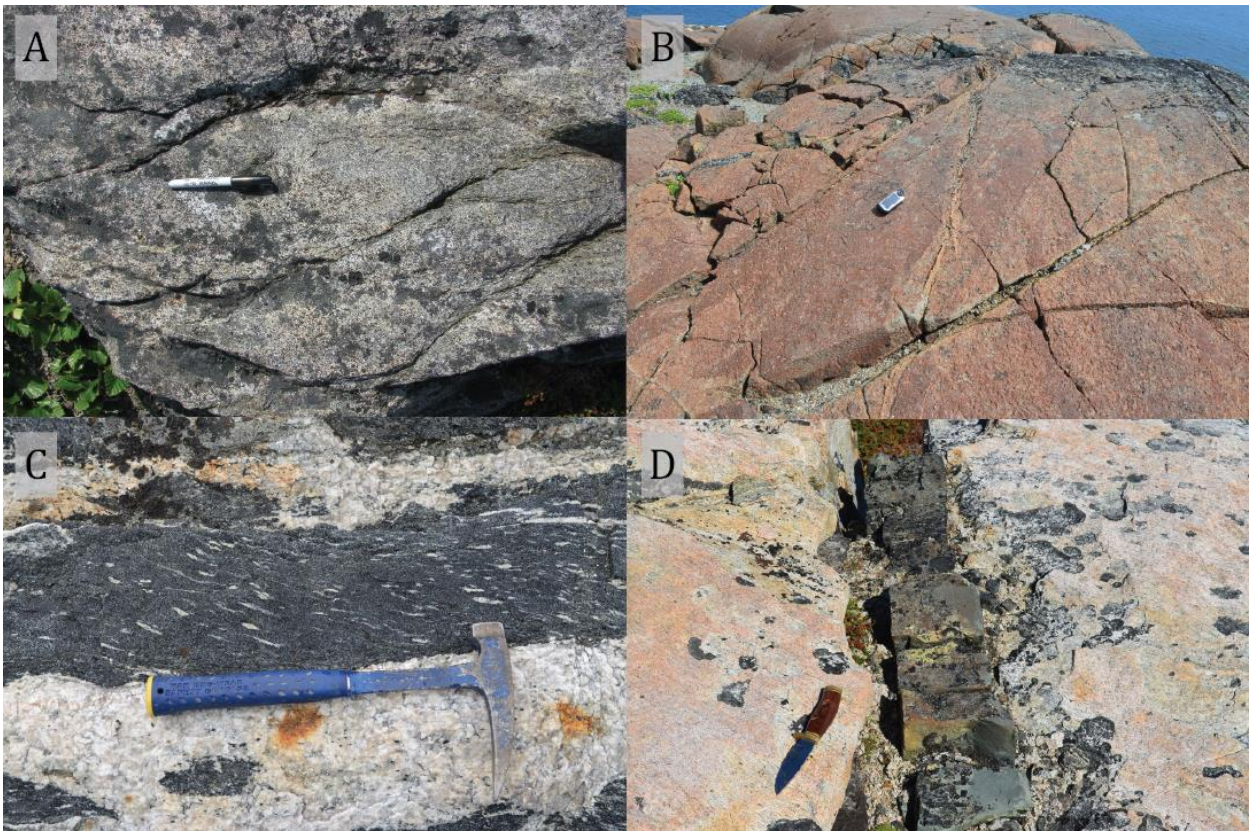

Figure 6 Field photographs of the different lithologies relevant to this study. A) Pillowed metavolcanic rocks from the Nulliak unit. B) Ultramafic rocks displaying a typical brown weathering surface. C) Deformed Saglek dike displaying elongated plagioclase phenocrysts, occurring as an enclave into the Uivak gneiss. D) Undeformed mafic dike intruding TTGs.

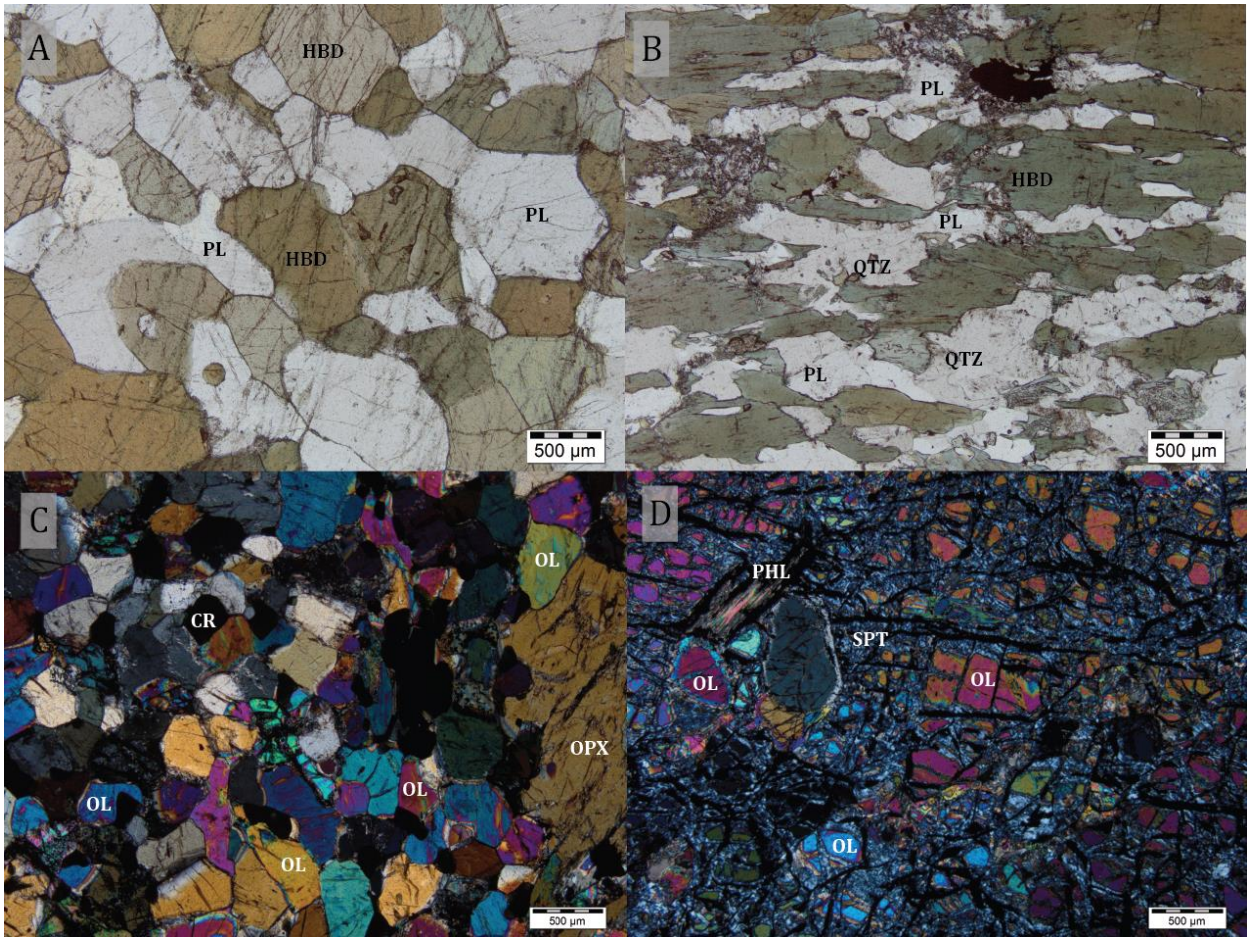

Figure 7 Microphotographs of the mafic metavolcanic (in plain polarized light) and ultramafic rocks (in cross-polarized light) A) Sample SG-090 displaying equigranular hornblende and plagioclase grains that are very weakly altered. B) Sample SG-079 displaying moderate grain deformation and alignment, as well as presence of quartz and weak to moderate alteration of plagioclase. C) Sample SG-010 displaying equigranular olivine, orthopyroxene and chromite grains, with limited alteration D) Sample SG-013 displaying strong serpentinization of olivine. (PL = Plagioclase, HBD = Hornblende, QTZ = Quartz, OL = Olivine, OPX = Orthopyroxene, PHL = Phlogopite, SPT = Serpentine)

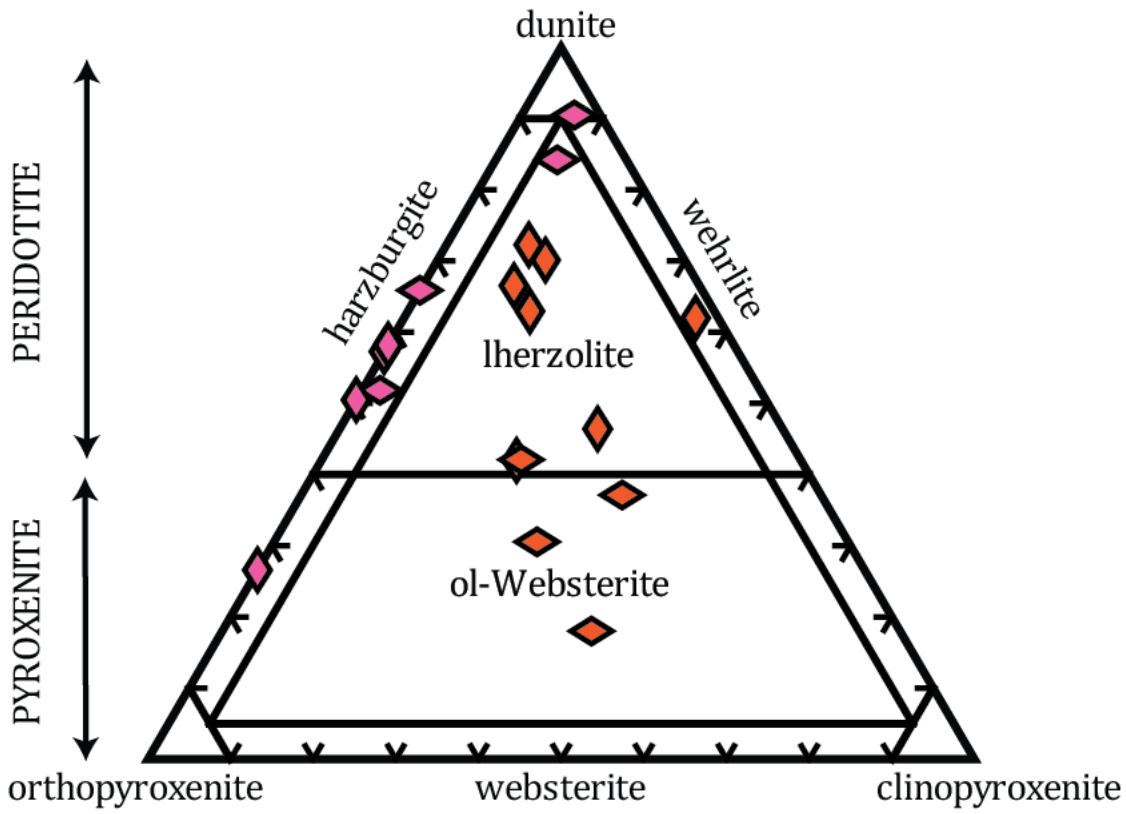

Figure 8 Rock classification diagram from Le Maitre (2002), of the ultramafic samples calculated CIPW-normative mineralogy (Irvine & Baragar., 1971). Vertical diamonds are samples from the Nulliak unit and the horizontal diamonds are samples from the Upernavik unit. Pink symbols are samples from the low-Fe ultramafic group and the orange symbols are samples from the Enriched ultramafic group from the classification of Wasilewski et al. (2019). Only the samples analysed for Sm-Nd isotopes for this study are plotted.

The major and trace elements compositions of the SHC mafic metavolcanic and ultramafic rocks can be found in Wasilewski et al. (2019) but the geochemical compositions of the samples analysed here for Sm-Nd isotopes are presented in Table A4 in the Appendix. Concentrations for the major elements are plotted on figures as recalculated anhydrous compositions. The mafic metavolcanic rocks are mostly basaltic in composition, with rare samples having more evolved basaltic andesite or andesitic compositions (Figure 9A). The mafic metavolcanic rocks display tholeiitic trends, with increasing FeO concentrations as MgO contents decrease (Figure 9B). Most samples studied here are from the "high-Ti group" defined by Wasilewski et al. (2019) as more evolved liquids, with a few samples from the "low-Ti group" (Figure 10) interpreted as cumulate-liquid mixtures. In terms of REE, all mafic metavolcanic samples are enriched compared to chondrites, but generally display

flat REE profiles with few samples exhibiting LREE enrichment (Figure 11). Slight complementary positive and negative Eu anomalies can be observed in the low-Ti and high-Ti metavolcanic rocks respectively.

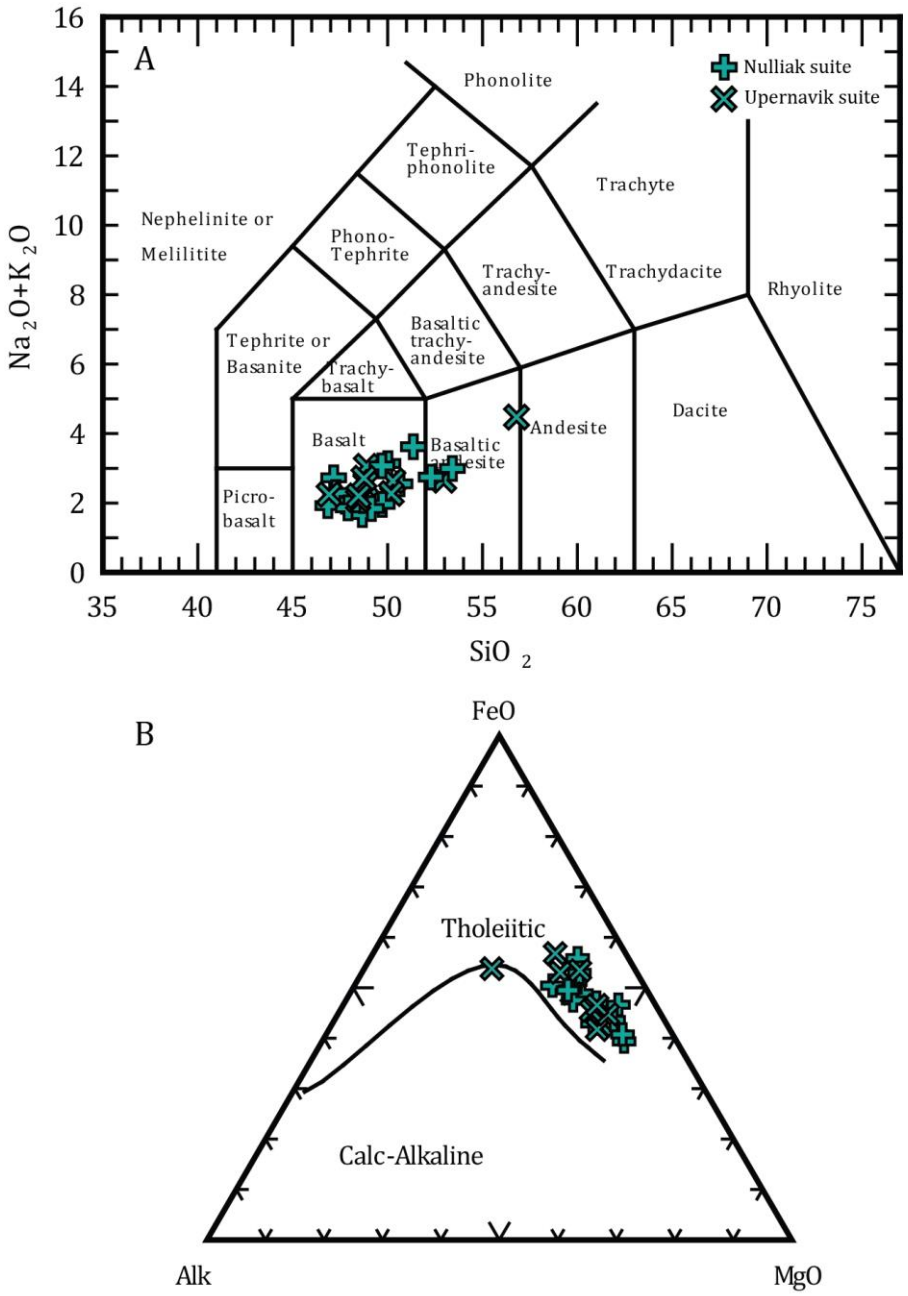

Figure 9 A) Total Alkali Silica (TAS), from Le Maitre (1989), diagram for the SHC mafic metavolcanic rocks analysed for this study, generally plotting in the basalt field, with the exception of the few samples plotting in the andesitic basalt and the andesite field. B) Alk + FeO + MgO (AFM) ternary diagram from Irvine & Baragar (1971). Data from Wasilewski et al. (2019).

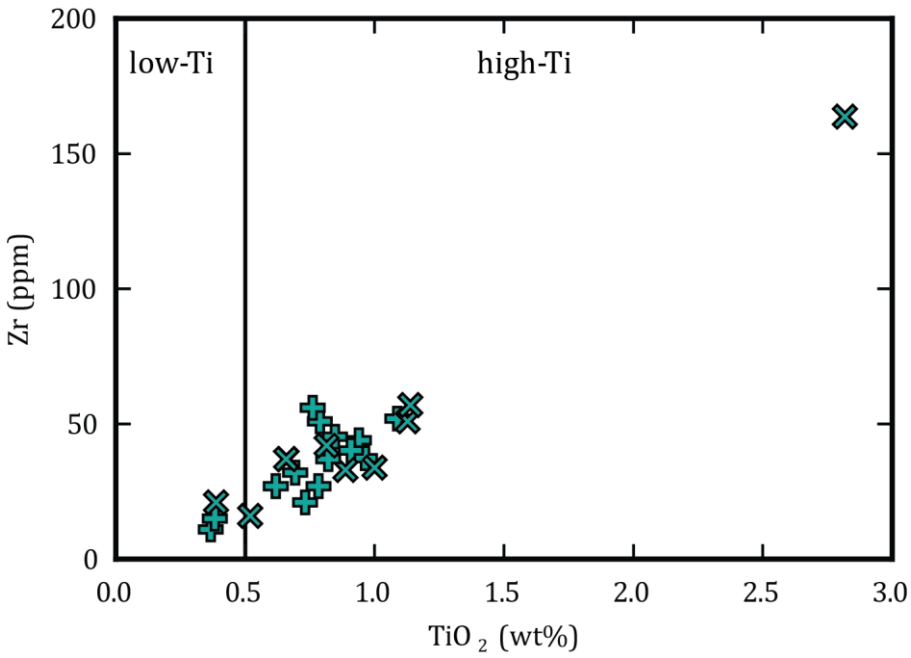

Figure 10 Zr vs TiO_2 of the mafic metavolcanic rocks illustrating that most samples take part of the high-Ti (>0.5 wt%) group. Classification and data from Wasilewski et al., (2019). The symbols are the same as the previous figure.

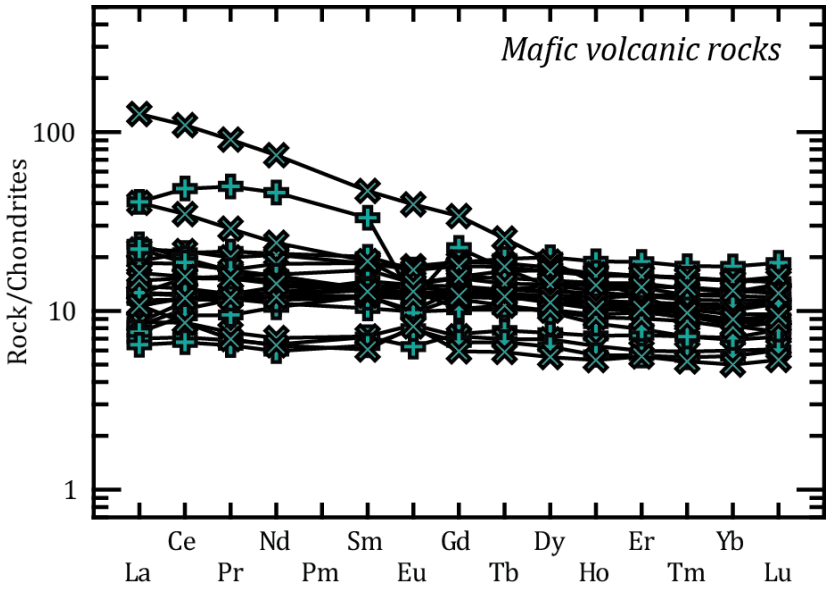

Figure 11 Chondrite-normalised rare earth element profile of the mafic metavolcanic rocks. Same symbols as for Figure 9. Normalizing values of Sun & McDonough (1989). Data from Wasilewski et al. (2019)

The ultramafic rocks have major element compositions relatively homogenous, with SiO_2 and MgO contents ranging from 42.1 to 50.2 wt% and 20.0 to 41.4 wt%, respectively. They are divided in two different groups distinguished by their Al/Ti ratios, with the harzburgitic rocks showing higher Al/Ti ratios compared to the lherzolitic rocks with are characterized by lower Al/Ti ratios

(Figure 12). The two groups of ultramafic rocks also display differences in terms of trace element compositions, where the high Al/Ti rocks have higher Cr concentrations, however they generally have lower concentrations in most incompatible elements compared to the low Al/Ti rocks. These two groups are therefore referred to as the high-Fe and the low-Fe ultramafic rocks, based on their Fe content (Wasilewski et al., 2019). The high-Fe ultramafic samples studied here exhibit relatively flat to slightly LREE enriched profiles whereas the low-Fe ultramafic rocks vary from relatively flat to LREE depleted profiles compared to the HREE (Figure 13). A number of low-Fe ultramafic samples displayed LREE enriched profiles interpreted to be the result of post-magmatic enrichment (Wasilewski et al., 2019), and therefore these samples were avoided for Sm-Nd isotope studies, as this LREE enrichment likely affected their original Sm/Nd ratios.

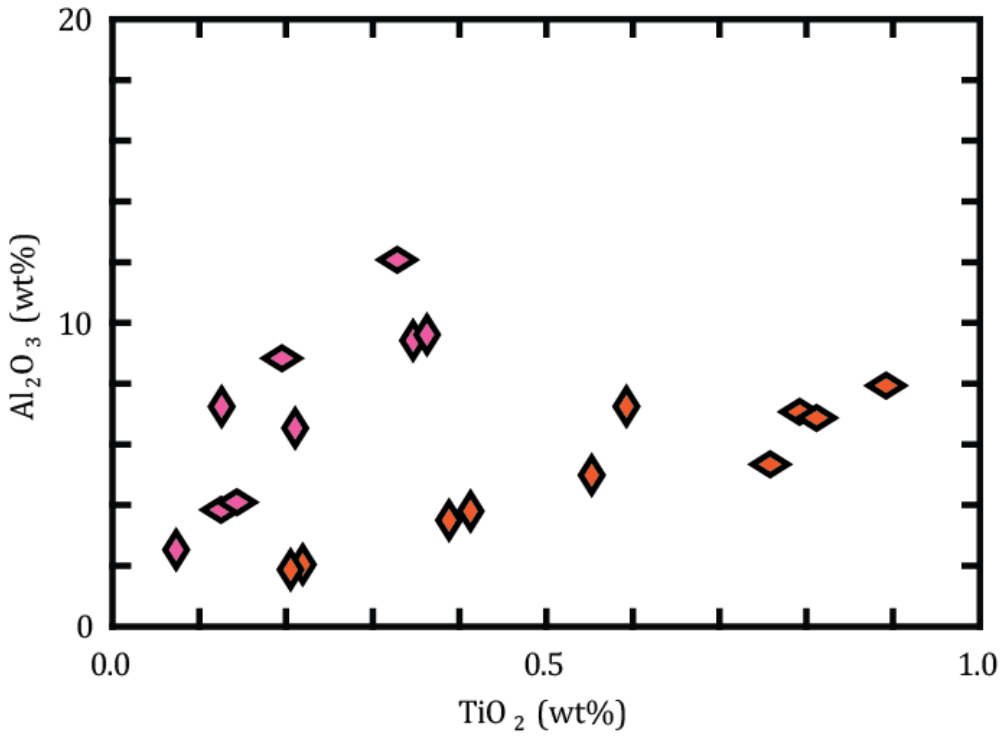

Figure 12 Al_2O_3 vs TiO_2 diagram of the ultramafic rocks studied here, displaying two distinct suites. Pink symbols are the low-Fe ultramafic samples and the orange symbols are the high-Fe ultramafic samples. Vertical symbols are samples from the Nulliak unit and horizontal symbols are samples from the Upernavik unit. Data from Wasilewski et al. (2019).

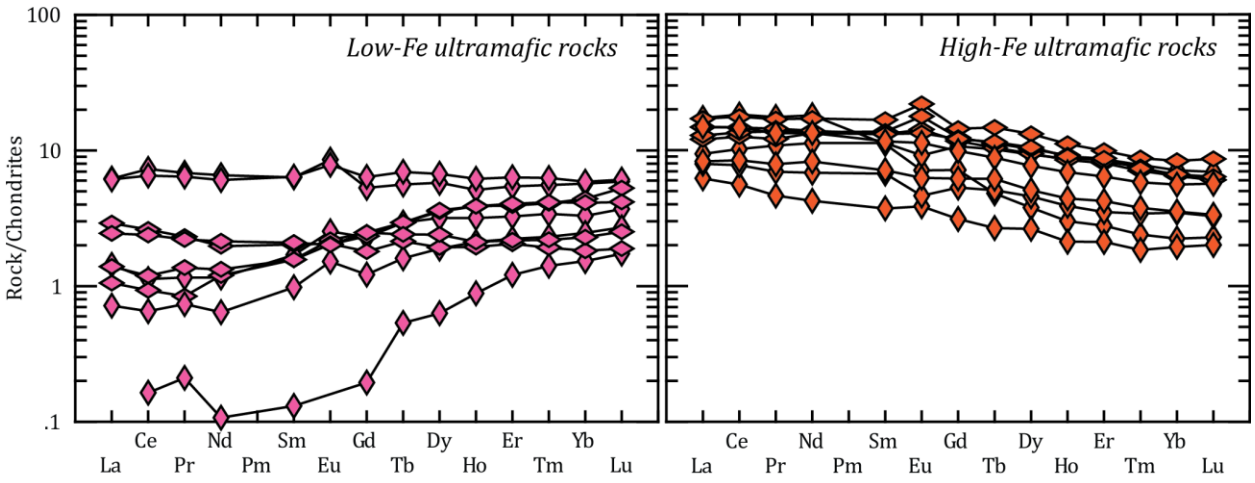

Figure 13 Chondrite-normalized rare earth element profiles of the ultramafic rocks from this study. Symbols used are the same as previous figures. Normalizing values of Sun & McDonough (1989). Data from Wasilewski et al. (2019).

5.1.2 Saglek dikes and undeformed mafic dikes

The Saglek dikes are elongated deformed porphyritic mafic rock units occurring as enclaves into the Uivak Gneiss and the Nulliak suite, and they are identified in the field by the presence of large plagioclase phenocrysts (Figure 6C). Because of their similar mineralogy and metamorphic texture to the metavolcanic rocks, the Saglek dikes are challenging to identify in the field when intruding the supracrustal suites. The younger undeformed mafic dikes are microgranular mafic rock units up to 30 meters wide. These have been observed to be intruding through the 3.24 Ga Lister Gneiss as illustrated in Figure 6D. From the sampled undeformed mafic dikes, a series of samples (SG-211 to SG-215) were collected across a ~30 m wide dike in order to get a representative sample set from a chilled margin into the centre of the dike.

The detailed petrography of the Saglek dikes and undeformed mafic dikes is presented in Tables A5 and A6, in the Appendix. Petrologically, the Saglek dikes are homogeneous with slight mineral proportion variations. They are mainly composed of typical metabasite upper amphibolite facies assemblages; amphibole + plagioclase with some samples exhibiting minor amounts of quartz ± clinopyroxene ± orthopyroxene ± olivine and some accessory minerals including Fe-Ti oxides,

sulphides (such as pyrite), chlorite and biotite (Figure 14 A&B). Most ferromagnesian minerals in the Saglek dikes are however amphiboles (between 40% and 50%), primarily present as hornblende and occasionally as actinolite. Hornblende minerals occur as euheudral to sub-euhedral stubby grains that vary in size from 0.5 mm to 2 mm and commonly display pyroxene rims. The plagioclase abundances vary between 20% and 35%. They occur as elongated and/or stubby grains that are generally euhedral to sub-euhedral although some grains are sub-rounded. They display moderate to strong sericitization. In terms of CIPW normative mineralogy, the Saglek dikes fall within the olivine gabbronorite field (Figure 15) with generally a lesser amount of normative orthopyroxene compared to clinopyroxene.

The undeformed mafic dikes are mineralogically homogeneous. As opposed to the Saglek dikes, the mafic dikes display more primary igneous mineralogical assemblages, composed of plagioclase + clinopyroxene + orthopyroxene ± amphibole ± sericite as well as some trace minerals including sulphides and iron oxides. Most mafic dike samples display ophitic to subophitic textures (Figure 14 C&D). The plagioclase abundance varies from 45% to 60%. They occur as elongated or acicular grains, and sometimes as stubby subeuhedral grains. The grain sizes vary between 0.25 mm and 1 mm. The plagioclase grains are generally well preserved, with a few samples displaying moderate to strong sericitization. The clinopyroxene and orthopyroxene abundances vary from 25% to 35% and 5% to 20% respectively. They occur as stubby subeuhedral grains that vary in size from 0.25 mm to 1 mm. In terms of CIPW normative mineralogy, the mafic dikes fall within the gabbronorite field (Figure 15) with generally higher abundances of clinopyroxene compared to orthopyroxene. In contrast to the Saglek dikes, the undeformed mafic dikes contain no olivine or normative olivine.

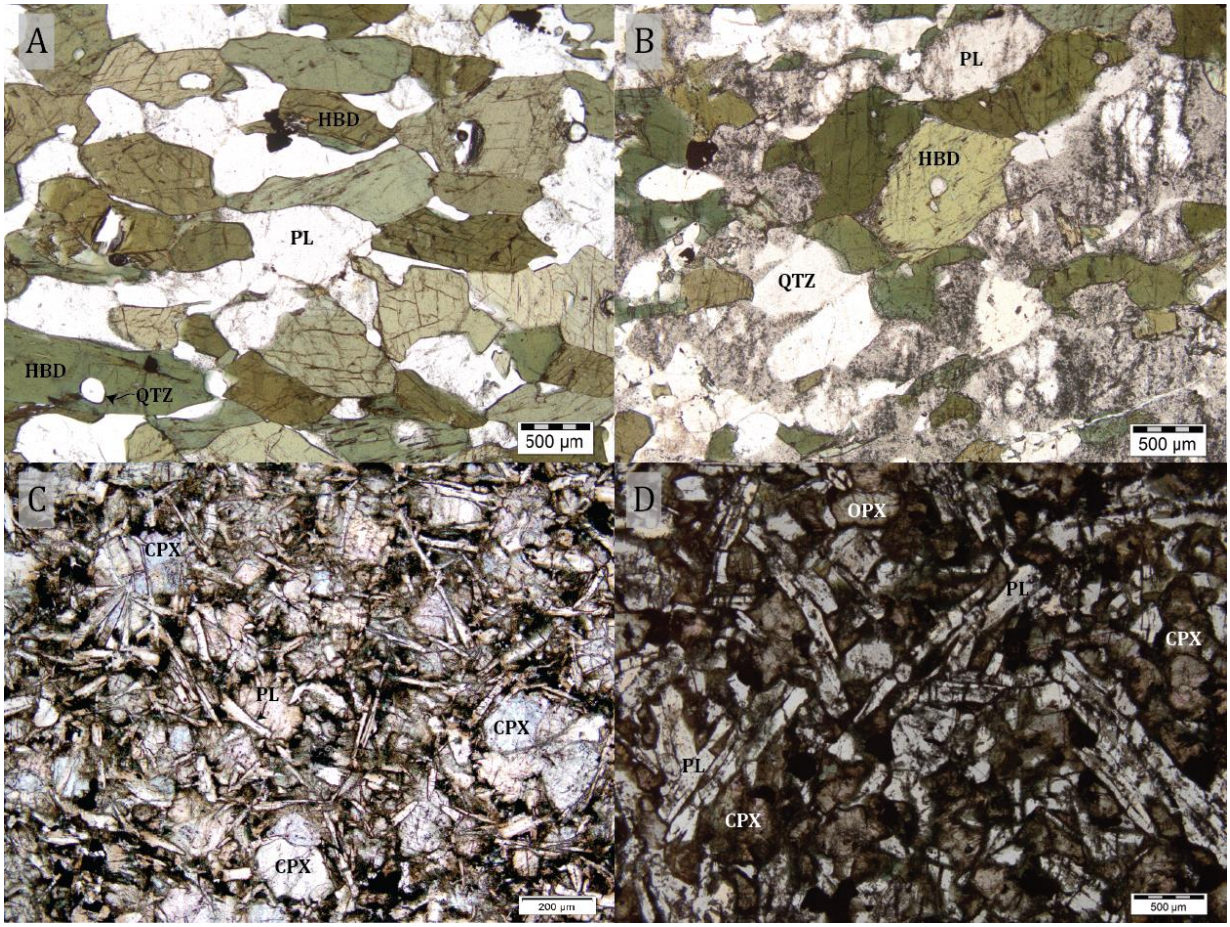

Figure 14 Microphotographs of the Saglek dikes (A&B) and undeformed mafic dikes (C&D) in plain polarized light, A) Sample SG-231 displaying hornblende mineral alignment and 60°/120° cleavage, as well as, the presence of a rounded quartz grains within the hornblende grains (poikilitic texture). B) Sample SG-250 displaying strong alteration of plagioclase as well as weak hornblende mineral alignment. C) Sample SG-040, displaying acicular plagioclase grains enveloped in the sub-euhedral clinopyroxene grains (sub-ophitic texture) D) Sample SG-220, displaying elongated plagioclase grains and moderately to strongly altered pyroxene grains. (HBD = Hornblende, QTZ = Quartz, PL = Plagioclase, CPX = Clinopyroxene, OPX = Orthopyroxene)

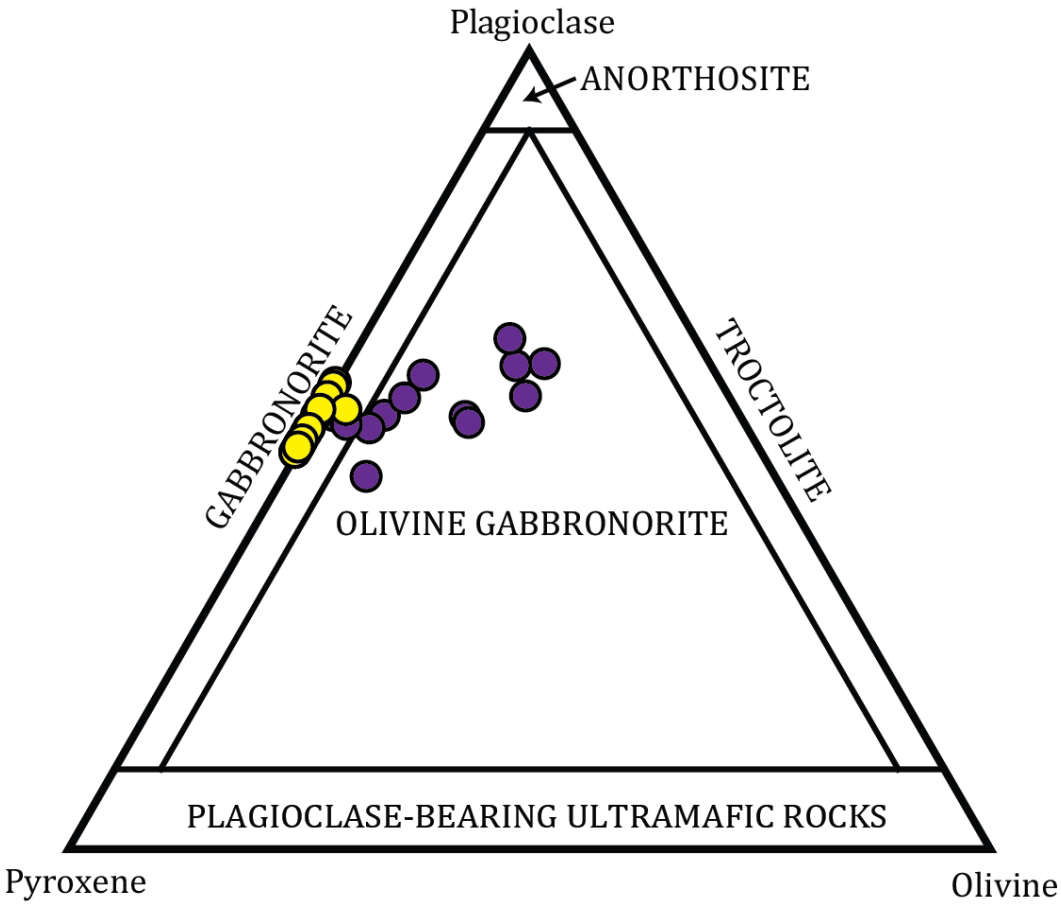

Figure 15 Rock classification diagram, from Le Maitre (2002), using the Saglek dikes (purple) and undeformed mafic dikes (yellow) calculated CIPW normative mineralogy (Irvine & Baragar., 1971).

The major and trace elements compositions for the Saglek dikes and the undeformed mafic dikes are presented in Table A7 in the Appendix. Most Saglek dikes have a basaltic composition, with few samples having basaltic andesite to andesitic compositions (Figure 16A). The Saglek dikes seem to follow a tholeiitic trend, with Fe and Ti contents increasing with decreasing MgO (Figure 16B). They have varying geochemical compositions in terms of major elements (Al, Mg, Ca, K, and P) (Figure 17A-D), with MgO compositions varying between 4.8 to 7.6 wt% and SiO_2 compositions varying between 45.7 wt% and 57.2 wt%. Most major elements do not exhibit clear variations with MgO contents, except for TiO_2 and FeO concentrations displaying well-defined increasing correlations with decreasing MgO. Immobile incompatible trace elements such as Zr and Nb generally show increasing concentrations with decreasing MgO, whereas more mobile

elements such as Sr do not exhibit clear correlations (Figure 17E-G). The La/Sm ratio for the Saglek dikes are generally low with a few samples exhibiting high La/Sm which do not correlate with MgO contents (Figure 17H). Most Saglek dikes exhibit flat REE patterns, with minor Eu negative anomalies (Figure 18). However, three samples exhibit a clear LREE enrichment (SG-250, SG-257, BR-83-122), and one of these samples also displays a weak HREE depletion (Figure 18).

Similarly to the Saglek dikes, the undeformed mafic dikes are basaltic in composition (Figure 16A) and they display a tholeiitic fractionation trends (Figure 16B). Their major elements concentrations cover a small range in terms of Mg, Al and Si; with SiO_2 concentrations varying from 51.1 to 47.7 wt% and MgO concentrations varying from 7.7 to 5.2 wt% (Figure 17A-D). CaO concentrations show positive correlations with MgO, where CaO contents decrease as MgO concentrations decrease. Both incompatible immobile elements, such as Zr, and mobile elements such as Sr, increase as MgO concentrations decreases (Figure 17E-G). Typically, the mafic dikes exhibit near-flat REE profiles (Figure 18), however, some samples exhibit light rare earth (LREE) enrichments, with La/Sm ratios generally increasing with decreasing MgO contents or increasing TiO_2 (Figure 17H). Variation in geochemical compositions can also be observed within larger dikes. The fine grained chill margin of the 30 meter wide mafic dike sampled across displays a relatively flat REE profile, whereas the more coarse grained and plagioclase-rich samples, towards the centre of the dike, show slight LREE enrichment with flat HREE profiles.

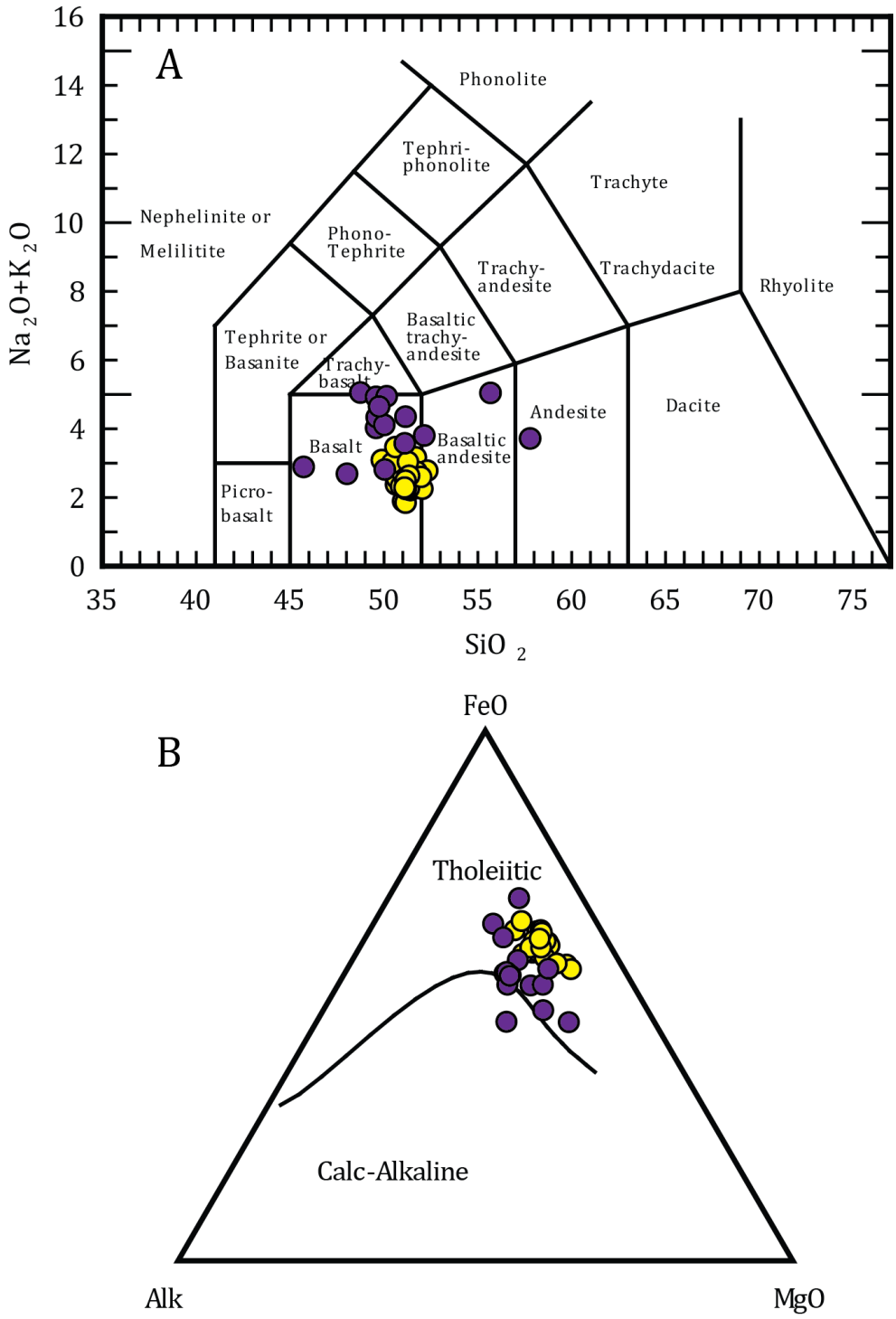

Figure 16 A) Total Alkali Silica (TAS) diagram illustrating the composition of the Saglek dikes (purple) and the undeformed mafic dikes (yellow) in terms of major elements, generally plotting in the basalt field, with the exception of the few samples plotting in the andesitic basalt and the andesite field. B) Alk+ FeO + MgO (AFM) ternary diagram from Irvine & Baragar (1971).

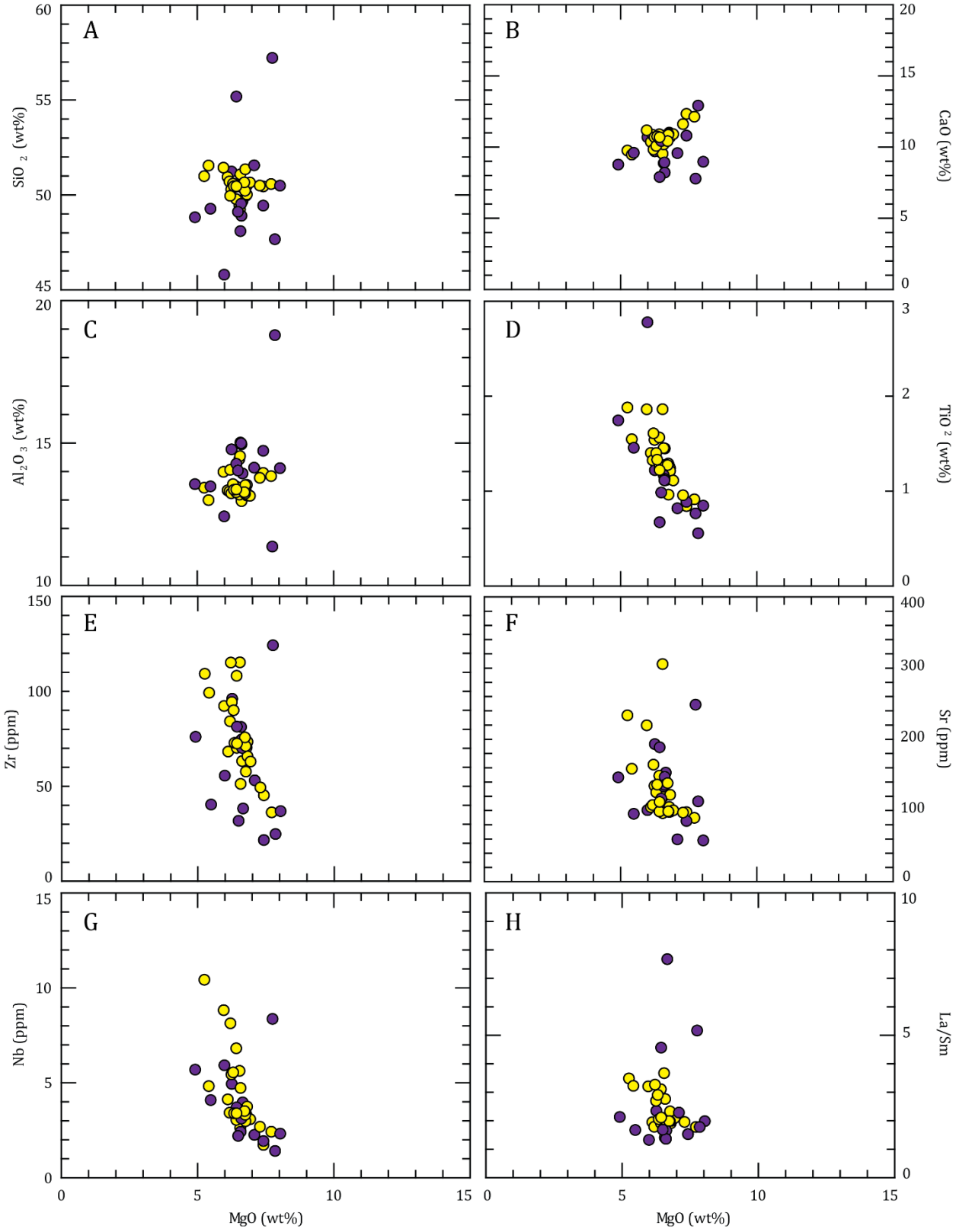

Figure 17 Major and trace element compositions of the Saglek dikes (purple) and undeformed mafic dikes (yellow). A-G) MgO vs selected major and trace elements. H) MgO vs La/Sm ratio.

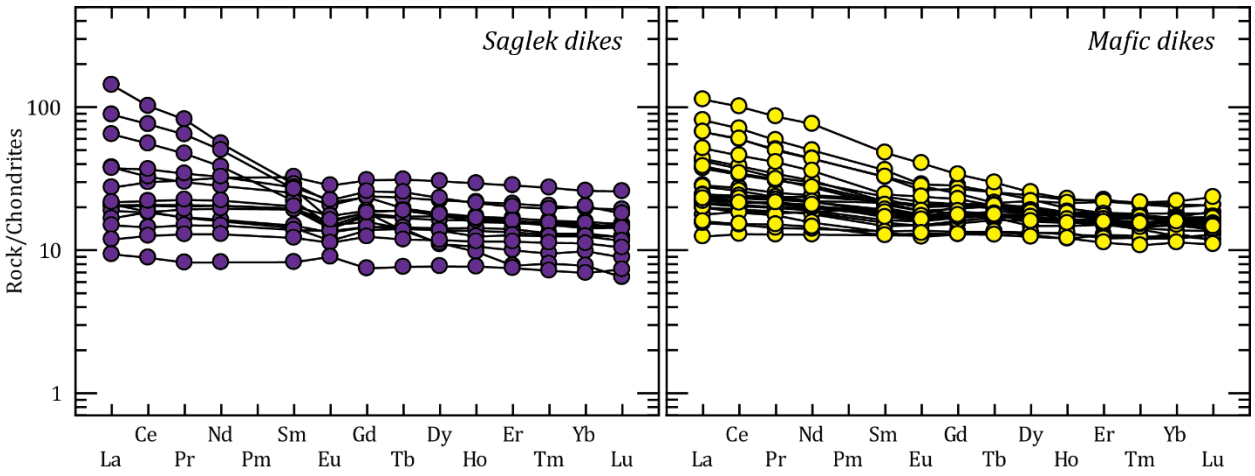

Figure 18 Chondrite-normalised rare earth element profile of the Saglek dikes and the undeformed mafic dikes. Normalizing values of Sun & McDonough (1989).

5.2 ^{147}Sm-^{143}Nd isotope results

5.2.1 Basaltic metavolcanic and ultramafic rocks

The Sm-Nd isotopic data for the ultramafic and mafic metavolcanic rocks is presented in Table 3. For geochronology purposes, samples were chosen to cover a wide range of Sm/Nd ratios. Some ultramafic samples, however, exhibit LREE enrichments with unusually low Sm/Nd ratios for typical ultramafic rocks. These samples were avoided for Sm-Nd isotope studies as the LREE enrichments may have resulted from post-magmatic processes (Wasilewski et al., 2019).

Most analysed mafic samples have yielded a relatively narrow range in $^{147}Sm/^{144}Nd$ ratios from 0.1748 to 0.2089, with three samples displaying lower $^{147}Sm/^{144}Nd$ ratios, as low as 0.1273, and two samples with slightly higher $^{147}Sm/^{144}Nd$ ratios, up to 0.2318. The present-day $^{143}Nd/^{144}Nd$ ratios for all mafic metavolcanic rocks range from 0.511468 to 0.515316. Ultramafic samples exhibit a wider range of $^{147}Sm/^{144}Nd$ ratios, from 0.1413 to 0.2923, with the low-Fe ultramafic samples generally displaying higher Sm/Nd ratios compared to the high-Fe ultramafic samples. The present-day $^{143}Nd/^{144}Nd$ for the ultramafic samples are ranging from 0.511468 to 0.515316.

The ^{147}Sm-^{143}Nd isochron diagram including all mafic metavolcanic and ultramafic samples yields an age of 3288 ± 230 Ma (MSWD=143, n=43), with an $^{143}Nd/^{144}Nd$ initial ratio of 0.508450 ± 0.00005, corresponding to an εNd initial value of +1.6 ± 1 (Figure 19). This isochron diagram exhibits significant scatter, with some low-Fe ultramafic samples lying well off the best-fit line. This 3288 Ma age is younger than both Sm-Nd ages obtained by Morino et al. (2017) of 3732 ± 87 Ma and 3362 ± 100 Ma for the rocks they define as being from the Nulliak unit and the Upernavik unit, respectively (Figure 19). If the rocks analysed here are rather grouped according to the Nulliak-Upernavik distinction, mafic and ultramafic rocks from the Nulliak unit yield an isochron age of 3501 ± 360 Ma (MSWD=118, n=25) whereas the rocks from the Upernavik unit define a best-fit line corresponding to an age of 3021 ± 200 Ma (MSWD=81, n=18).

Sample	Lithology	Unit	Nd (ppm)	Sm (ppm)	$^{147}Sm/^{144}Nd$	$^{143}Nd/^{144}Nd \pm 2\sigma$
SG-065	Andesite	Upernavik	34.99	7.371	0.1273	0.511524 ± 5
SG-011	Metavolcanic	Nulliak	8.596	1.974	0.2047	0.512959 ± 5
SG-021	Metavolcanic	Nulliak	21.41	5.156	0.1455	0.511301 ± 8
SG-029A	Metavolcanic	Nulliak	5.522	1.868	0.2045	0.512884 ± 4
SG-035	Metavolcanic	Nulliak	7.612	2.471	0.1963	0.512744 ± 5
SG-044	Metavolcanic	Nulliak	9.872	3.070	0.1899	0.512552 ± 4
SG-046	Metavolcanic	Nulliak	3.063	1.123	0.2217	0.513118 ± 5
SG-051	Metavolcanic	Nulliak	5.580	2.140	0.2318	0.513357 ± 4
SG-071	Metavolcanic	Upernavik	8.790	2.757	0.1896	0.512558 ± 4
SG-072	Metavolcanic	Upernavik	8.269	2.698	0.1972	0.512720 ± 4
SG-075	Metavolcanic	Upernavik	3.360	1.042	0.1875	0.512581 ± 4
SG-079	Metavolcanic	Upernavik	5.635	1.856	0.1991	0.512766 ± 4
SG-090	Metavolcanic	Nulliak	5.319	1.641	0.1865	0.512531 ± 4
SG-092	Metavolcanic	Nulliak	7.464	2.205	0.1786	0.512305 ± 5
SG-095	Metavolcanic	Nulliak	7.095	2.052	0.1748	0.512229 ± 4
SG-101	Metavolcanic	Nulliak	6.045	1.970	0.1970	0.512689 ± 5
SG-109B	Metavolcanic	Nulliak	5.205	1.798	0.2089	0.512997 ± 5
SG-110	Metavolcanic	Nulliak	2.931	0.9508	0.1961	0.512782 ± 5
SG-112	Metavolcanic	Nulliak	5.523	1.724	0.1887	0.512594 ± 4
SG-123	Metavolcanic	Upernavik	3.117	0.9556	0.1853	0.512542 ± 4
SG-126	Metavolcanic	Upernavik	11.13	2.854	0.1551	0.511904 ± 4
SG-128	Metavolcanic	Upernavik	6.980	2.044	0.1771	0.512253 ± 5
SG-129	Metavolcanic	Upernavik	5.696	1.908	0.2025	0.512822 ± 4
SG-130	Metavolcanic	Upernavik	6.701	2.005	0.1809	0.512308 ± 4
SG-006	Low-Fe UM	Nulliak	0.5838	0.2837	0.2938	0.515311 ± 9
SG-006(D)	Low-Fe UM	Nulliak	0.5608	0.2698	0.2908	0.515321 ± 16
SG-006(AVG)	Low-Fe UM	Nulliak	0.5723	0.2767	0.2923	0.515316 ± 15
SG-009	Low-Fe UM	Nulliak	3.125	0.9152	0.1770	0.512461 ± 5
SG-010	Low-Fe UM	Nulliak	3.100	1.003	0.1956	0.512851 ± 5
SG-013	High-Fe UM	Nulliak	8.392	1.961	0.1413	0.511468 ± 7
SG-015	High-Fe UM	Nulliak	2.110	0.5989	0.1716	0.512132 ± 6
SG-022	Low-Fe UM	Nulliak	0.1052	0.0404	0.2322	0.512860 ± 5
SG-023	High-Fe UM	Nulliak	5.008	1.717	0.2072	0.513005 ± 5
SG-063	High-Fe UM	Upernavik	8.050	2.512	0.1887	0.512553 ± 5
SG-064	Low-Fe UM	Upernavik	0.5364	0.2607	0.2938	0.514625 ± 8
SG-066	Low-Fe UM	Upernavik	0.6418	0.2682	0.2526	0.514089 ± 6
SG-067	High-Fe UM	Upernavik	6.362	2.065	0.1962	0.512680 ± 7
SG-068	High-Fe UM	Upernavik	6.595	2.079	0.1905	0.512581 ± 5
SG-069	High-Fe UM	Upernavik	6.893	2.157	0.1891	0.512536 ± 4
SG-099	High-Fe UM	Nulliak	3.272	0.9528	0.1760	0.512311 ± 9
SG-100	High-Fe UM	Nulliak	6.418	1.864	0.1756	0.512309 ± 6
SG-205	High-Fe UM	Nulliak	3.734	1.150	0.1863	0.512497 ± 4
SG-221	Low-Fe UM	Nulliak	0.3305	0.1441	0.2636	0.514204 ± 13
SG-240	Low-Fe UM	Upernavik	0.9937	0.3047	0.1854	0.512545 ± 14
SG-243	Low-Fe UM	Upernavik	1.067	0.3481	0.1972	0.512750 ± 7

Table 3: Sm-Nd isotopic data of the mafic metavolcanic samples and the ultramafic samples, where UM = ultramafic samples. Samples marked (D) are duplicate samples from a different sample dissolution. Samples marked (AVG) are the average of multiple analysis of the same sample.

Nd and Sm concentrations were determined by isotope dilution.

2 σ errors for $^{143}Nd/^{144}Nd$ are in the last decimal place.

Errors for the $^{147}Sm/^{144}Nd$ ratio are 0.5%

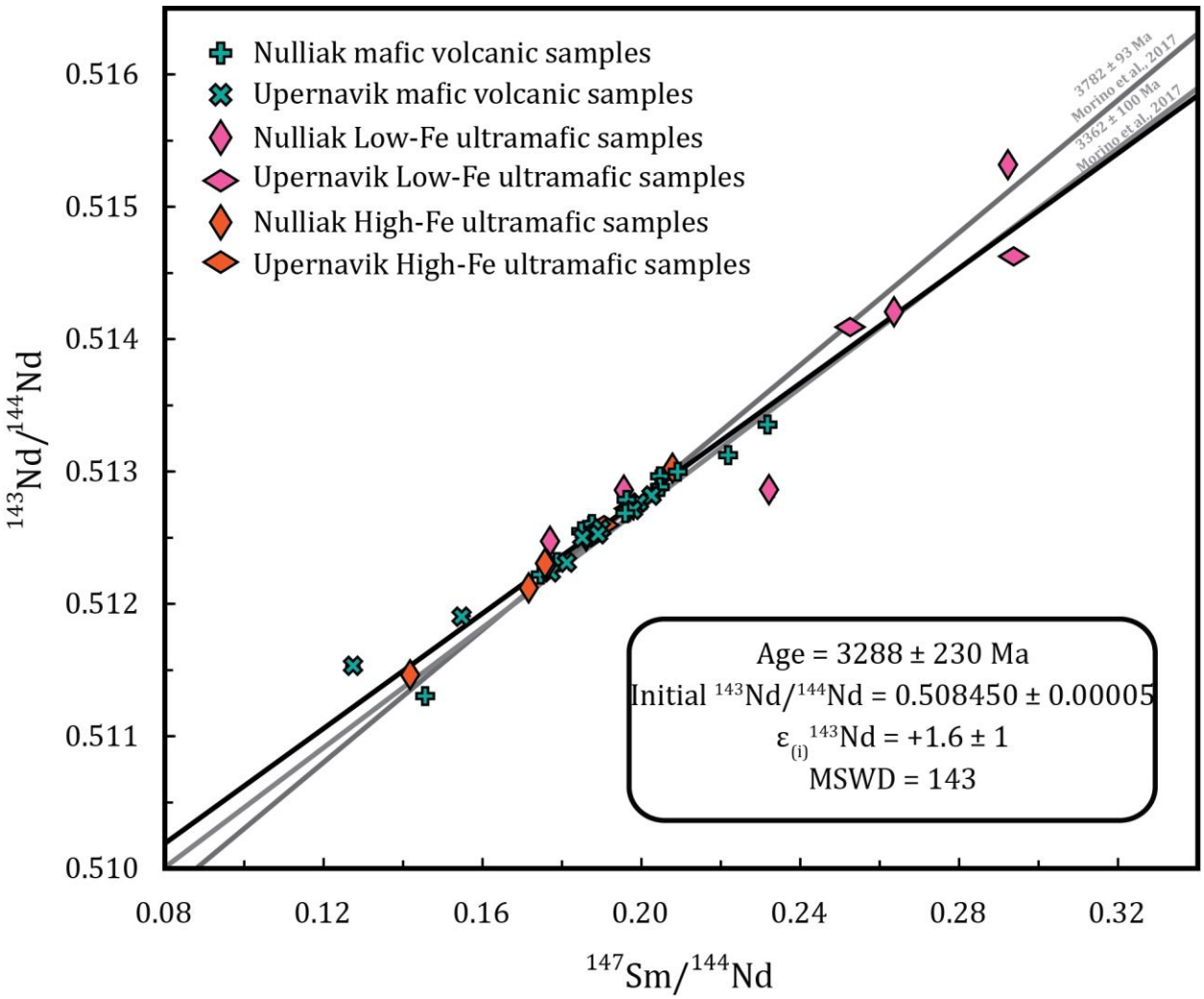

Figure 19 $^{147}Sm/^{144}Nd$ vs $^{143}Nd/^{144}Nd$ isochron diagram of the mafic metavolcanic samples and ultramafic samples. Grey lines correspond to the slopes from the Sm-Nd Eoarchean and Mesoarchean isochron diagrams from Morino et al. (2017). Errors on individual samples are smaller than the symbols.

5.2.2 Saglek dikes and undeformed mafic dikes

The Sm-Nd isotopic data of the Saglek dikes and the undeformed mafic dikes is presented in Table 4. Most Saglek dike samples analysed have yielded $^{147}Sm/^{144}Nd$ ratios ranging from 0.1721 to 0.1998 with three samples having significantly lower $^{147}Sm/^{144}Nd$ between 0.1044 and 0.1206. The present-day $^{143}Nd/^{144}Nd$ ratios for the full set of Saglek dikes range from 0.510666 to 0.512801. A ^{147}Sm-^{143}Nd isochron diagram including all analysed samples yields an age of 3528 ± 100 Ma with a relatively low scatter (MSWD=19, n=14), and an initial $^{143}Nd/^{144}Nd$ initial ratio of 0.508144 ± 0.000022 corresponding to an εNd of +1.7 ± 0.4 (Figure 20).

Sample	Lithology	Nd (ppm)	Sm (ppm)	$^{147}Sm/^{144}Nd$	$^{143}Nd/^{144}Nd \pm 2\sigma$
BR-82-119b	Saglek dike	14.60	4.825	0.1998	0.512801± 3
BR-83-122	Saglek dike	25.20	4.350	0.1043	0.510666 ± 12
BR-83-46b	Saglek dike	12.95	3.794	0.1771	0.512255 ± 5
SG-225	Saglek dike	9.590	2.977	0.1876	0.512526 ± 4
SG-226	Saglek dike	9.746	2.993	0.1857	0.512474 ± 5
SG-231	Saglek dike	7.527	2.242	0.1801	0.512342 ± 5
SG-237	Saglek dike	9.124	2.862	0.1897	0.512554 ± 6
SG-250	Saglek dike	19.38	3.865	0.1206	0.510895 ± 5
SG-251	Saglek dike	16.45	4.685	0.1722	0.512162 ± 6
SG-253	Saglek dike	11.12	3.437	0.1868	0.512513 ± 4
SG-256	Saglek dike	7.297	2.356	0.1952	0.512708 ± 4
SG-257	Saglek dike	24.45	4.688	0.1159	0.510805 ± 4
SG-263	Saglek dike	6.483	2.104	0.1962	0.512713 ± 5
SG-289	Saglek dike	3.966	1.247	0.1901	0.512634 ± 6
SG-001	Mafic dike	22.85	5.331	0.1411	0.511916 ± 6
SG-036	Mafic dike	6.185	1.955	0.1911	0.512610 ± 5
SG-040	Mafic dike	6.365	2.008	0.1907	0.512612 ± 2
SG-050	Mafic dike	11.01	3.296	0.1809	0.512474 ± 2
SG-052	Mafic dike	19.80	6.885	0.1452	0.511682 ± 4
SG-058	Mafic dike	10.75	2.835	0.1810	0.512460 ± 3
SG-059	Mafic dike	33.29	3.464	0.1250	0.511284 ± 4
SG-094	Mafic dike	10.59	3.208	0.1832	0.512498 ± 2
SG-098	Mafic dike	19.81	4.714	0.1439	0.511998 ± 2
SG-118	Mafic dike	9.679	2.889	0.1804	0.512431 ± 5
SG-120	Mafic dike	8.534	2.008	0.2008	0.512765 ± 7
SG-121	Mafic dike	13.69	3.296	0.1530	0.512000 ± 5
SG-211	Mafic dike	9.616	2.890	0.1817	0.512479 ± 4
SG-212	Mafic dike	13.87	3.764	0.1641	0.512121 ± 5
SG-213	Mafic dike	15.36	3.868	0.1522	0.511936 ± 5
SG-214	Mafic dike	17.71	4.293	0.1466	0.511836 ± 4
SG-215	Mafic dike	13.75	3.573	0.1571	0.512013 ± 5
SG-217	Mafic dike	9.672	2.963	0.1852	0.512522 ± 4
SG-218	Mafic dike	8.841	2.716	0.1857	0.512532 ± 4
SG-219	Mafic dike	8.712	2.670	0.1853	0.512527 ± 5
SG-220	Mafic dike	9.539	2.918	0.1849	0.512524 ± 5
SG-222	Mafic dike	7.911	2.336	0.1785	0.512387 ± 5
SG-249	Mafic dike	10.09	3.041	0.1823	0.512486 ± 6
SG-262	Mafic dike	10.44	3.128	0.1811	0.512461 ± 5
SG-268	Mafic dike	10.07	3.035	0.1822	0.512478 ± 9
SG-269	Mafic dike	7.117	2.167	0.1840	0.512504 ± 5

Table 4: Sm-Nd isotopic data of the Saglek dikes and undeformed mafic dikes samples.
Nd and Sm concentrations were determined by isotope dilution.
2 σ errors for $^{143}Nd/^{144}Nd$ are in the last decimal place
Errors for the $^{147}Sm/^{144}Nd$ ratio are 0.5%

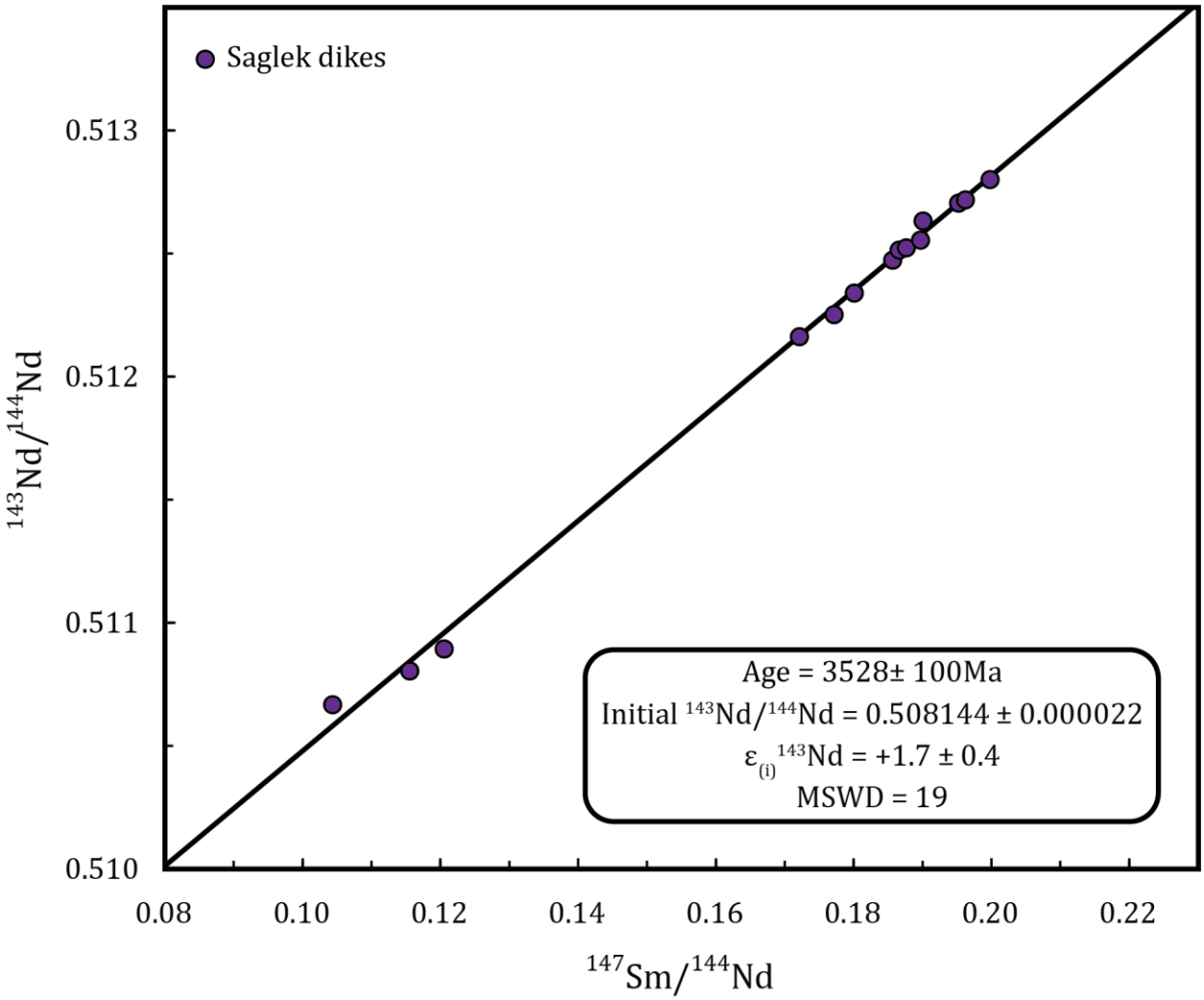

Figure 20 $^{147}Sm/^{144}Nd$ vs $^{143}Nd/^{144}Nd$ isochron diagram of the Saglek dike samples. Errors on individual samples are smaller than the symbols.

The undeformed mafic dike samples display a wider range of $^{147}Sm/^{144}Nd$ ratios, from 0.1249 to 0.2008, and present-day $^{143}Nd/^{144}Nd$ ratios ranging from 0.511284 to 0.512765. The mafic dikes cluster into two groups with different Sm/Nd ratios. The group with Sm/Nd ratios closer to chondritic values appears to yield more homogeneous isotopic composition compared to the samples with subchondritic Sm/Nd. A ^{147}Sm-^{143}Nd isochron diagram including all samples yield an age of 2677 ± 230 Ma (MSWD=117, n=26), with a $^{143}Nd/^{144}Nd$ initial ratio of 0.509255 ± 0.000029 corresponding to an εNd value of +1.7 ± 0.6 (Figure 21). The mafic dikes with lower Sm/Nd ratios display significant scatter with a number of samples lying well off the best-fit line.

An isochron including only the 5 samples collected across the same 30m mafic dike (SG-211 to SG-215) yields an age of 2771 ± 290 Ma (MSWD = 4.5; n=5), similar to the isochron age including all undeformed mafic dikes samples.

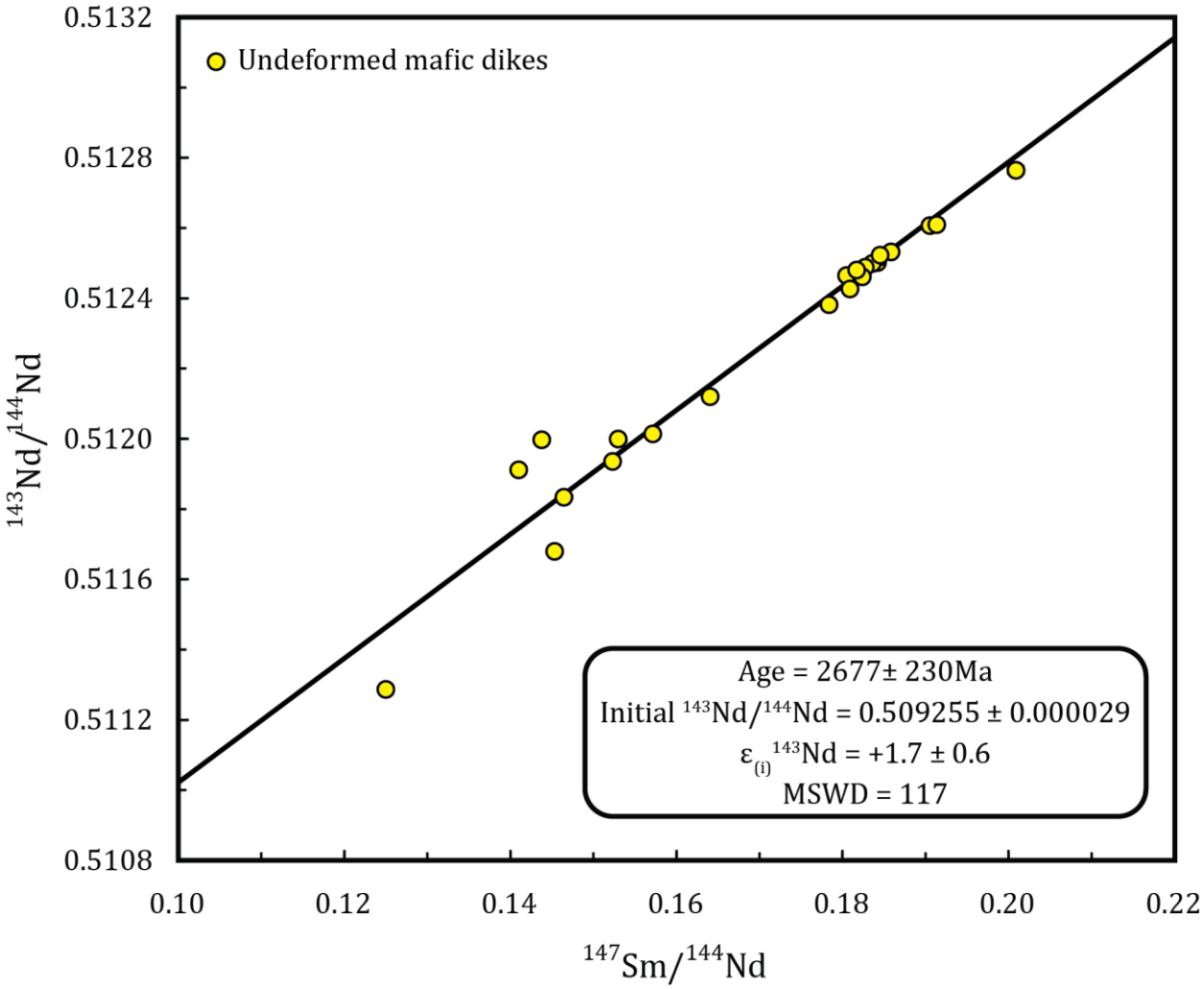

Figure 21 $^{147}Sm/^{144}Nd$ vs $^{143}Nd/^{144}Nd$ isochron diagram of the undeformed mafic dike samples. Errors on individual samples are smaller than the symbols.

6. Discussion

6.1 Assessment of igneous primary character of the SHC mantle-derived rocks composition

The SHC has been subjected to a protracted thermal history including multiple felsic magmatic and crustal reworking events from ~3.9 Ga to ~2.7 Ga (e.g. Komiya et al. 2017) as well as high-grade metamorphic events (Schiøtte et al., 1986, 1989; Kusiak et al. 2018). It is therefore important

to evaluate the degree to which the whole-rock chemistry of the mantle-derived samples studied here has been affected as they might have been modified by post-magmatic events. Assessing the primary character of the REE is crucial in order to interpret the Sm-Nd isotopic compositions of these rocks and establish if the measured Sm/Nd ratios are pristine or the result of post-magmatic processes.

6.1.1 Element mobility

Most immobile trace elements such as Ti, Zr, Nb, Y, Ta, V, Hf and REE define well-correlated trends for the mafic and ultramafic rocks, suggesting limited post-magmatic remobilization of these elements (Wasilewski et al., 2019). The mafic metavolcanic samples studied here generally display flat REE profiles with only a few samples exhibiting LREE enrichments. Some mafic metavolcanic samples with higher La/Sm, however, also display relatively high K_2O contents (Figure 22), suggesting LREE enrichments might be associated with post-magmatic potassic fluids. Some of the ultramafic samples, especially the low-Fe ultramafic samples, display variable LREE depletions and enrichments, and some display unusual LREE enrichments with La/Sm ratios slightly correlated with mobile elements, suggesting that LREE enrichment is in fact the result of post-magmatic processes (Wasilewski et al., 2019). Ultramafic samples displaying such characteristics were avoided for Sm-Nd isotopic work here. Nevertheless, the isotopic compositions of the ultramafic samples should be considered with caution, especially for samples with enriched LREE concentrations, which are unusual for olivine-pyroxene cumulate rocks.

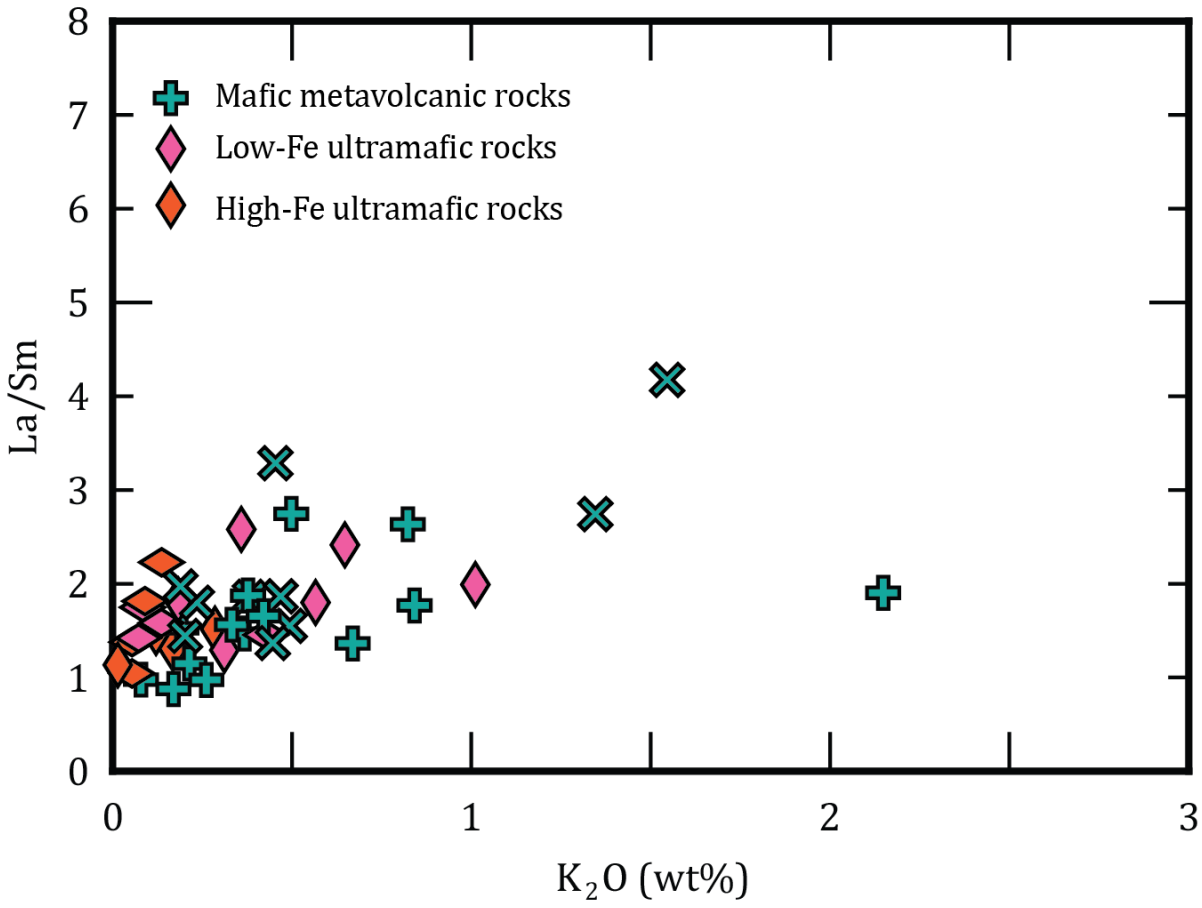

Figure 22 La/Sm vs K_2O plot for mafic metavolcanic rocks and ultramafic rocks included in this study. Data from Wasilewski et al. (2019).

The Saglek dikes have been subjected to the regional metamorphism as supported by their amphibolite facies mineralogical assemblages. Therefore, post-magmatic processes could also have affected their whole-rock geochemical composition. The immobile incompatible trace element concentrations (Ti, Zr, Nb, Th, Hf) of the Saglek dikes are scattered but display correlations consistent with igneous differentiation (Figure 23A&B). Mobile incompatible elements (Rb, Sr, K, Ba), however, do not display clear correlations with fractionation proxies such as Zr, TiO_2 or Mg# (Figure 23C&D), suggesting some remobilisation of the large ion lithophile elements by post-magmatic processes. Most Saglek dikes exhibit relatively flat REE profiles with the exception of three samples that exhibit higher La/Sm (Figure 18). Figure 23E

shows a general increase of the La/Sm ratio with increasing Zr for the majority of the Saglek dikes, suggesting that the REE enrichment may be the result of igneous differentiation for most Saglek dikes. Samples SG-250, SG-257 and BR-83-122 however have marked higher La/Sm ratios, which are not correlated with immobile incompatible elements such as Zr (Figure 23E), suggesting possible post-magmatic LREE enrichments. These three samples also display slight HREE depletions with Gd/Yb higher than the other Saglek dikes. Due to the lack of clear correlations between La/Sm ratios and mobile elements such as K (Figure 23F), the LREE enrichment may not be the result of element remobilisation through metasomatic fluids.

Given the igneous mineralogical compositions and preserved igneous ophitic texture of the undeformed mafic dikes, they likely have not been affected by regional metamorphism and metasomatism to the same extent as the Saglek dikes. These dikes display strong correlations between the immobile trace elements (Zr, Ti, Nb, Th), consistent with their concentrations controlled by igneous processes such as differentiation. Correlations between mobile and immobile incompatible trace elements, such as Ba and K vs. Zr are not as well defined but concentrations generally increase with differentiation, suggesting limited remobilisation of the more mobile elements (Figure 23). The undeformed mafic dikes exhibit flat to LREE enriched profiles (Figure 18), with La/Sm ratios generally well correlated with differentiation indices such as Zr or Ti (Figure 23E) suggesting that the LREE enrichment of some dikes may be a primary igneous feature rather than the result of post-magmatic remobilisation.

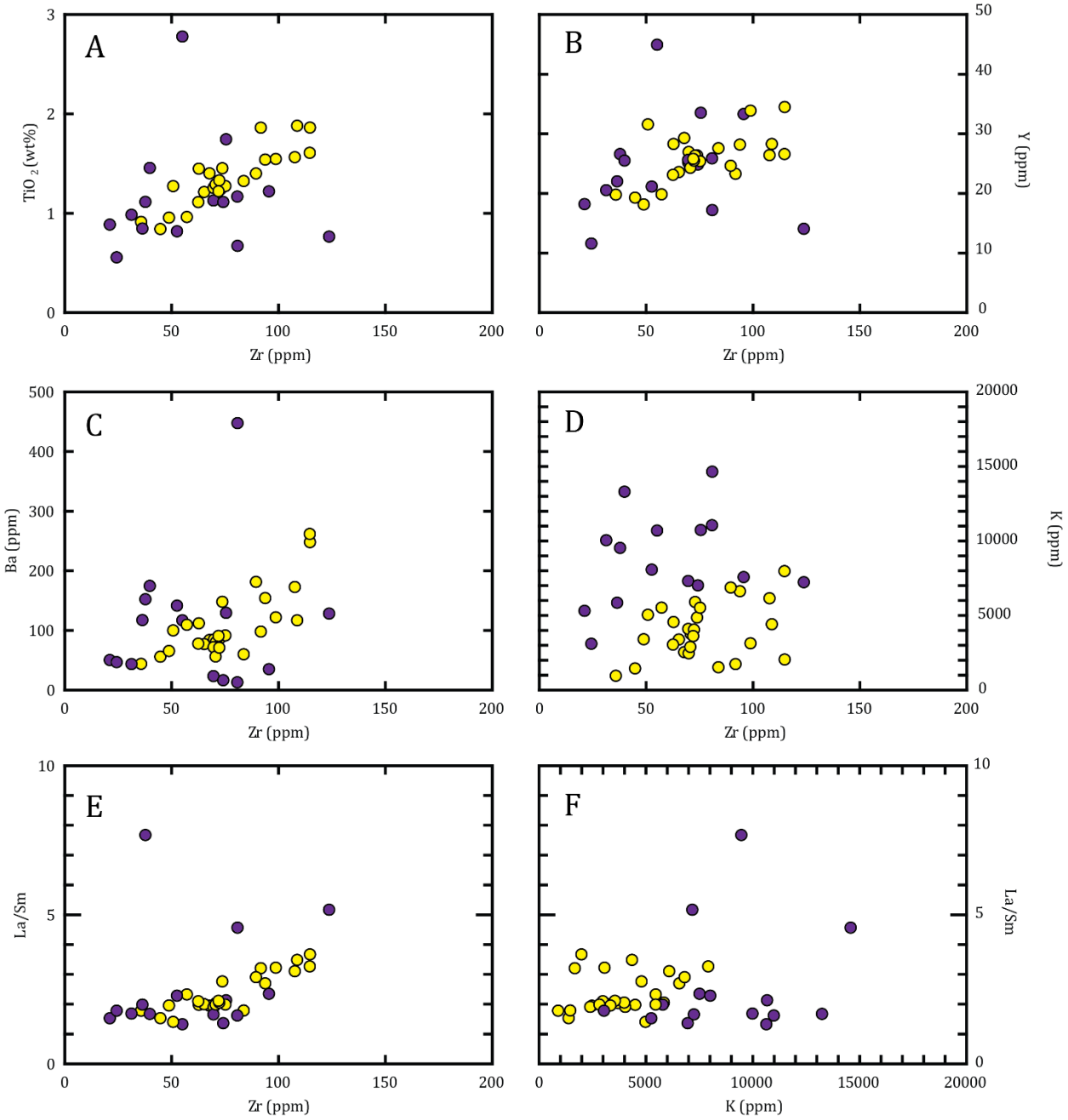

Figure 23 Geochemical diagrams of the Saglek dikes (purple) and the undeformed mafic dikes (yellow) A-E) Selected major and trace elements composition vs Zr F) La/Sm ratios vs K

6.1.2 Igneous differentiation

As discussed previously, most mantle-derived rocks analysed here display limited mobility of the REE, suggesting that the variation in La/Sm may be due to igneous differentiation. Wasilewski et al. (2019) have suggested that both the Nulliak and the Upernavik mafic suites are consistent with

tholeiitic flows that differentiated into two groups, high-Ti samples and low-Ti samples, by fractional crystallisation. The high-Ti samples are consistent with residual liquids whereas the low-Ti samples represent pyroxene-rich cumulate-liquid mixtures.

As for the ultramafic rocks, the distinct compositions of the high-Fe ultramafic and low-Fe ultramafic rocks suggest two distinct parental magmas from which these suite may have originated. Wasilewski et al. (2019) suggest that these suites were cumulates formed from a parental magma that was komatiitic basalt in composition (Figure 24). They also suggested that the fractionation of the low-Fe ultramafic cumulates may have produced a mafic magma that would have a comparable composition as the parental magma that differentiated into the low and high-Ti mafic metavolcanic rocks, thus implying a petrogenetic link between the mafic metavolcanic rocks and the low-Fe ultramafic rocks (Figure 24).

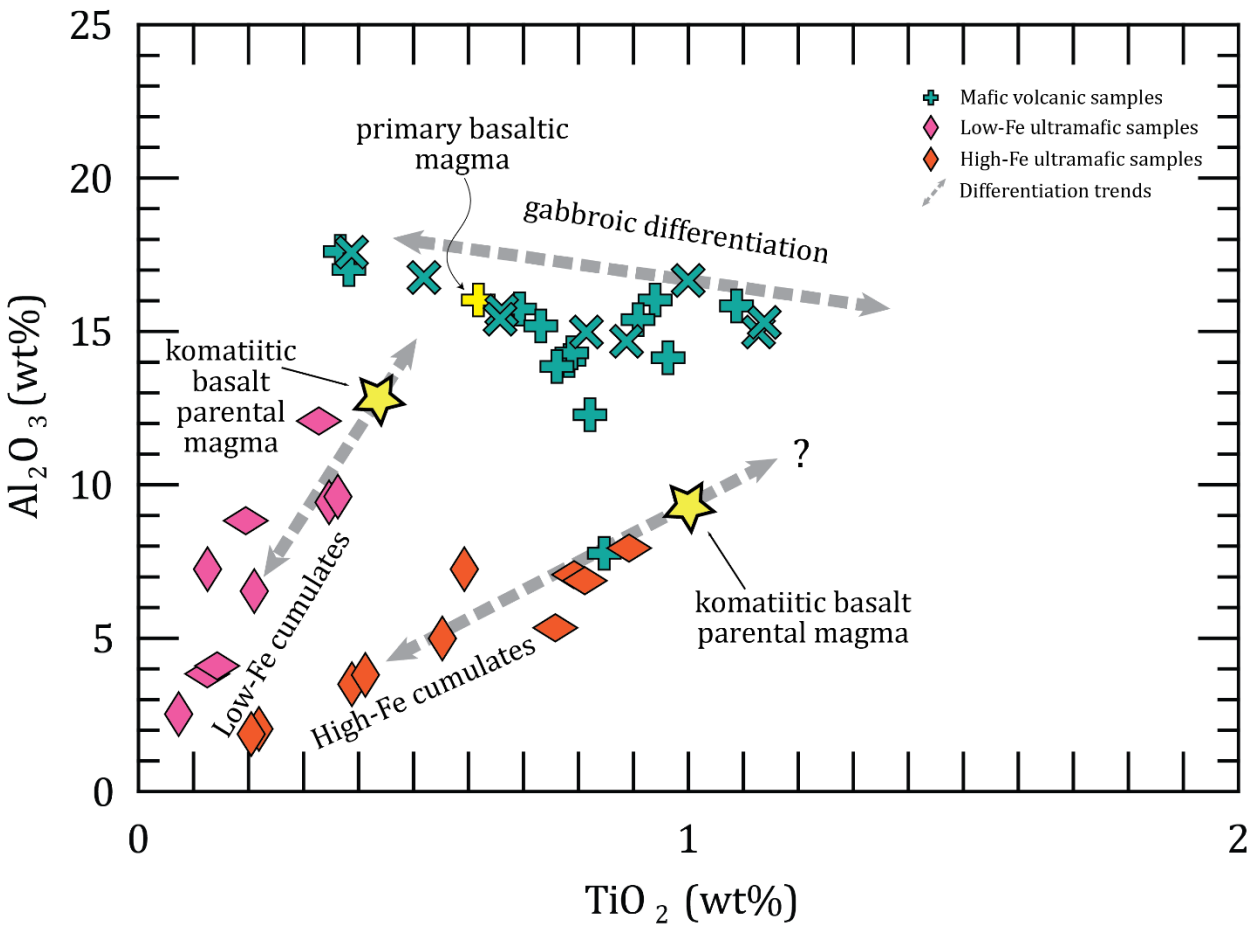

Figure 24 Al_2O_3 vs TiO_2 diagram of the mafic metavolcanic rocks and ultramafic rock, illustrating the two distinct ultramafic suites with their respective calculated parental magmas (yellow stars). As well as the differentiation that formed the mafic metavolcanic rocks. Modified from Wasilewski et al. (2019).

Although the trace element compositions of the Saglek dikes seem to have been relatively unaffected by secondary fluid mobilisation, a few samples exhibit strong LREE enrichment. Since the La/Sm ratios for the most LREE-enriched samples are not correlated with high concentrations of other incompatible trace elements such as Zr or Ti, it is important to carefully examine the cause of the LREE enrichment in order to assess if it is the result of primary igneous processes.

Most Saglek dikes display flat REE profiles with slight negative Eu anomalies, and only one sample displaying a positive Eu anomaly. Complementary Eu anomalies suggest that the REE compositions of the Saglek dikes are controlled by fractional crystallization. Using sample SG-263 as starting composition, the range of REE concentrations observed in most Saglek dikes could

be explained by a minimum of 60% fractional crystallisation of 50% plagioclase + 20% orthopyroxene + 30% clinopyroxene from a gabbroic magma (Figure 25A). Even with the high degree of fractional crystallisation required by this model, it fails to reproduce the LREE enrichment observed in the three samples with high La/Sm ratios (BR-83-122, SG-250 and SG-257). The Saglek dikes were often sampled where they intrude TTG and are thus susceptible to contamination by the felsic host rock. Figure 25B compares the REE compositions of the LREE-enriched Saglek dikes with the SHC granitoids. The Paleo to Eoarchean TTG present during the emplacement of the Saglek dikes are dominated by typical TTG and high-Mg tonalites (Wasilewski et al., in prep). Because most TTGs have LREE concentrations similar the LREE-enriched Saglek dikes, it would require close to 100% of contamination by the TTG to reproduce the La/Sm of the LREE-enriched Saglek dikes. Despite the fact that two of these samples are andesitic in composition, this degree of contamination by felsic TTG is inconsistent with their overall geochemical composition. The high-Mg tonalities, however, generally have higher LREE concentrations compared to the TTG and could be a more suitable contaminant to explain the LREE enrichment of the three Saglek dikes. Figure 25B shows that ~25% binary mixing with high-Mg tonalites can well reproduce the REE profiles of the LREE-enriched Saglek dikes. We therefore suggest that the LREE compositions of these dikes are the result of crustal contamination from high-Mg tonalites. This hypothesis is further supported by their initial Nd isotopic compositions. Figure 26 shows the initial εNd values of the Saglek dikes, calculated at 3528 Ma (the age obtained from the isochron, Figure 20). The initial εNd values are homogeneous except for the three LREE-enriched samples as well as sample SG-289, displaying higher and lower initial εNd values at 3528 Ma (Figure 26). In fact, these dikes display initial εNd values that are close to the εNd values calculated for surrounding high-Mg tonalites and TTGs (Figure 26). The initial

εNd values at 3528 Ma of the LREE-enriched dikes SG-250 and SG-257 would be consistent with contamination with surrounding high-Mg tonalites (Figure 26). The model shown on figure 26 would suggest ~30-40% mixing to reproduce the lower εNd values of dike samples SG-250 and SG-257. This is somewhat higher than what is suggested by the REE mixing model of figure 25B, but the slight difference is expected given the range of REE concentrations on the tonalitic samples. It is thus difficult to constrain the exact extent of contamination of the dikes, nonetheless, it shows that the initial isotopic compositions of these four Saglek dike samples have been affected and modified by contamination from the host rock and are not suitable for isochron dating.

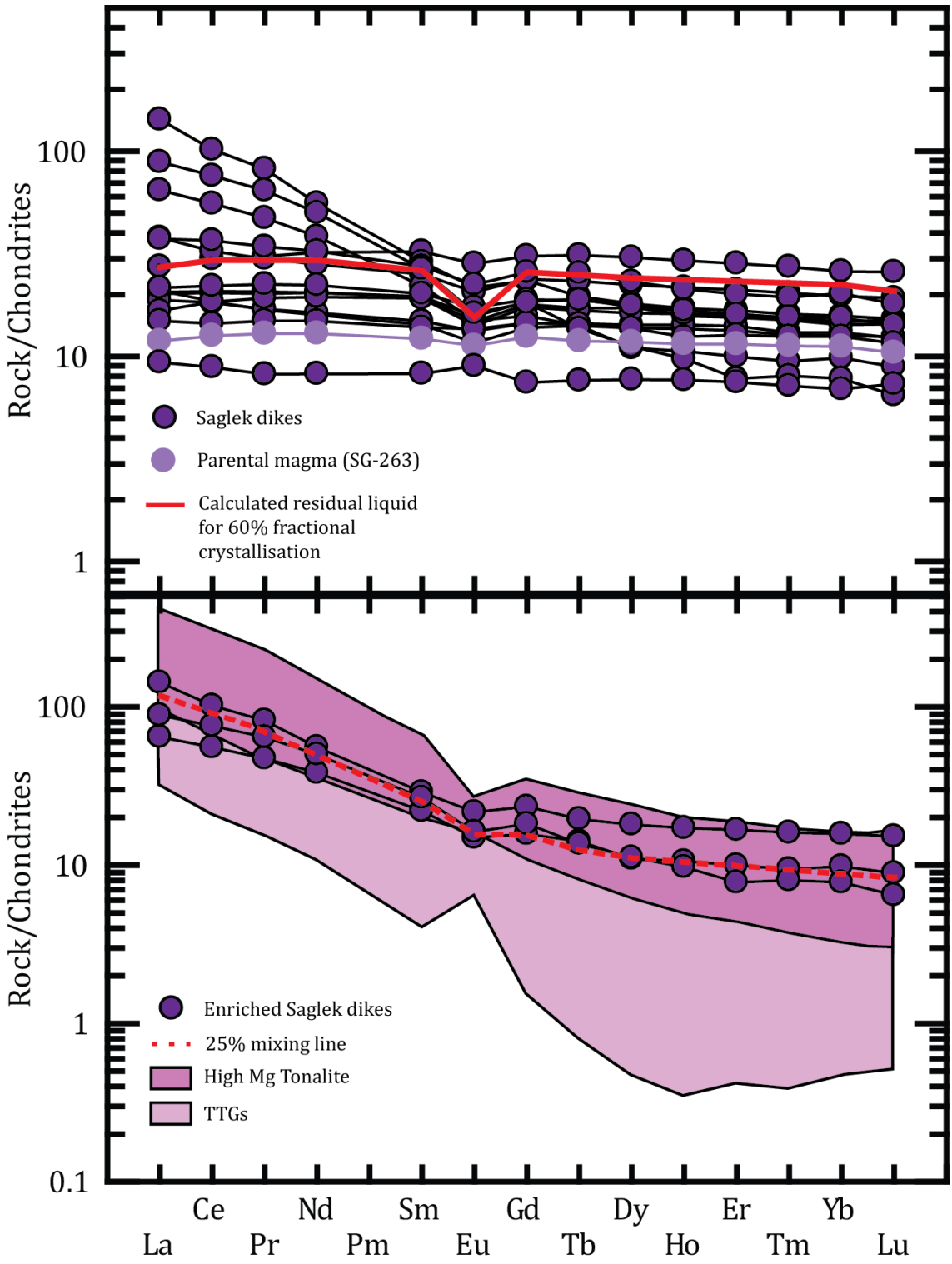

Figure 25 A) Fractional crystallisation model of the Saglek dikes from their REE compositions. This model uses SG-263 as the parental magma, the red line represents 60% residual liquid from a gabbroic assemblage 50% plagioclase + 20% orthopyroxene + 30% clinopyroxene. B) Saglek dikes enriched in LREE (SG-250, SG-257 and BR-83-122) with the range of REE concentrations of some surrounding TTGs and high-Mg tonalites. Includes a 25% mixing line between SG-263 (parental magma) and a high-Mg tonalite. Normalisation values from Sun & McDonough (1989) and partition coefficients from Winter (2001) and the GERM database (https://earthref.org/GERM/). High-Mg tonalite and TTG data from Wasilewski et al., (in prep).

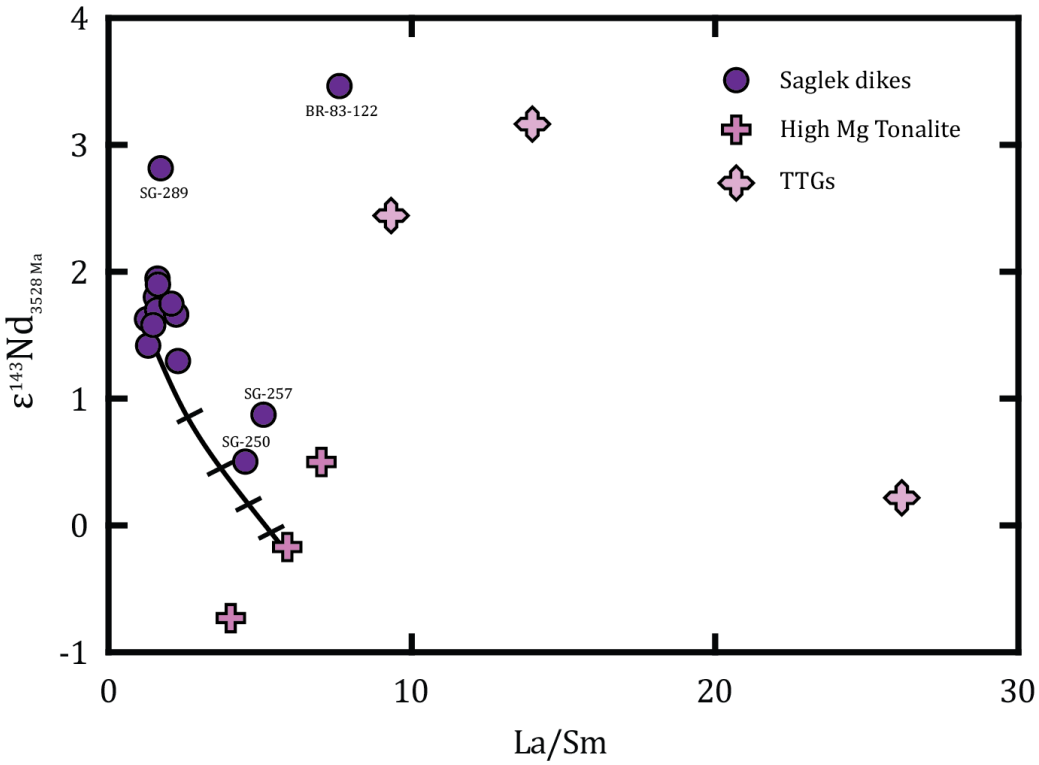

Figure 26 εNd values calculated at 3528 Ma vs. La/Sm ratios of the Saglek dikes and some of the surrounding TTGs and high-Mg tonalites. The black line represents a mixing line between samples SG-263 and SG-210c, with 20% increments. Data for the high-Mg tonalites and TTGs from Wasilewski et al., (in prep).

Most undeformed mafic dikes display flat REE profiles with a number of samples displaying a LREE enrichment along with a small HREE depletion. The range of concentrations observed in most mafic dikes can be in part explained by fractional crystallisation. Figure 27A shows that differentiation of 45% clinopyroxene + 30% orthopyroxene + 25% plagioclase from a gabbroic primary magma (SG-036) can reproduce the REE concentrations of most undeformed mafic dikes. This model can account for the increase on REE concentration, but does not lead to an increase in the La/Sm ratios, as observed in the LREE-enriched dikes. The model, however, uses the mafic dike samples with the lowest REE concentrations with flat LREE profiles. Sample SG-211, which is the chilled margin of the 30 meter mafic dike sampled across, however, shows a slight LREE-enrichment. Using this sample as the starting primary composition, Figure 27B shows that fractional crystallization of a similar assemblage, within larger dikes, can well reproduce the LREE

enrichment observed in the samples collected in the coarser grain dike interior. Samples displaying the highest LREE enrichments (SG-001, SG-052, SG-059, SG-098 and SG-121) are, however, difficult to explain by fractional crystallization models, as it would require more than 50% crystallisation to satisfy those higher La/Sm ratios and REE concentrations. We therefore suggest that the LREE enrichment of these samples may not be the result of igneous primary processes. Similarly to the enriched Saglek dikes samples, by comparing the enriched mafic dikes compositions to the composition of the surrounding TTGs, we observe that they have comparable trends with a LREE enrichment along with a HREE depletion (Figure 27C). Figure 27C shows that ~20% mixing of the high-Mg tonalites with the chill margin (sample SG-211) can produce LREE enrichment similar to what is observed in the most enriched mafic dikes. The LREE enrichment of these dikes can also be well reproduced by AFC models (Figure 27C). Despite the exact processes that lead to the LREE composition of these enriched dikes, their high La/Sm ratios are consistent with contamination with surrounding granitoids. In addition, these enriched dikes exhibit variable initial εNd values compared to the majority of the mafic dikes for which REE compositions can be modeled by primary igneous processes and display homogeneous initial εNd (Figure 28). In fact, some of these enriched dikes yield initial εNd values that are close to the initial values calculated from the surrounding TTGs and high-Mg tonalites (Figure 28). Figure 28 also shows a mixing line between the dike sample SG-036 and TTG sample SG-080, which suggests that the initial Nd isotopic composition of the enriched mafic dikes with lower εNd values has likely been modified due to contamination from the surrounding host rocks. These samples should therefore be avoided for isochron dating. Although contamination with TTG cannot account for the higher εNd values of the dike samples SG-001 and SG-098, their distinct Nd isotopic composition also suggests disturbance of the Sm-Nd system.

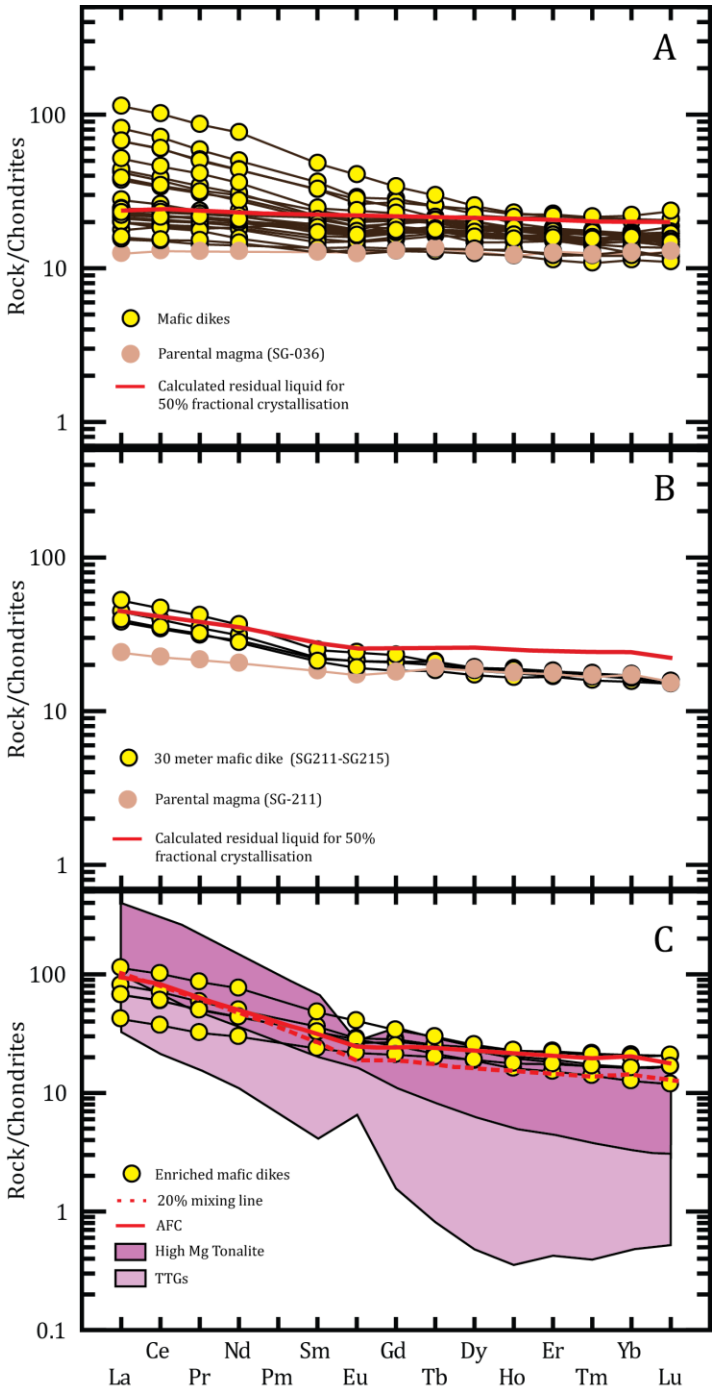

Figure 27 A) Fractional crystallisation model of the undeformed mafic dikes from their REE composition. This model uses SG-036 as parental magma, the red line represents 50% residual liquid from a gabbroic assemblage 25% plagioclase + 30% orthopyroxene + 45% clinopyroxene. B) Fractional crystallisation model of the 30 meter mafic dike using SG-211 (chill margin) as parental magma, the red line represents 50% of residual liquid from a gabbroic assemblage 25% plagioclase + 30 % orthopyroxene + 45% clinopyroxene. C) Mafic dikes exhibiting a LREE enrichment (SG-001, SG-052, SG-059, SG-098, SG-121) including the range of REE concentrations from the surrounding TTGs. The dotted line represent 20% mixing with the surrounding TTG. The solid red line shows an AFC model for 25% of crystallisation of the same mineralogical assemblage used for these previous models, with an R value of 0.4, and a surrounding TTG as a contaminant. Normalisation values from Sun & McDonough (1989) and partition coefficient from Winter (2001) and the GERM database (https://earthref.org/GERM/). High-Mg tonalite and TTGs data from Wasilewski et al., (in prep).

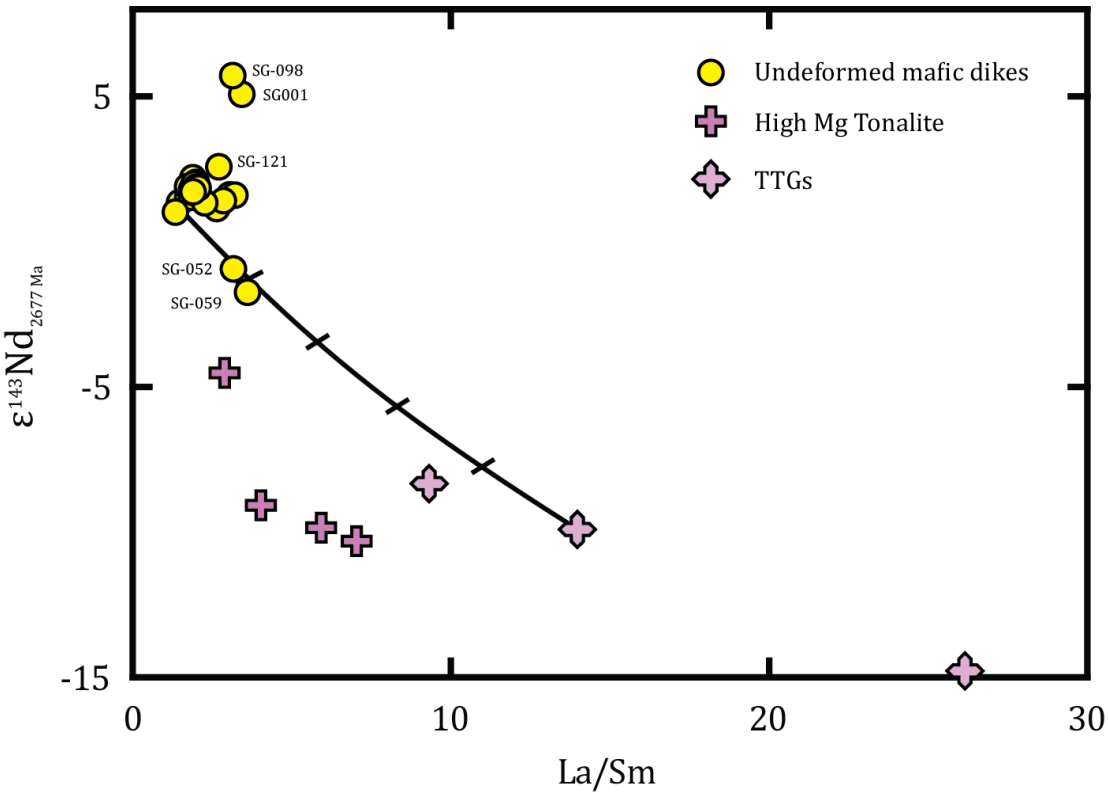

Figure 28 εNd values calculated at 2677 Ma vs La/Sm for the undeformed mafic dikes and some of the surrounding TTGs and high-Mg tonalites. The black line represents a mixing line between sample SG-036 and SG-080, with 20% increments. Isotopic data for the high-Mg tonalite and TTGs from Wasilewski et al, in prep.

6.2 Chronology of the SHC mafic magmatism

Precisely dating mafic and ultramafic rocks can be challenging because they usually do not contain minerals such as zircon, which can provide precise and robust ages. Samarium-Nd isochrons can be useful to constrain the age of mafic and ultramafic rocks, but post-magmatic processes can lead to REE mobilisation and therefore affect this long-lived system. This is particularly true for Archean terrains, such as the Saglek-Hebron Gneiss Complex, which has been subjected to a protracted thermal history and reached upper amphibolite to granulite metamorphic conditions. Therefore, for a Sm-Nd isochron to hold any geochronological significance, it is crucial to ensure that the isotopic system has remained closed since the emplacement of the considered samples. Additionally, samples used to build Sm-Nd isochrons must be co-genetic and share the same initial isotopic composition. Morino et al. (2017) have obtained Sm-Nd isochron ages of 3782 ± 93 Ma

and 3362 ± 100 Ma on SHC ultramafic rocks with a few mafic metavolcanic samples. However, some of the ultramafic samples they studied display unusual LREE enrichments, similar to the ultramafic samples studied by Wasilewski et al. (2019) they interpreted as the result of post-magmatic remobilisation of LREE. The Sm-Nd ages obtained by Morino et al. (2017) contrast with Re-Os isochron ages of 3096 ± 170 Ma and 3612 ± 130 Ma on the SHC ultramafic rocks (Ishikawa et al., 2017). Here, in order to better constrain the age of the SHC metavolcanic rocks, we closely examine the Sm-Nd isotopic composition of a new extensive set of samples, focussing on the mafic metavolcanic rocks with ultramafic samples having REE concentrations consistent with primary compositions. Samarium-Nd isotopic compositions of the Saglek dikes and undeformed mafic dikes are also used to provide new age constraints on the SHC mafic magmatism.

6.2.1 Age of the SHC metavolcanic and ultramafic rocks

The Sm-Nd isochron presented on Figure 19 includes all mafic metavolcanic and ultramafic samples analysed for this study. It is apparent from the highly scattered data (MSWD = 143) that the age of 3288 ± 230 Ma given by the best-fit line is unlikely to provide accurate geochronological information on these rocks. This suggest that the Sm-Nd system has been disturbed for a number of samples and/or that the samples are not all co-genetic and should not be considered all together on the same isochron.

Figure 19 shows that the lithology displaying the most scatter in Sm-Nd ratios is the low-Fe ultramafic rocks, whereas the high-Fe ultramafic rocks and the mafic metavolcanic rocks, when considered separately, define better regressions in a $^{147}Sm/^{144}Nd$ vs $^{143}Nd/^{144}Nd$ space. Most mafic metavolcanic samples plot on relatively good regression lines in the isochron diagram, except for the most LREE-enriched ($^{147}Sm/^{144}Nd < 0.16$) samples, which have Nd isotopic compositions

falling off the general trend defined by the other mafic samples, suggesting isotopic disturbance for these LREE-enriched samples. An isochron diagram for all the mafic metavolcanic samples, excluding samples SG-021, SG-065 and SG-126, which plot off the best fit-line, yields an age of 3028 ± 270 Ma (n= 21, MSWD = 27), with an initial $^{143}Nd/^{144}Nd$ ratio of 0.508776 ± 0.000025 corresponding to an initial εNd value of +1.3 ± 0.5 (Figure 29). Most SHC mafic metavolcanic rocks display relatively flat REE profiles, therefore the large errors on the isochron age for the metavolcanic samples is partly due to their relatively limited variation in Sm/Nd. Nonetheless, this age is younger than both Sm-Nd ages reported by Morino et al. (2017), although it overlaps within error with the 3362 ± 100 Ma age they obtained for the rocks they interpreted as belonging the Upernavik unit. Figure 29 shows that the slope of the best-fit line is partly controlled by the two samples with higher Sm/Nd ratios (>0.22). The slope of the isochron becomes steeper when these two samples are not considered, yielding an older age of 3443 ± 310 Ma, closer to the age of the Upernavik unit obtained by Morino et al. (2017) but still younger than the 3782 ± 93 Ma Eoarchean age they proposed for the Nulliak rocks. The younger ages obtained for the mafic metavolcanic rocks are also in disagreement with the interpretation of Shimojo et al. (2016) suggesting that the Nulliak metavolcanic rocks are >3.92 Ga, based on U-Pb ages of the Iqualuk Gneiss they interpreted as intruding the Nulliak supracrustal rocks. However, this age agrees with Whitehouse et al. (2019), who argue that there is a lack of field and geochronological evidence supporting an age of >3.92Ga for the metavolcanic rocks that form the Nulliak suite. This either suggests that the mafic metavolcanic rocks that form the supracrustal rocks are not as old as they were thought to be, or that their Sm-Nd isotopic system has not remained closed since the emplacement of the rocks.

Figure 29 also shows that the mafic metavolcanic rocks from the Nulliak and Upernavik assemblage display similar Sm-Nd isotopic compositions. If the least disturbed Nulliak and Upernavik mafic metavolcanic samples are considered individually, they yield similar ages of 3457 ± 380 Ma and 3351 ± 780 Ma, respectively. The age for the Nulliak rocks contrasts with the results of Morino et al. (2017) where they obtained a ^{147}Sm-^{143}Nd isochron age of 3782 ± 93 Ma, whereas the age we obtained for the Upernavik only is comparable to the age of 3362 ± 100 Ma from Morino et al. (2017), although our isochron, with only the mafic Upernavik rocks, displays a significant error. The Sm-Nd isochrons from Morino et al. (2017) however mostly include ultramafic rocks, which can be difficult to ascribe to Nulliak or Upernavik supracrustal units. A number of ultramafic samples also display unusual LREE-enriched compositions. The extended isotopic dataset we present here for the mafic metavolcanic rocks shows that it is difficult to distinguish between mafic rocks from the Nulliak and the Upernavik units based on their ^{147}Sm-^{144}Nd isotopic compositions. The similar Sm-Nd isotopic composition for the Nulliak and Upernavik mafic rocks we obtained is consistent with the interpretation of Wasilewski et al (2019), who suggested that the mafic metavolcanic rocks from the Nulliak and Upernavik units are indistinguishable in terms of petrology and geochemistry, and proposed that all mafic metavolcanic rocks represent one single suite.

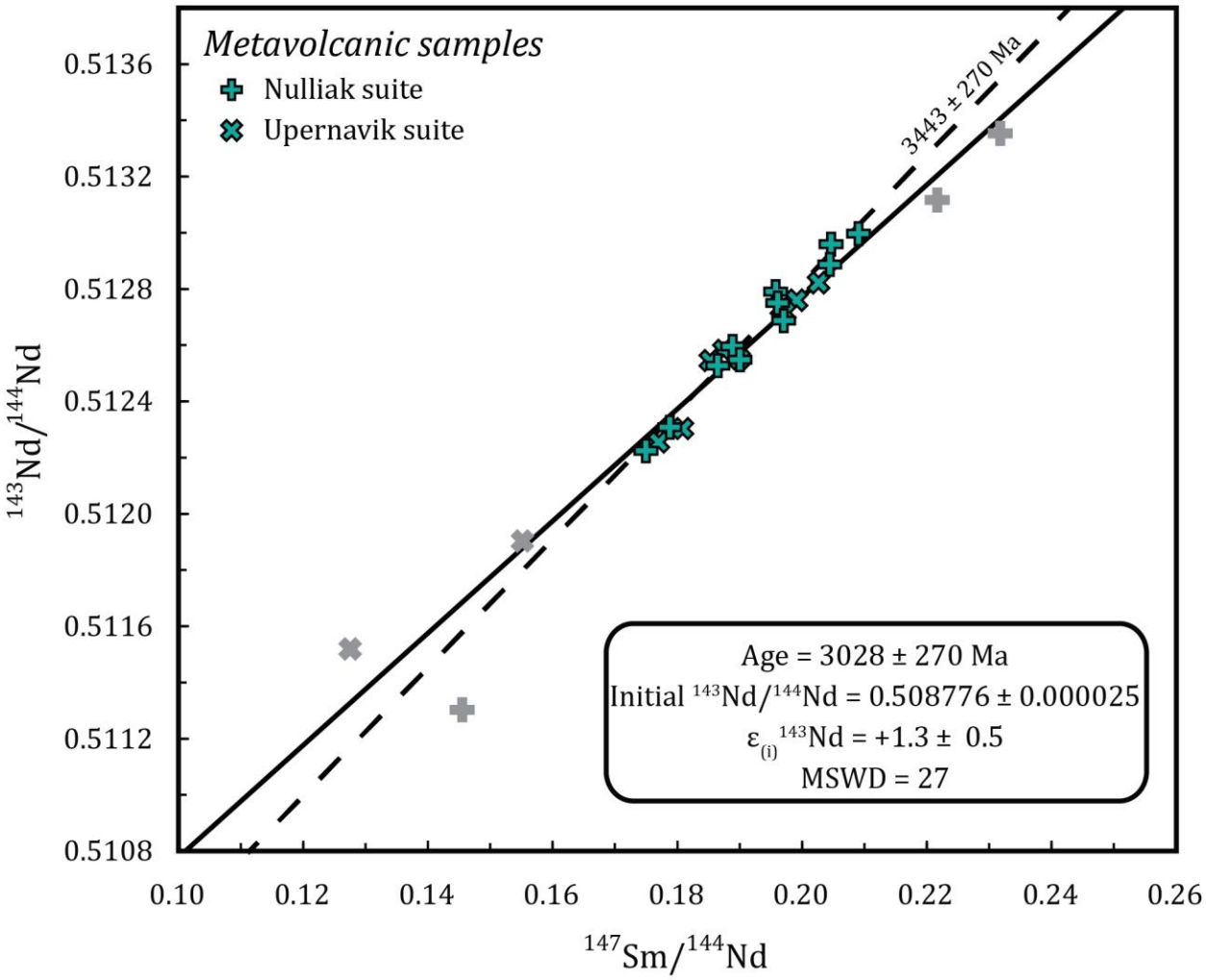

Figure 29 $^{147}Sm/^{144}Nd$ vs $^{143}Nd/^{144}Nd$ isochron diagram of the SHC metavolcanic samples. The grey symbols represent sample outliers that are not considered in the regressions. The dashed line represents the isochron without the two samples with high Sm/Nd ratios (>0.22) with an age of 3443 Ma. Errors on each data point are smaller than the symbols.

Whole-rock geochemical compositions for the mafic metavolcanic rocks and the low-Fe ultramafic rocks suggest a possible petrogenetic link between these two rock groups (Figure 24). The low-Fe ultramafic rocks could represent co-genetic ultramafic cumulates that fractionated to produce the primary basaltic magmas forming the metavolcanic rocks. Based on these petrological constraints, we consider both the mafic metavolcanic rocks and the low-Fe ultramafic rocks to be co-genetic and combined them on the same Sm-Nd isochron diagram. When the mafic metavolcanic rocks are considered together with the low-Fe ultramafic samples, the isochron yields an age of 3274 ± 280 Ma (n= 33, MSWD = 184) (Figure 30). However, some ultramafic samples are significantly

off the best-fit line. Although these samples do not display any evidence of alteration or crustal contamination in terms of geochemistry and petrology, their isotopic ratios display clear evidence of disturbance. When these ultramafic samples and the LREE-enriched mafic disturbed samples are not considered, the isochron diagram yields an older age of 3819 ± 190 Ma (n=25, MSWD = 34) (Figure 30), with an initial $^{143}Nd/^{144}Nd$ ratio of 0.507790 ± 0.000031, which corresponds to an initial εNd value of +2.3 ± 0.6 (Table 5). The scatter observed in both the isochron diagram and the calculated initial εNd values for individual samples (Figure 31), suggests some extent of disturbance within the Sm-Nd isotopic system of the mafic metavolcanic rocks and the low-Fe ultramafic rocks, and must therefore be considered with caution.

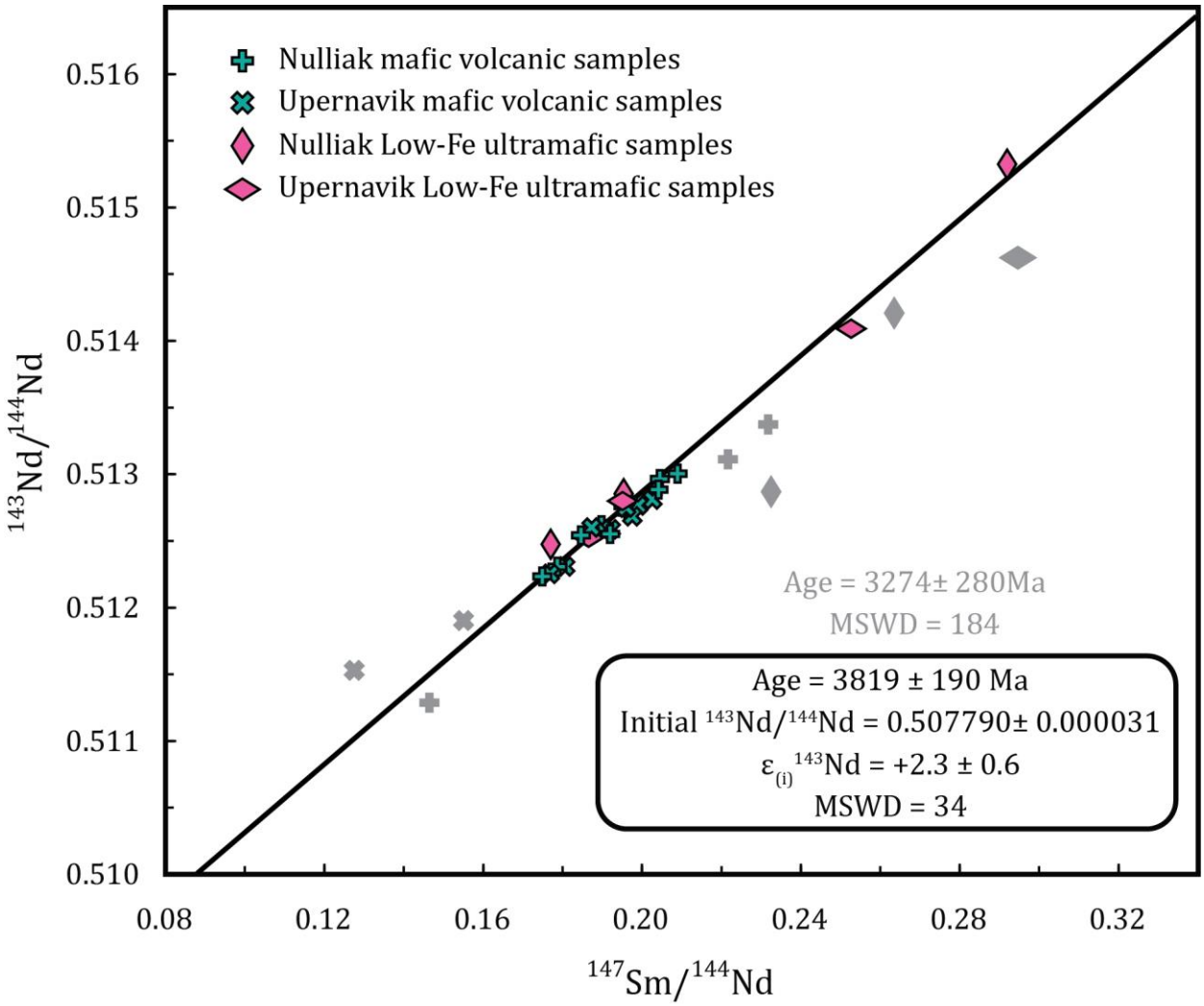

Figure 30 $^{147}Sm/^{144}Nd$ vs $^{143}Nd/^{144}Nd$ isochron diagram of the mafic metavolcanic samples and low-Fe ultramafic samples. Grey symbols represent outliers that are not considered for the regression, yielding the 3819 Ma age. Errors of each data point are smaller than the symbols.

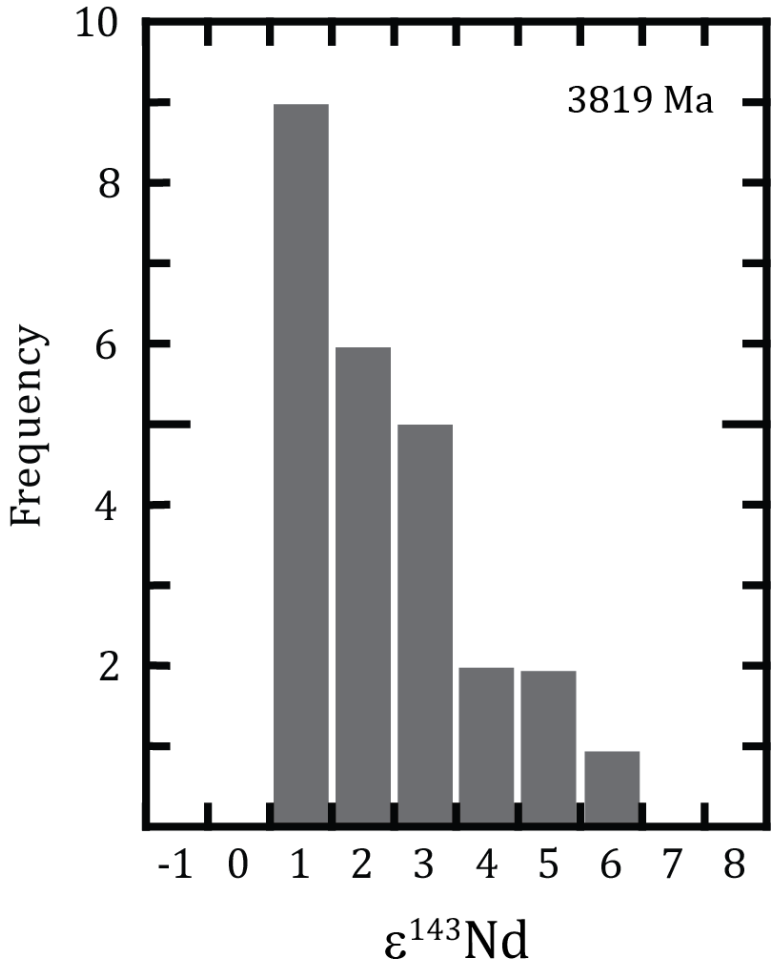

Figure 31 Histogram of the initial εNd values of the mafic metavolcanic samples and low-Fe ultramafic samples calculated at 3819 Ma. εNd values calculated from CHUR values from Bouvier et al. (2008).

Wasilewski et al. (2019) suggested that the high-Fe ultramafic rocks represent a distinct lithological unit. They are characterised by higher FeO content and lower Al_2O_3/TiO_2 compared to the low-Fe ultramafic rocks, with higher concentrations in incompatible trace elements. According to Wasilewski et al. (2019), the high-Fe ultramafic rocks represent olivine-rich cumulates derived from a parental magma with a komatiitic basalt composition and sharing some geochemically affinities with Al-depleted komatiites. Figure 24 moreover suggests that the high-Fe rocks are not petrogenetically linked with the mafic metavolcanic rocks. Therefore, the high-Fe samples need to be considered on their own in an isochron diagram, as they appear not to be co-genetic with the low-Fe ultramafic rocks or the mafic metavolcanic rocks. The isochron

diagram including only the high-Fe ultramafic samples yields an age of 3433 ± 220 Ma (n=10, MSWD = 10.4) (Figure 32), with an initial $^{143}Nd/^{144}Nd$ ratio of 0.508269 ± 0.000026 which corresponds to an initial εNd value of +1.8 ± 0.5 (Table 5). One could argue that this age is heavily controlled by a single sample with a Sm/Nd unusually low for ultramafic rocks, but even if this sample is interpreted to have been affected by post-magmatic LREE-enrichment, the best-fit line obtained when it is removed, yields a similar age of 3369 Ma but with a larger error of 410 Ma due to the narrower Sm/Nd spread.

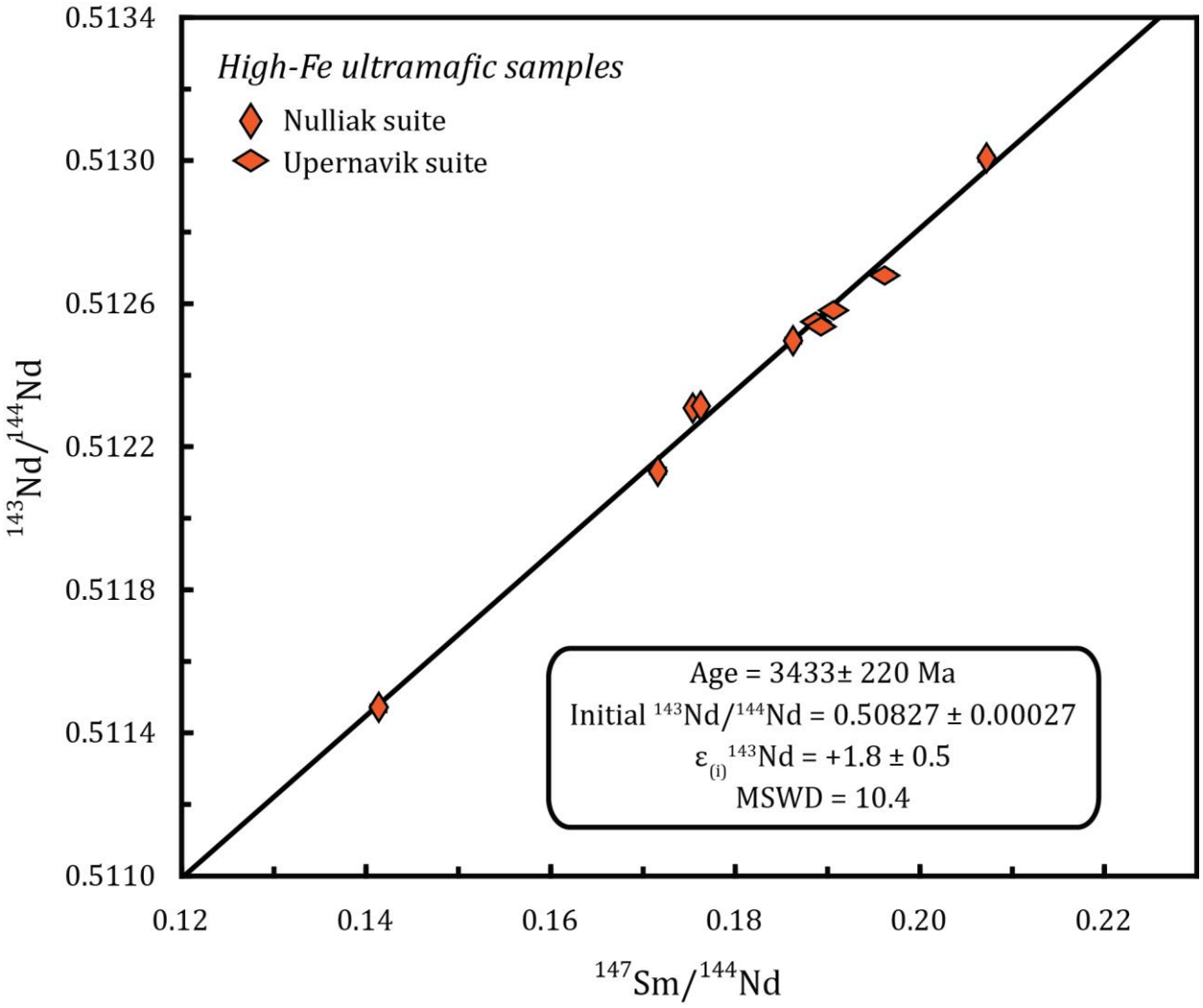

Figure 32 $^{147}Sm/^{144}Nd$ vs $^{143}Nd/^{144}Nd$ isochron diagram of the high-Fe ultramafic samples. Error on each data point are smaller than the symbols.

The age of 3433 ± 220 Ma given by the high-Fe ultramafic rocks Sm-Nd isochron, falls within error with the Re-Os age of 3612 ± 130 Ma obtained by Ishikawa et al (2017) for the same lithology they interpret as metakomatiites. This would imply that the high-Fe ultramafic rocks are 300-400 million years younger than the basaltic metavolcanic rocks interpreted to be from the Nulliak supracrustal unit from figure 30. This age is also consistent with the age of 3362 ± 100 Ma obtained by Morino et al. (2017) on rocks they interpreted as the Upernavik supracrustal unit. Their Mesoarchean isochron, however, includes mafic metavolcanic rocks and ultramafic rocks corresponding to both the high-Fe ultramafic and low-Fe ultramafic rocks. Despite yielding a similar isochron age, however this contrasts with the interpretation of Wasilewski et al. (2019) who argues that the high-Fe ultramafic rocks are not genetically related to the metavolcanic and low-Fe ultramafic rocks. This highlights the need to establish clear genetic link between lithologies in order to consider them on the same isochron diagram. Morino et al. (2017) argue for two different suites of mafic-ultramafic supracrustal rocks (i.e. Nulliak and Upernavik units) based on their ^{142}Nd isotopic compositions. The mafic and ultramafic samples they studied that displayed an excess in ^{142}Nd fall on a ~3.8 Ga ^{147}Sm-^{143}Nd isochron, whereas samples lacking this ^{142}Nd anomaly fall on a younger ~3.4 Ga isochron. They therefore interpreted these two suites as the Eoarchean Nulliak and Mesoarchean Upernavik respectively, both including mafic metavolcanic rocks and ultramafic rocks from the high-Fe ultramafic and low-Fe ultramafic group. Rouleau et al. (2018) has recently conducted ^{142}Nd analyses on a subset of samples studied here, and found that all mafic and ultramafic samples exhibit comparable ^{142}Nd positive anomalies. If we only considerer the mafic and ultramafic samples that display ^{142}Nd excesses, these define a much

younger ^{147}Sm-^{143}Nd isochron age of 2974 ± 290 Ma (n=9), suggesting that there may not be a systematic correlation between the age on the SHC mantle-derived rocks and their ^{142}Nd isotopic composition.

Despite being highly selective and considering only the samples that appear to show the least disturbed isotopic compositions, the isochron diagrams for the metavolcanic rocks and ultramafic cumulates still exhibit noticeable scatter, particularly the mafic-low-Fe ultramafic rock isochron (Figure 30). This suggests that the long-lived Sm-Nd isotopic system in the oldest SHC mafic and ultramafic lithologies has been disturbed to some extent and must be used with caution in order to put precise geochronology constraints on these rocks. Nonetheless, we consider that the Sm-Nd isotopic compositions of the mafic metavolcanic and co-genetic ultramafic rocks support an Eoarchean age of ~3.8 Ga for the SHC metavolcanic rocks, consistent with the Eoarchean Sm-Nd age of Morino et al (2017). The Nd isotopic compositions of the high-Fe ultramafic samples, when interpreted as not co-genetic with the mafic metavolcanic rocks, support a Mesoarchean age of ~3.4 Ga.

6.2.2 Age of the Saglek dikes and undeformed mafic dikes

The exact age of the Saglek dikes is poorly constrained in the literature, despite the fact that they represent an important lithology as they are used for relative geochronology, in the field, to differentiate the Nulliak and Upernavik suite, and therefore important in order to better understand the evolution of the SHC. It has been proposed that the Saglek dikes are younger than the Nulliak assemblage, but older than the Upernavik unit (Hurst et al., 1975; Collerson et al., 1976; Bridgwater et al., 1991; Shimojo et al., 2016). The isochron shown on Figure 20 includes all analysed Saglek dike samples. Excluding from this isochron the LREE-enriched samples (SG-250, SG-257 and BR-83-122) that display evidence of crustal contamination, together with sample SG-

289 that falls off the best-fit line, the Sm-Nd isochron yields an age of 3565 ± 120 Ma (n=10, MSWD = 1.17) (Figure 33), with an initial $^{143}Nd/^{144}Nd$ ratio of 0.508094 ± 0.000007 which corresponds to an initial εNd value of +1.7 ± 0.1 (Table 5). This age is comparable to the age obtained when all Saglek dikes samples are considered but with significantly less scatter (MSWD=1.17). Despite the fact that the Saglek dikes have been metamorphosed to relatively high metamorphic grades, as supported by their mineralogy dominated by hornblende, their homogeneous initial Nd isotopic compositions (Figure 26) and very low scatter on the isochron diagram, suggest that the Sm-Nd isotopic system has remain relatively undisturbed, contrasting with the mafic metavolcanic rocks. We thus interpret the isochron age of 3565 Ma as their emplacement age. This age is consistent with the broad Mesoarchean age previously suggested for the Saglek dikes (Hurst et al., 1975; Collerson et al., 1976; Bridgwater et al., 1991; Shimojo et al., 2016), but the Sm-Nd data presented here provides the first actual measured age reported for these dikes.

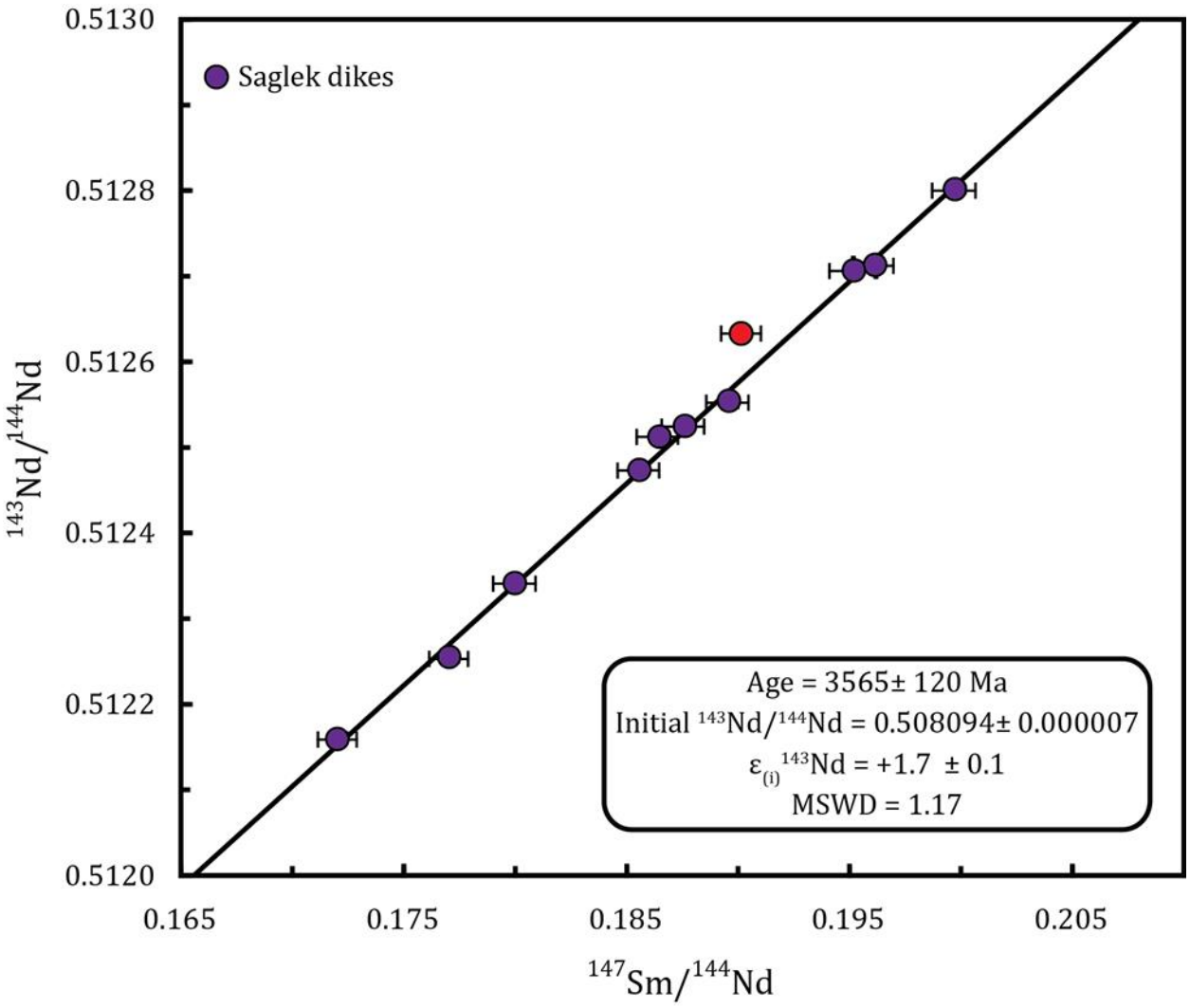

Figure 33 $^{147}Sm/^{144}Nd$ vs $^{143}Nd/^{144}Nd$ isochron diagram of the Saglek dikes. The red sample represents the outlier (SG-289).

Similar to the Saglek dikes, the undeformed mafic dike samples with LREE-enriched compositions inconsistent with primary compositions should not be considered to constrain their Sm-Nd age. Figure 34 presents the Sm-Nd isochron for the least disturbed mafic dikes. When the dikes displaying evidence for contamination are removed, the isochron diagram yields an age of 2694 ± 79 Ma (n= 21, MSWD = 3.2) with an initial $^{143}Nd/^{144}Nd$ ratio of 0.509231 ± 0.000007 which corresponds to an initial εNd value of +1.7 ± 0.1 (Table 5). This age falls within the internal isochron age of the 30 meter differentiated dike (2771 ± 290 Ma) but with less scatter and better

precision due to the wider compositional range. These mafic undeformed dikes display preserved igneous textures and mineralogy, and therefore they often have been interpreted to be Proterozoic in age, emplaced after the Neoarchean peak metamorphism of ~2700 Ma (Wendt & Collerson., 1999; Kusiak et al., 2018). Their Sm-Nd isotopic composition is however consistent with a Neoarchean age, more contemporaneous with the emplacement of late granites associated with tectonic juxtaposition around 2.8-2.7 Ga (Bridgwater et al., 1991). Thus, the emplacement of the mafic dikes may be associated with a major tectonic event that occurred during the Neoarchean, which also resulted in a major thermal and magmatic event. The preserved igneous ophitic textures and mineralogical assemblage of the undeformed Neoarchean dikes suggest that they were not extensively affected by the peak metamorphic conditions at 2.7 Ga or even later metamorphic events of 2.6 Ga, 2.5 Ga and 2.2 Ga identified by Kusiak et al. (2018). Table 5 summarizes the Sm-Nd isochron ages obtained for the least disturbed samples from the different mantle-derived lithologies in the SHC. This shows that the SHC recorded more than one billion years of mafic magmatism.

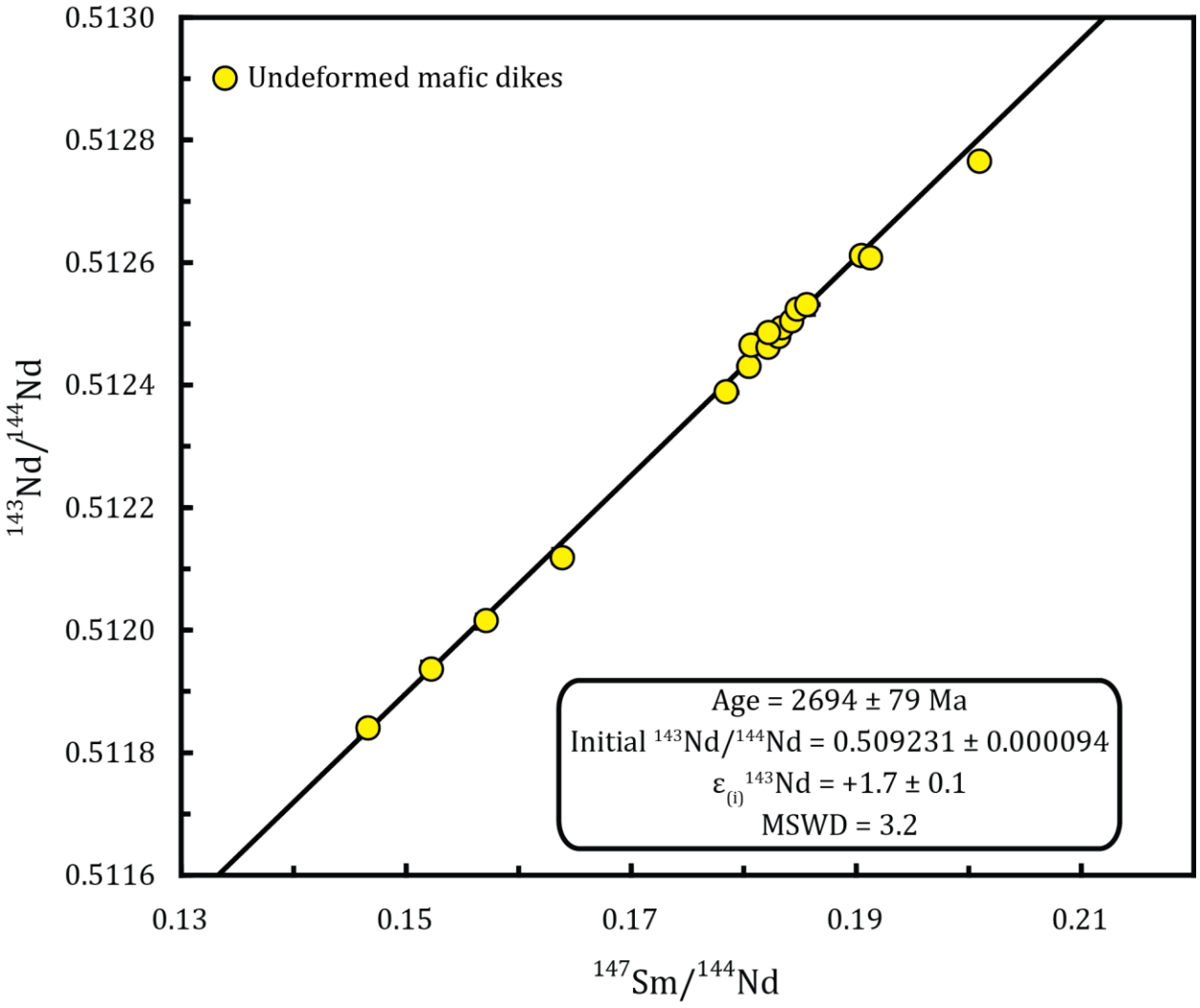

Figure 34 $^{147}Sm/^{144}Nd$ vs $^{143}Nd/^{144}Nd$ isochron diagram of the undeformed mafic dikes.

Unit	Age	Initial εNd values
Mafic metavolcanic and low-Fe ultramafic rocks	3819 ± 190 Ma	+ 2.3 ± 0.6
High-Fe ultramafic rocks	3433 ± 220 Ma	+ 1.8 ± 0.5
Saglek dikes	3565 ± 120 Ma	+ 1.7 ± 0.1
Undeformed mafic dikes	2694 ± 79 Ma	+ 1.7 ± 0.1

Table 5 Summary of the calculated Sm-Nd ages and initial εNd values for each mantle-derived unit. εNd values calculated from CHUR values from Bouvier et al. (2008).

6.3 Are the Saglek dikes related to the Southwest Greenland Ameralik dikes?

The Saglek-Hebron Gneiss Complex belongs to the North Atlantic craton, and several studies have suggested that it is closely related the Itsaq gneiss complex in Southwest Greenland (Baadsgaard et al., 1979; Collerson et al., 1982; Hurst et al., 1975; McGregor, 1973). Bridgwater et al. (1975) suggested that the Saglek dikes may be equivalent to the Ameralik dikes intruding into the Itsaq gneiss complex. A few of the Ameralik dikes show ^{142}Nd deficits compared to the terrestrial Nd standard (Rizo et al., 2012), which could reflect the geochemical fingerprints of the Hadean enriched reservoir complementary to the early depleted mantle previously identified in the Itsaq gneiss complex (e.g. Boyet et al., 2006, Rizo et al., 2011). The Saglek dikes represent therefore the potential candidates to have recorded an early-enriched source, similar to the mantle sampled by the Ameralik dikes.

The Ameralik dikes are commonly meter size doleritic dikes characterized by the occurrence of plagioclase phenocrysts, similar to what is observed in the Saglek dikes. Larger Ameralik dikes are noritic in composition commonly displaying olivine and pyroxene cumulates (McGregor et al., 1973; Bridgwater et al., 1975; Nutman et al., 2004; Rizo et al., 2012). The larger noritic Ameralik dikes yielded an age of 3413 ± 57 Ma based on Sm-Nd whole-rock and mineral separate isochrons (Nutman et al., 2004) and a U-Pb zircon age of 3512 ± 7 Ma (Nielsen et al., 2002). Rizo et al. (2012) reported Sm-Nd isotopic data supporting an emplacement age of 3403 ± 250 Ma for the doleritic Ameralik dikes, consistent with the weighted average ^{207}Pb/^{206}Pb mean age of 3421 ± 34 Ma they obtained for zircons, baddeleyites and monazites in the noritic dikes. These ages are slightly younger but overlap within error the Sm-Nd age of 3565 ± 120 Ma we report here for the Saglek dikes. The similarities in terms of petrology and geochemistry, as well as the similar age could be consistent with the Saglek and the Ameralik dikes being derived from the same source.

However, when the samples from both dike groups are plotted on the same isochron diagram (Figure 35), it is apparent that their Sm-Nd isotopic compositions reflect distinct sources. Both groups of dikes yield similar slopes (i.e. similar ages), but they clearly define distinct trends, corresponding to different initial $^{143}Nd/^{144}Nd$ isotopic compositions. The higher initial εNd value of +3.0 for the Ameralik suggests a more depleted source compared the initial εNd value of +1.7 for the Saglek dikes (Figure 36).

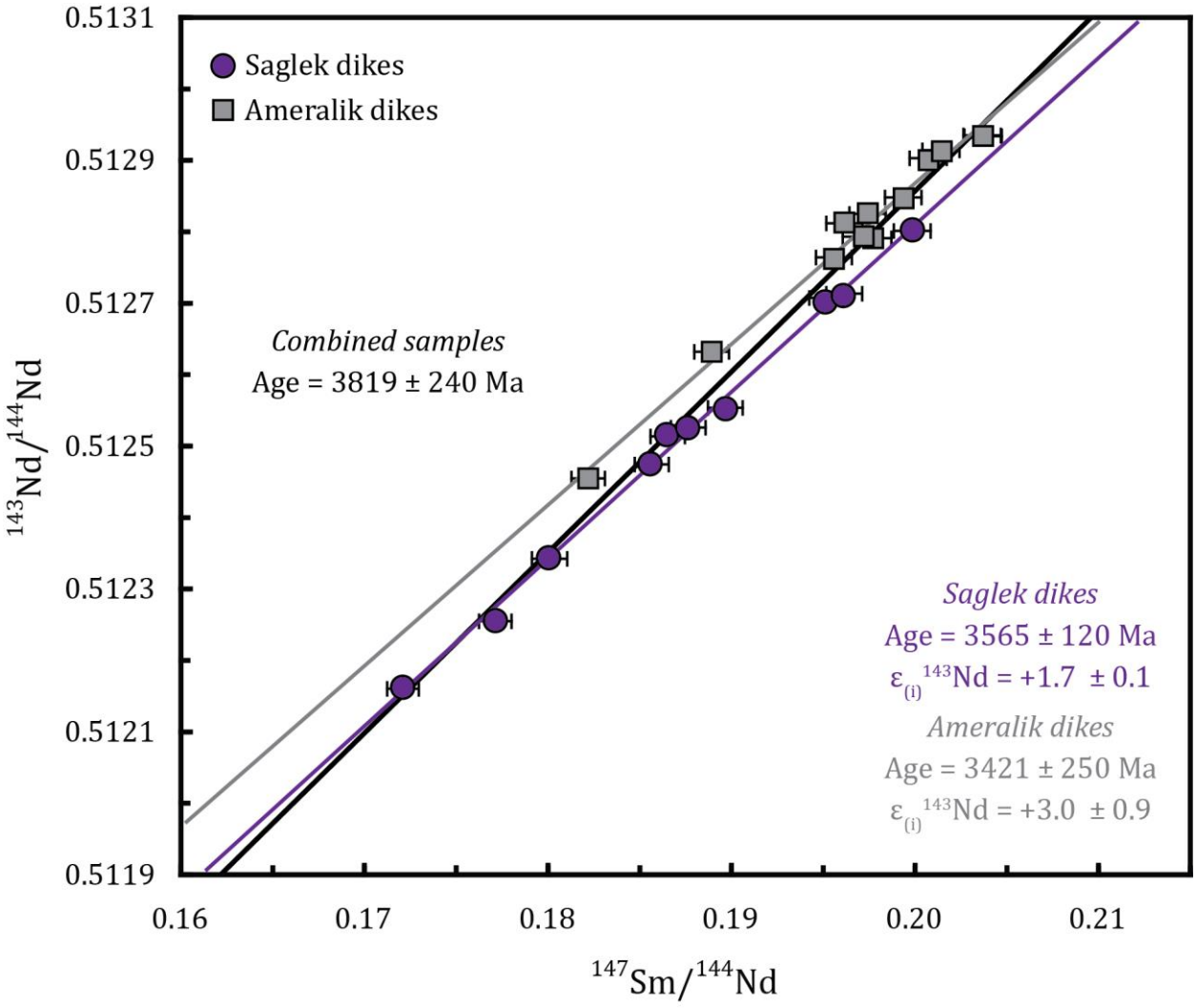

Figure 35 $^{147}Sm/^{144}Nd$ vs $^{143}Nd/^{144}Nd$ isochron diagram of the Saglek dikes and the Ameralik dikes. If all Saglek and Ameralik dike samples are considered together, they yield an age of 3819 Ma. Sm-Nd isotopic data for the Ameralik dikes from Rizo et al. (2012).

6.4 Evolution of the SHC mantle source

Given that the SHC includes multiple generations of mantle-derived rocks emplaced at ~3.8 Ga, ~3.5 Ga, ~3.4 Ga and ~2.7 Ga, it offers the unique opportunity to study the evolution of the mantle for more than 1 billion years of its early history. The initial εNd isotopic compositions given by the isochrons with the least disturbed rocks can be used to track the isotopic evolution of the SHC mantle source. All generations of mantle-derived rocks yield positive εNd values, (i.e. suprachondritic), which is indicative of a source depleted in incompatible trace elements, and therefore has a high Sm/Nd ratio. Only the Eoarchean rocks display an initial Nd isotopic compositions similar the depleted mantle (Figure 36). The isochron for the mafic metavolcanic rocks and low-Fe ultramafic rocks including only the least disturbed samples yields an initial εNd value of +2.3 ± 0.6 (Figure 36), comparable within error to the initial εNd value of 1.5 ± 0.6 obtained by Morino et al. (2017) from their Eoarchean isochron. This value of ~+2 is consistent with a depleted mantle source (Figure 36). Morino et al. (2017) proposed a mantle source with a $^{147}Sm/^{144}Nd$ ratio of 0.211 for the oldest SHC mantle-derived rocks, which would have formed by an early differentiation event occurring at 4.40 Ga, to account for their initial εNd value and their ^{142}Nd excesses of ~8 ppm. This mantle source could also be consistent with our ^{147}Sm-^{143}Nd data for the Eoarchean rocks, but more ^{142}Nd isotopic date would need to be acquired in order confirm if all the mafic and ultramafic rocks, which we interpret as being Eoarchean in age, are derived from an early formed mantle source with an excess in ^{142}Nd. Based on their geochemical composition, Wasilewski et al. (2019) have interpreted the high-Fe ultramafic rocks as representing a distinct mantle-derived lithology, which closely resembles Al-depleted komatiites. The initial εNd value of +1.8 ± 0.5 for these rocks, which we dated at 3433 Ma, is slightly lower than the depleted mantle at that time (Figure 36), suggesting that their mantle source may be

different from the source of the older Eoarchean rocks. Morino et al. (2017) obtained a lower initial εNd value of 0.4 ± 0.4 for the mantle-derived rocks they interpreted as Mesoarchean. This chondritic εNd value, together with the fact that these rocks did not yield ^{142}Nd anomalies, lead them to suggest that the SHC Mesoarchean rocks are derived from a distinct mantle compared to the Eoarchean rocks. Preliminary ^{142}Nd results on high-Fe ultramafic rocks, however, showed that these ultramafic rocks have high ^{142}Nd/^{144}Nd comparable to the Eoarchean rocks (Rouleau et al., 2018), suggesting that if the mantle sources of the Mesoarchean high-Fe ultramafic rocks and the Eoarchean mafic metavolcanic along with the low-Fe ultramafic rocks are distinct, they may share a similar Hadean history. The ages and initial isotopic compositions obtained from isochron diagrams is directly tied to the geological interpretation and the lithologies that are interpreted to be co-genetic. The discrepancy between our results and those of Morino et al. (2017) may be on part due to diverging geological interpretations, but regardless of which SHC rocks are interpreted to be Mesoarchean in age, the mantle source sampled by the ~3.4 Ga mantle-derived rocks appears to be less depleted than the mantle source of the Eoarchean rocks. This is also supported by the ~3.5 Ga Saglek dikes yielding an initial εNd value of +1.7 ± 0.1 (Figure 36). Similar to the high-Fe ultramafic rocks, this is consistent with derivation from a source slightly less depleted in incompatible elements than the "normal" depleted mantle (Figure 36). Interestingly, the undeformed mafic dikes yield an identical εNd value of +1.7 ± 0.1, although they are ~800 million years younger than the Saglek dikes. The εNd value we obtained for all the different generations of mantle-derived rocks appear, in fact, to be the same within error. This suggests that if all generations of mafic-ultramafic rocks have been derived from a single mantle source, this source diverged from the depleted mantle in the Eoarchean to evolve with a chondritic Sm/Nd ratio for at least 1 billion years (Figure 36). If multiple mantle sources are instead involved in the formation

of the SCH mantle-derived rocks, the older rocks appear to have been produced from a depleted source similar to the depleted mantle, whereas the younger rocks are consistent with derivation from a depleted source, but not as depleted as the present-day mantle. Contribution from an older unradiogenic crust, which typically yield low to negative εNd values (i.e. enriched in incompatible trace elements), could also explain the loser $^{143}Nd/^{144}Nd$ of the Neoarchean dikes compared to the "normal" depleted mantle. Since the undeformed dikes used for the Sm-Nd isochron do not display evidence of mixing with surrounding TTG (Figure 28), if crustal contamination is the process that lowered their initial εNd value, it could possibly have occurred before the emplacement of the dikes, in a magma chamber where some extent of crustal assimilation may have taken place. Therefore creating a suite of rocks derived from a source that is uniform with an initial isotopic composition less depleted than the depleted mantle.

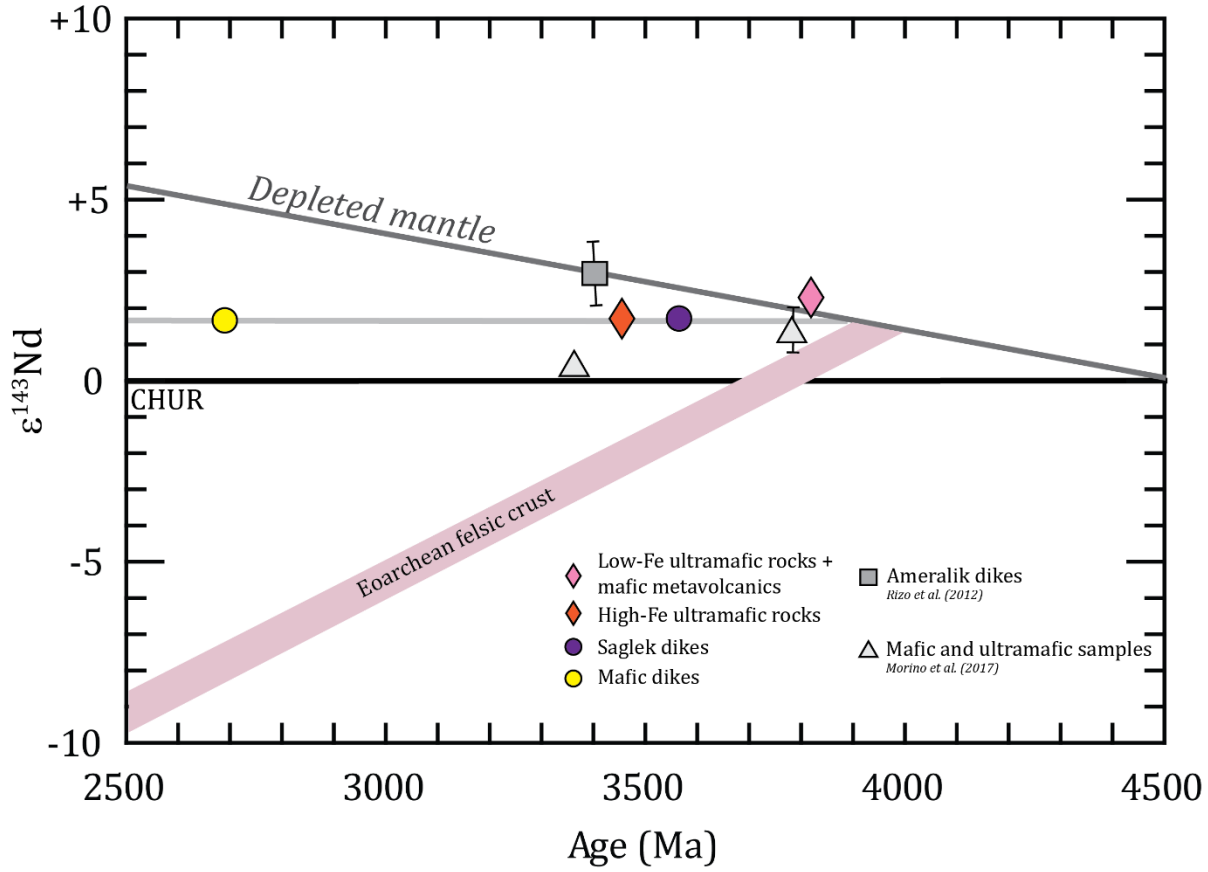

Figure 36 Initial εNd values vs time. The εNd values are obtained from the isochron diagram of each unit. The light grey line represent a source diverging from the depleted mantle and evolving with a chondritic Sm/Nd ratio. Along with εNd values of the Ameralik dikes from Rizo et al. (2012) and mafic and ultramafic samples εNd values from Morino et al. (2017). The pink Eoarchean array is based on the data from Wasilewski et al. (in prep). Note that some units have error smaller than the symbols. εNd values calculated from CHUR values from Bouvier et al. (2008).

7. Conclusion

The SHC hosts several generations of mantle-derived rocks over more than one billion years, making it ideal to study the evolution of mafic magmatism events over time. Petrological, geochemical and isotopic data have proven to be useful tools to characterize and constrain the ages of the various mantle-derived rocks present in the SHC. The mafic metavolcanic rocks are described as amphibolites with a basaltic composition, and the ultramafic rocks range from harzburgitic to lherzolitic compositions, and were divided into two distinct groups (Wasilewski et al., 2019). The Saglek dikes exhibit an amphibolite facies mineralogical assemblage whereas the

undeformed mafic dikes have shown a primitive gabbroic mineralogy as well as igneous textures. Both generations of mafic dikes display basaltic compositions with tholeiitic trends.

Assessment of element mobility and models of crystallisation and mixing have ensured the quality of the isotopic data of the samples used to calculate our final reported ages. The multiple generations of mantle-derived rocks have been dated at 3.8 Ga, 3.6 Ga, 3.5 Ga and 2.7 Ga. The new Sm-Nd data of the mafic metavolcanic rocks and the ultramafic rocks yield similar ages to the previously reported ages, however these ages are based on new petrogenetical interpretations. This new data has also provided the first reported age for the Saglek dikes and the undeformed mafic dikes. It was shown that all the generations of mantle-derived rocks yield positive εNd values, where only the Eoarchean rocks shows a mantle source with a Nd composition similar to the depleted mantle. The Mesoarchean ultramafic rocks, Saglek dikes and Neoarchean mafic dikes display close to identical initial εNd values, despite an age difference of 800 Ma. Suggesting the contribution of distinct mantle sources or, if all generations of mantle-derived rocks in the SHC were produced from the same mantle source, this source would have evolved with a nearly chondritic Sm/Nd ratio. Previously thought to be equivalent, the Saglek and Ameralik dikes yield similar Mesoarchean ages. However, the higher initial εNd value of the Ameralik dikes suggests a more depleted source compared the initial εNd value of the Saglek dikes.

Future work on these samples should consist of isotopic studies using long-lived and short-lived isotopic systems, as it would provide more information of the source of these mantle-derived rocks as well as confirm the ages reported in this study. It would also provide more evidence on the nature of the relation between the Saglek dikes and the Ameralik dikes.

References

Baadsgaard, H., Collerson, K. D., & Bridgwater, D., 1979. The Archean gneiss complex of northern Labrador. 1. Preliminary U-Th-Pb geochronology. Canadian Journal of Earth Sciences, 951–961.

Baadsgaard, H., Cumming, G. L., & Woden, J. M., 1984. U-Pb geochronology of minerals from the Midwest uranium deposit, northern Saskatchewan. Canadian Journal of Earth Sciences, 21, 642–648.

Black, L. P., Williams, I. S., & Compston, W., 1986. Four zircon ages from one rock: the history of a 3930 Ma-old granulite from Mount Sones, Enderby Land, Antarctica. Contributions to Mineralogy and Petrology, 94(4), 427–437.

Bouvier, A., Vervoort, J.D., Patchett, J.P., 2008. The Lu–Hf and Sm–Nd isotopic composition of CHUR: constraints from unequilibrated chondrites and implications for the bulk composition of terrestrial planets. Earth and Planetary Science Letters 273, 48–57.

Bowring, S. a., & Williams, I. S., 1999. Priscoan (4.00-4.03 Ga) orthogneisses from northwestern Canada. Contributions to Mineralogy and Petrology, 134 (July 1998), 3–16.

Boyet, M. and Carlson, R.W., 2006. A new geochemical model for the Earth's mantle inferred from 146Sm–142Nd systematics. Earth and Planetary Science Letters, 250(1-2), pp.254-268.

Bridgwater, D., & Collerson, K. D., 1976. The major petrological and geochemical characters of the 3,600 m.y. Uivak gneisses from Labrador. Contributions to Mineralogy and Petrology, 54(1), 43–59.

Bridgwater, D., & Collerson, K. D., 1977. On the origin of Early Archean gneisses: a reply. Contributions to Mineralogy and Petrology, 62, 179–191.

Bridgwater, D., & Schiøtte, L., 1991. The Archean gneiss complex of northern Labrador. A review of current results, ideas and problems. Bulletin of the Geological Society of Denmark, 39(3–4), 153–166.

Bridgwater, D., Collerson, K. D., Hurst, R. W., & Jesseau, C. W., 1975. Field characters of the early precambrian rocks from Saglek, Coast of Labrador. Geological Survey of Canada, 75(1), 287–296.

Bridgwater, D., Watson, J.V. and Windley, B.F., 1973. A Discussion on the evolution of the Precambrian crust-The Archaean craton of the North Atlantic region. Phil. Trans. R. Soc. Lond. A, 273(1235), pp.493-512.

Cates, N. L., & Mojzsis, S. J., 2007. Pre-3750 Ma supracrustal rocks from the Nuvvuagittuq supracrustal belt, northern Québec. Earth and Planetary Science Letters, 255(1–2), 9–21.

Collerson, K. D., 1983. The Archean gneiss complex of northern Labrador. 2. Mineral ages, secondary isochrons, and diffusion of strontium during polymetamorphism of the Uivak gneisses. Can. J. Earth Sci., 20, 707–718.

Collerson, K. D., Campbell, L. M., Weaver, B. L., & Palacz, Z. A., 1991. Evidence for extreme mantle fractionation in early Archean ultramafic rocks from northern Labrador. Nature, 349(6306), 209–214.

Collerson, K. D., Jesseau, C. W., & Bridgwater, D., 1976. Contrasting types of bladed olivine in ultramafic rocks from Archean of Labrador. Canadian Journal of Earth Sciences, 13(3), 442–450.

Collerson, K. D., Kerr, A., Vocke, R. D., & Hanson, G. N., 1982. Reworking of sialic crust as represented in late Archean-age gneisses, northern Labrador. Geology. 10 (4), 202-208

Collerson, K.D. and Bridgwater, D., 1979. Metamorphic development of early Archean tonalitic and trondhjemitic gneisses: Saglek area, Labrador. In Developments in Petrology (Vol. 6, pp. 205-273). Elsevier.

Compston, W., & Kroner, A., 1988. Multiple zircon growth within early Archean tonalitic gneiss from Ancient Gneiss Complex, Swaziland. Earth and Planetary Science Letters, 87, 13–28.

Darling, J. R., Moser, D. E., Heaman, L. M., Davis, W. J., O'Neil, J., & Carlson, R., 2013. Eoarchean to neoarchean evolution of the Nuvvuagittuq Supracrustal belt: New insights from U-Pb zircon geochronology. American Journal of Science, 313(9), 844–876.

DePaolo, D.J. and Wasserburg, G.J., 1979. Petrogenetic mixing models and Nd-Sr isotopic patterns. Geochimica et Cosmochimica Acta, 43(4), pp.615-627.

DePaolo, D.J., 2012. Neodymium isotope geochemistry: an introduction (Vol. 20). Springer Science & Business Media.

Dyck, B., Reno, B.L. and Kokfelt, T.F., 2015. The Majorqaq Belt: a record of Neoarchaean orogenesis during final assembly of the North Atlantic Craton, southern West Greenland. Lithos, 220, pp.253-271.

Fletcher, I.R., Rosman, K.J.R., 1982. Precise determination of initial εNd from Sm–Nd isochron data. Geochimica et Cosmochimica Acta 46, 1983–1987.

Furnes, H., Rosing, M., Dilek, Y., de Wit, M., 2009. Isua supracrustal belt (Greenland) — a vestige of a 3.8 Ga suprasubduction zone ophiolite, and the implications for Archean geology. Lithos 113, 115–132.

Gill, R.C.O. & Bridgwater, D. 1976. The Ameralik dykes of West Greenland, the earliest known basic rocks intruding stable continental crust. Earth and Planetary Science Letters, 29, 276–282.

Hurst, R. W., Bridgwater, D., Collerson, K. D., & Wetherill, G. W., 1975. 3600-m,y, Rb-Sr ages from very early Archean gneisses from Saglek Bay, Labrador. Earth and Planetary Science Letters, 27, 393–403.

Irvine, T. N., & Baragar, W. R. A., 1971. A Guide to the Chemical Classification of the Common Volcanic Rocks. Canadian Journal of Earth Sciencesd, 8, 523–548.

Ishikawa, A., Suzuki, K., Collerson, K. D., Liu, J., Pearson, D. G., & Komiya, T., 2017. Rhenium-osmium isotopes and highly siderophile elements in ultramafic rocks from the Eoarchean Saglek Block, northern Labrador, Canada: implications for Archean mantle evolution. Geochimica ET Cosmochimica Acta, 216, 286–311.

Komiya, T., Yamamoto, S., Aoki, S., Koshida, K., Shimojo, M., Sawaki, Y., Aoki, K., Sakata, S., Yokoyama, T.D., Maki, K., Ishikawa, A., Hirata, T., Collerson, K. D., 2017. A prolonged granitoid formation in Saglek Block, Labrador: Zonal growth and crustal reworking of continental crust in the Eoarchean. Geoscience Frontiers, 8(2), 355–385.

Komiya, T., Yamamoto, S., Aoki, S., Sawaki, Y., Ishikawa, A., Tashiro, T., Koshida, K., Shimojo, M., Aoki, K., & Collerson, K. D., 2015. Geology of the Eoarchean, > 3.95 Ga, Nulliak supracrustal rocks in the Saglek Block, northern Labrador, Canada: The oldest geological evidence for plate tectonics. Tectonophysics, 662, 40–66.

Kröner, A., 2007. The Ancient Gneiss Complex of Swaziland and Environs: Record of Early Archean Crustal Evolution in Southern Africa. Earth's Oldest Rocks, 465–480.

Kusiak, M. A., Dunkley, D. J., Whitehouse, M. J., Wilde, S. A., Sałacińska, A., Konečný, P., Szopa, K., Gawęda, A., & Chew, D., 2018. Peak to post-peak thermal history of the Saglek Block of Labrador: A multiphase and multi-instrumental approach to geochronology. Chemical Geology, 484(May), 210–223.

Kusiak, M. A., Whitehouse, M. J., Wilde, S. A., Dunkley, D. J., Menneken, M., Nemchin, A. A., & Clark, C., 2014. Changes in zircon chemistry during Archean UHT metamorphism in the Napier Complex, Antarctica. American Journal of Science, 313(9), 933–967.

Le Maître, R. W., 2002. Igneous Rocks: A Classification and Glossary of Terms (2nd Ed.). New York: Cambridge University Press.

Le Maitre, R., 1989. A classification of igneous rocks and glossary of terms. Recommendations of the international union of geological sciences subcommission on the systematics of igneous rocks, 193.

Liu, J., Touboul, M., Ishikawa, A., Walker, R. J., & Graham Pearson, D., 2016. Widespread tungsten isotope anomalies and W mobility in crustal and mantle rocks of the Eoarchean Saglek Block, northern Labrador, Canada: Implications for early Earth processes and W recycling. Earth and Planetary Science Letters, 448, 13–23.

Ludwig, K.R., 1991. ISOPLOT; A Plotting and Regression Program for Radiogenic-Isotope Data; version 2.53, Open-File Rep.

McGregor, V. R., 1973. The early Precambrian gneisses of the Godthab district West Greenland. Phil. Trans. R. Soc. Lond. A., 273, 343–358.

Morino, P., Caro, G., & Reisberg, L., 2018. Differentiation mechanisms of the early Hadean mantle: Insights from combined176Hf-142,143Nd signatures of Archean rocks from the Saglek Block. Geochimica et Cosmochimica Acta, 240, 43–63.

Morino, P., Caro, G., Reisberg, L., & Schumacher, A., 2017. Chemical stratification in the post-magma ocean Earth inferred from coupled 146,147Sm–142,143Nd systematics in ultramafic rocks of the Saglek block (3.25–3.9 Ga; northern Labrador, Canada). Earth and Planetary Science Letters, 463, 136–150.

Nielsen,S. G., Baker, A. J.&Krogstad, E. J., 2002 Petrogenesis of an early Archean (3.4Ga) norite dyke, Isua, West Greenland: evidence for early Archean crustal recycling? Precambr. Res. 118, 133–148

Nutman, A. P., & Collerson, K. D., 1991. Very early Archean crustal-accretion complexes preserved in the North Atlantic craton. Geology, 19, 791–794.

Nutman, A. P., & Friend, C. R. L., 2009. New 1:20,000 scale geological maps, synthesis and history of investigation of the Isua supracrustal belt and adjacent orthogneisses, southern West Greenland: A glimpse of Eoarchaean crust formation and orogeny. Precambrian Research, 172(3–4), 189–211.

Nutman, A. P., Bennett, V. C., Friend, C. R. L., Hidaka, H., Yi, K., Lee, S. R., & Kamiichi, T., 2013. The Itsaq Gneiss Complex of Greenland: Episodic 3900 to 3660 Ma juvenile crust formation and recycling in the 3660 to 3600 Ma Isukasian orogeny. American Journal of Science, 313(9), 877–911.

Nutman, A. P., Fryer, B. J., & Bridgwater, D., 1989. The early Archaean Nulliak (supracrustal) assemblage, northern Labrador. Can. J. Earth Sci., 26, 2159–2168.

Nutman, A. P., Kinny, P. D., Compston, W., & Williams, I. S., 1991. SHRIMP U-Pb zircon geochronology of the Narryer Gneiss Complex, Western Australia. Precambrian Research, (52), 275–300.

Nutman, A. P., McGregor, V. R., Friend, C. R. L., Bennett, V. C., & Kinny, P. D., 1996. The Itsaq Gneiss Complex of southern West Greenland; the world's most extensive record of early crustal evolution (3900-3600 Ma). Precambrian Research, 78(1–3), 1–39.

Nutman, A., Friend, C., Bennett, V., McGregor, V., 2004. Dating of the Ameralik dyke swarms of the Nuuk district, southern West Greenland: mafic intrusion events starting from c . 3510 Ma, 161, 421–430.

O'Neil, J., Carlson, R. W., Francis, D., & Stevenson, R. K., 2008. Neodymium-142 evidence for hadean mafic crust. Science, 321(5897), 1828–1831.

O'Neil, J., Carlson, R. W., Papineau, D., Levine, Y. E., & Francis, D., in press. The Nuvvuagittuq greenstone belt: A glimpse of Earth's earliest crust. In Earth's Oldest Rocks 2nd Edition. Elsevier B.V.

O'Neil, J., Carlson, R. W., Paquette, J. L., & Francis, D., 2012. Formation age and metamorphic history of the Nuvvuagittuq Greenstone Belt. Precambrian Research, 220–221, 23–44.

O'Neil, J., Francis, D., & Carlson, R. W., 2011. Implications of the Nuvvuagittuq Greenstone Belt for the Formation of Earth's Early Crust. Journal of Petrology, 52(5), 985–1009.

O'Neil, J., Maurice, C., Stevenson, R. K., Larocque, J., Cloquet, C., David, J., & Francis, D. 2007. Chapter 3.4 The Geology of the 3.8 Ga Nuvvuagittuq (Porpoise Cove) Greenstone Belt, Northeastern Superior Province, Canada. Developments in Precambrian Geology, 15(07), 219–250.

O'Neil, J., Rizo, H., Boyet, M., Carlson, R. W., & Rosing, M. T., 2016. Geochemistry and Nd isotopic characteristics of Earth's Hadean mantle and primitive crust. Earth and Planetary Science Letters, 442, 194–205.

Regelous, M., & Collerson, K. D., 1996. 147Sm-143Nd, 146Sm-142Nd systematics of early Archaean rocks and implications for crust-mantle evolution. Geochimica ET Cosmochimica Acta, 60(18), 3513–3520.

Reimink, J. R., Chacko, T., Stern, R. A., & Heaman, L. M., 2016. The birth of a cratonic nucleus: Lithogeochemical evolution of the 4.02-2.94 Ga Acasta Gneiss Complex. Precambrian Research, 281, 453–472.

Rizo, H., Boyet, M., Blichert-Toft, J. and Rosing, M., 2011. Combined Nd and Hf isotope evidence for deep-seated source of Isua lavas. Earth and Planetary Science Letters, 312(3-4), pp.267-279.

Rizo, H., Boyet, M., Blichert-toft, J., Neil, J. O., Rosing, M. T., & Paquette, J. (2012). Nd deficits in Isua Archaean rocks. Nature, 490(7422), 96–100. https://doi.org/10.1038/nature11565

Rouleau, A., Rizo, H., O'Neil, J., Wasilewski, B., 2018. Combined 182W and 142Nd Study of Mantle-Derived Rocks from the Saglek-Hebron Gneiss Complex. Goldschmidt Abstracts, 2018 2189

Ryan, B. A., 1977. Progressive structural reworking of the Uivak Gneisses, Jerusalem Harbour, Northern Labrador. Department of Geology Memorial University of Newfoundland.

Ryan, B., 1990. Basement-cover relationships and metamorphic patterns in the foreland of the Torngat Orogen in the Saglek-Hebron area, Labrador. Geoscience Canada, 17(4).

Ryan, B., & Martineau, Y., 2012. Revised and coloured edition of 1992 map showing the Geology of the Saglek Fiord - Hebron Fiord area, Labrador (NTS 14L/2,3,6,7). Scale: 1:100 000. Government of Newfoundland and Labrador, Department of Natural Resources, Geological Survey, Map 2012-15, Open File 14L/0091.

Schiøtte, L., Bridgwater, D., Collerson, K. D., Nutman, A. P., & Ryan, A. B., 1986. Chemical and isotopic effects of Late Archean high-grade metamorphism and granite injection on early Archean gneisses, Saglek-Hebron, northern Labrador. In K. H. W. J.B. Dawson, D.A. Carswell, J. Hale (Ed.), the nature of the lower continental crust (pp. 261–273). Geol. Soc. Lond. Spec. Publ.

Schiøtte, L., Compston, W., & Bridgwater, D., 1989. Ion probe U–Th–Pb zircon dating of polymetamorphic orthogneisses from northern Labrador, Canada. Canadian Journal of Earth Sciences, 26(8), 1533–1556.

Schiøtte, L., Compston, W., & Bridgwater, D., 1989a. U-Th-Pb ages of single zircons in Archaean supracrustals from Nain Province, Labrador, Canada. Can. J. Earth Sci., 26, 2636–2644.

Schiøtte, L., Nutman, A. P., & Bridgwater, D., 1992. U-Pb ages of single zircons within Upernavik metasedimentary rocks and regional implications for the tectonic evolution of the Archaean Nain Province, Labrador. Can. J. Earth Sci., 29, 260–276.

Shimojo, M., Yamamoto, S., Sakata, S., Yokoyama, T. D., Maki, K., Sawaki, Y., Ishikawa, A., Aoki, K., Aoki, S., Koshida, K., Tashiro, T., Hirata, T., Collerson, K.D., & Komiya, T., 2016. Occurrence and geochronology of the Eoarchean,~3.9Ga, Iqaluk Gneiss in the Saglek Block, northern Labrador, Canada: Evidencefor the oldest supracrustal rocks in the world. Precambrian Research, 278, 218–243.

Song, B., Nutman, A. P., Liu, D., & Wu, J., 1996. 3800 to 2500 Ma crustal evolution in the Anshan area of Liaoning Province, northeastern China. Precambrian Research, 78(1–3), 79–94.

Sun, S.S., McDonough, W.F., 1989. Chemical and isotopic systematics of oceanic basalts; implications for mantle composition and processes. In: Saunders, A.D., Norry, M.J. (Eds.), Magmatism in the Ocean Basins. London, Geological Society of London, pp. 313–345.

Tanaka, T., Togashi, S., Kamioka, H., Amakawa, H., Kagami, H., Hamamoto, T., Yuharad, M., Orihashie, Y., Yonedaf, S., Shimizug, H., Kunimarug, T., Takahashih, K., Yanagii, T., Nakanoj, T., Fujimakik, H., Shinjol, R., Asaharaa, Y., Tanimizua, M., Dragusanu, C., 2000. JNdi-1: a neodymium isotopic reference in consistency with LaJolla neodymium. Chem. Geol.168 (3), 279–281.

Van Kranendonk, M. J., 1990. Late Archean geologic history of the Nain Province, North River-Nutak map area, Labrador, and its tectonic significance. Geoscience Canada, 17(4), 231–237.

Wasilewski, B., O'Neil, J., Rizo, H., Paquette, J-L., Gannoun, A-M., Boyet, M. In prep. Geochemistry, geochronology and Lu-Hf isotopic signature of granitoids from the Saglek-Hebron Complex (Northern Labrador, Canada)

Wasilewski, B., O'Neil, J., Rizo, H., 2019. Geochemistry and petrogenesis of the early Archean mafic crust from the Saglek-Hebron Complex (Northern Labrador).

Wendt, J. I., & Collerson, K. D. 1999. Early Archæan U / Pb fractionation and timing of late Archæan high-grade metamorphism in the Saglek – Hebron segment of the North Atlantic Craton, 93, 281–297.

White, W.M., 2013. Geochemistry. John Wiley & Sons.

Whitehouse, M. J., Dunkley, D. J., Kusiak, M. A., Wilde, S. A., 2019. On the true antiquity of Eoarchean chemofossils – assessing the claim for Earth's oldest biogenic graphite in the Saglek Block of Labrador. Elsevier.

Wilde, S. A, Valley, J. W., Peck, W. H., & Graham, C. M., 2001. Evidence from detrital zircons for the existence of continental crust and oceans on the Earth 4.4 Gyr ago. Nature, 409(6817), 175–178.

Wilde, S. A., & Spaggiari, C., 2007. Chapter 3.6 The Narryer Terrane, Western Australia: A Review. In Earth's Oldest Rocks (Vol. 15, pp. 275–304). Elsevier.

Windley, B.F. and Garde, A.A., 2009. Arc-generated blocks with crustal sections in the North Atlantic craton of West Greenland: crustal growth in the Archean with modern analogues. Earth-Science Reviews, 93(1-2), pp.1-30.

Winter, J., Feininger, T., 2001. An Introduction to Igneous and Metamorphic Petrology. Prentice-Hall Inc

Wu, F. Y., Zhang, Y. Bin, Yang, J. H., Xie, L. W., & Yang, Y. H., 2008. Zircon U-Pb and Hf isotopic constraints on the Early Archean crustal evolution in Anshan of theNorth China Craton. Precambrian Research, 167(3–4), 339–362.

Appendix

Table A1: Sample location and coordinates in Easting and Northing UTM NAD 27 zone 20

Sample	Lithology	Unit	Location	Easting	Northing
SG-011	Mafic metavolcanic rock	Nulliak	Ukkalek Island	522810	6461353
SG-021	Mafic metavolcanic rock	Nulliak	Ukkalek Island	522676	6461130
SG-029A	Mafic metavolcanic rock	Nulliak	Pangertok Inlet	491355	6470197
SG-035	Mafic metavolcanic rock	Nulliak	Pangertok Inlet	491247	6470184
SG-044	Mafic metavolcanic rock	Nulliak	Pangertok Inlet	491234	6470293
SG-046	Mafic metavolcanic rock	Nulliak	Pangertok Inlet	491285	6470345
SG-051	Mafic metavolcanic rock	Nulliak	Pangertok Inlet	491726	6469933
SG-065	Andesite	Upernavik	Kangidluasuk Inlet	512688	6478616
SG-071	Mafic metavolcanic rock	Upernavik	Kangidluasuk Inlet	512451	6478457
SG-072	Mafic metavolcanic rock	Upernavik	Kangidluasuk Inlet	512444	6478360
SG-075	Mafic metavolcanic rock	Upernavik	Kangidluasuk Inlet	512637	6478211
SG-079	Mafic metavolcanic rock	Upernavik	Kangidluasuk Inlet	513114	6478006
SG-090	Mafic metavolcanic rock	Nulliak	Aupaluttoq	522486	6439978
SG-092	Mafic metavolcanic rock	Nulliak	Aupaluttoq	522628	6440162
SG-095	Mafic metavolcanic rock	Nulliak	Aupaluttoq	522733	6440261
SG-101	Mafic metavolcanic rock	Nulliak	Aupaluttoq	522942	6440450
SG-109B	Mafic metavolcanic rock	Nulliak	Aupaluttoq	523517	6440334
SG-110	Mafic metavolcanic rock	Nulliak	Aupaluttoq	523611	6440181
SG-112	Mafic metavolcanic rock	Nulliak	Aupaluttoq	523717	6440091
SG-115	Mafic metavolcanic rock	Nulliak	Aupaluttoq	523681	6439924
SG-123	Mafic metavolcanic rock	Upernavik	Upernavik Island	502469	6483981
SG-126	Mafic metavolcanic rock	Upernavik	Upernavik Island	502460	6484045
SG-128	Mafic metavolcanic rock	Upernavik	Upernavik Island	501508	6482743
SG-129	Mafic metavolcanic rock	Upernavik	Upernavik Island	501503	6482792
SG-130	Mafic metavolcanic rock	Upernavik	Upernavik Island	501490	6482839
SG-006	Ultramafic rock	Nulliak	Ukkalek Island	522662	6461603
SG-009	Ultramafic rock	Nulliak	Ukkalek Island	522717	6461519
SG-010	Ultramafic rock	Nulliak	Ukkalek Island	522714	6461519
SG-013	Ultramafic rock	Nulliak	Ukkalek Island	522811	6461191
SG-015	Ultramafic rock	Nulliak	Ukkalek Island	522807	6461187
SG-022	Ultramafic rock	Nulliak	Ukkalek Island	522635	6461145
SG-023	Ultramafic rock	Nulliak	Ukkalek Island	522601	6461303
SG-063	Ultramafic rock	Upernavik	Kangidluasuk Inlet	512629	6478655
SG-064	Ultramafic rock	Upernavik	Kangidluasuk Inlet	512690	6478633
SG-066	Ultramafic rock	Upernavik	Kangidluasuk Inlet	512559	6478682
SG-067	Ultramafic rock	Upernavik	Kangidluasuk Inlet	512554	6478561
SG-068	Ultramafic rock	Upernavik	Kangidluasuk Inlet	512546	6478561
SG-069	Ultramafic rock	Upernavik	Kangidluasuk Inlet	512551	6478553
SG-099	Ultramafic rock	Nulliak	Aupaluttoq	522931	6440466
SG-100	Ultramafic rock	Nulliak	Aupaluttoq	522937	6440458
SG-205	Ultramafic rock	Nulliak	Opposite coast of Nulliak Island	522755	6463676
SG-221	Ultramafic rock	Nulliak	Kangidluasuk Inlet	513991	6481276
SG-240	Ultramafic rock	Upernavik	Torr bay	509842	6480373
SG-243	Ultramafic rock	Upernavik	Torr bay	509859	6480435
SG-001	Mafic Dike	N/A	Hebron fjord	513752	6441990
SG-036	Mafic Dike	N/A	Pangertok	491248	6470194
SG-040	Mafic Dike	N/A	Pangertok	491327	6470259

Sample	Lithology	Unit	Location	Easting	Northing
SG-050	Mafic Dike	N/A	Pangertok	491744	6469968
SG-052	Mafic Dike	N/A	Pangertok	491737	6469733
SG-058	Mafic Dike	N/A	Pangertok	491659	6469784
SG-059	Mafic Dike	N/A	Pangertok	491625	6469829
SG-094	Mafic Dike	N/A	Aupaluttoq	522724	6440240
SG-098	Mafic Dike	N/A	Aupaluttoq	522865	6440434
SG-118	Mafic Dike	N/A	Kangidluasuk Inlet	511798	6479821
SG-120	Mafic Dike	N/A	Kangidluasuk Inlet	512061	6482301
SG-121	Mafic Dike	N/A	Kangidluasuk Inlet	513501	6482912
SG-211	Mafic Dike	N/A	Kangidluasuk East	513429	6482910
SG-212	Mafic Dike	N/A	Kangidluasuk East	513426	6482910
SG-213	Mafic Dike	N/A	Kangidluasuk East	513420	6482906
SG-214	Mafic Dike	N/A	Kangidluasuk East	513418	6482902
SG-215	Mafic Dike	N/A	Kangidluasuk East	513417	6482891
SG-217	Mafic Dike	N/A	Kangidluasuk East	513255	6481182
SG-218	Mafic Dike	N/A	Kangidluasuk East	513250	6481195
SG-219	Mafic Dike	N/A	Kangidluasuk East	513249	6481203
SG-220	Mafic Dike	N/A	Kangidluasuk East	513245	6481210
SG-222	Mafic Dike	N/A	Kangidluasuk East	514023	6481311
SG-249	Mafic Dike	N/A	Big Island	518861	6488019
SG-261	Mafic Dike	N/A	Big Island	520546	6488579
SG-262	Mafic Dike	N/A	Big Island	520547	6488554
SG-268	Mafic Dike	N/A	White Point	523217	6476533
SG-269	Mafic Dike	N/A	White Point	523218	6476516
BR-82-119b	Saglek Dike	N/A	Pangertok	491630	6481720
BR-83-122	Saglek Dike	N/A	Between Saglek and Hebron Fjord	509570	6466410
BR-83-46b	Saglek Dike	N/A	Between Saglek and Hebron Fjord	510630	6474530
SG-225	Saglek Dike	N/A	Nulliak Island	523503	6462825
SG-226	Saglek Dike	N/A	Nulliak Island	523503	6462834
SG-231	Saglek Dike	N/A	Nulliak Island	523657	6462844
SG-232	Saglek Dike	N/A	Nulliak Island	523704	6462809
SG-237	Saglek Dike	N/A	Nulliak Island	523529	6462815
SG-250	Saglek Dike	N/A	Big Island	518843	6488027
SG-251	Saglek Dike	N/A	Big Island	518856	6487973
SG-253	Saglek Dike	N/A	Big Island	518863	6487959
SG-256	Saglek Dike	N/A	Big Island	520443	6488533
SG-257	Saglek Dike	N/A	Big Island	520493	6488585
SG-263	Saglek Dike	N/A	Big Island	520589	6488564
SG-289	Saglek Dike	N/A	Kyuktok	498025	6477836

Table A2: Detection limit of the major elements concentrations measured on the XRF at the University of Ottawa

Elements	Detection limit (wt%)
Na_2O	0.007
MgO	0.018
Al_2O_3	0.009
SiO_2	0.02
P_2O_5	0.017
K_2O	0.033
CaO	0.052
TiO_2	0.047
MnO	0.074
Fe_2O_3	0.116

Table A3: Column chemistry protocol

Primary Columns
Biorad columns (10 ml) filled with 2 ml
AG50W-X8, 200-400 mesh

Step	Eluent	Volume
Conditioning	2 N HCl	10 ml
		10 ml
Load Sample	**2 N HCl**	**2 ml**
Rinse	2 N HCl	1 ml
		1ml
Discard	2 N HCl	8 ml
		8 ml
Discard	2.5 N HCl	10 ml
Collect LREE	**6 N HCl**	**10 ml**
Wash	6 N HCl	10 ml
	6 N HCl	10 ml
	MQ H20	10 ml
	6 N HCl	10 ml
	MQ H20	10 ml
Store	MQ H20 + squirt HCl	

Large Quartz Primary columns
AG50W-X8, 200-400 mesh, 18cm x 1 cm ID in 4M HCl

Step	Eluent	Volume
Conditioning	2.5 N HCl	30 ml
Load sample	**2.5 N HCl**	**4 ml**
Rinse	2.5 N HCl	2 ml
		2 ml
Discard	2.5 N HCl	90 ml
Discard	4 N HCl	20 ml
Collect LREE	**4 N HCl**	**50 ml**
Wash	6 N HCl	100 ml
Backwash	**MQ H20 + squirt HCl**	

LN-spec resin column

Quartz columns: LN spec resin 50-100 μm 300 mg, 68 mm x 4 mm

Step	Eluent	Volume
Conditioning	0.2 N HCl	3 ml
Load Sample	**0.2 N HCl**	**0.25 ml**
Rinse	0.2 N HCl	0.25 ml
Discard	0.2 N HCl	4.5 ml
Collect Nd	**0.2 N HCl**	**5.5 ml**
Rinse	0.5 N HCl	0.5 ml
Collect Sm	**0.5 N HCl**	**2.75 ml**
Wash	6 N HCl	10 ml
	MQ H20 + squirt HCl	10 ml
Store	MQ H20 + squirt HCl	

Table A4: Whole-rock chemistry of the ultramafic and mafic samples studied here. Major element concentrations are reported in wt% and trace element concentrations are reported in ppm. Elements with concentrations below detection limits are marked as BDL. (Low-Fe = low-Fe ultramafic rocks; High-Fe = High-Fe ultramafic rocks; M = Mafic metavolcanic rocks)

Sample	SG006	SG009	SG010	SG013	SG015	SG022	SG023	SG063	SG064
Lithology	Low-Fe	Low-Fe	Low-Fe	High-Fe	High-Fe	Low-Fe	High-Fe	High-Fe	Low-Fe
Unit	Nulliak	Nulliak	Nulliak	Nulliak	Nulliak	Nulliak	Nulliak	Upernavik	Upernavik
SiO_2	50.16	48.48	45.07	43.91	44.25	46.77	44.78	45.60	42.76
TiO_2	0.21	0.35	0.36	0.22	0.21	0.07	0.59	0.89	0.33
Al_2O_3	6.53	9.42	9.61	2.04	1.87	2.53	7.24	7.93	12.07
FeO	9.29	9.94	11.54	12.78	11.63	7.71	13.61	12.43	9.92
MnO	0.17	0.15	0.17	0.22	0.19	0.18	0.24	0.19	0.13
MgO	29.45	21.07	27.11	35.59	36.10	41.35	21.24	22.48	28.63
CaO	2.59	7.88	4.17	3.05	3.89	0.06	9.32	8.49	4.78
Na_2O	0.40	1.31	0.55	0.11	0.18	0.00	1.11	0.41	0.20
K_2O	0.17	0.29	0.12	0.65	0.36	0.47	0.31	0.14	0.05
P_2O_5	0.00	0.00	0.02	0.00	0.02	0.00	0.04	0.06	0.02
LOI	4.65	1.32	0.69	4.31	2.71	4.25	1.01	4.64	8.47
Sc	BDL	BDL	BDL	BDL	BDL	BDL	29.0	BDL	BDL
V	110	142	150	54.0	55.0	44.0	179	211	194
Cr	2520	2490	2630	1430	1510	5410	2150	1780	3190
Co	83.0	82.0	102	121	125	106	97.0	52.0	82.0
Ni	1600	880	1080	2260	2380	2570	800	400	830
Cu	40.0	40.0	BDL	20.0	BDL	BDL	50.0	50.0	BDL
Ga	6.00	9.00	9.00	4.00	3.00	3.00	9.00	10.0	9.00
Ge	1.50	1.20	1.20	1.20	1.30	1.60	1.50	1.20	1.10
Rb	4.00	4.00	1.00	32.0	18.0	26.0	4.00	2.00	2.00
Sr	17.0	69.0	62.0	39.0	15.0	BDL	76.0	99.0	16.0
Y	5.20	9.00	10.6	5.00	3.50	1.50	12.5	16.7	6.70
Zr	5.00	15.0	16.0	10.0	11.0	6.00	34.0	53.0	17.0
Nb	BDL	BDL	BDL	1.20	BDL	BDL	0.900	1.20	0.40
Cs	0.800	0.200	BDL	1.60	1.50	4.80	BDL	0.300	0.600
Ba	6.00	8.00	7.00	280	36.0	9.00	9.00	21.0	BDL
La	0.34	1.47	1.45	4.10	1.47	BDL	2.23	4.05	0.25
Ce	0.690	4.47	4.00	11.2	3.42	0.100	6.24	10.8	0.570
Pr	0.11	0.650	0.610	1.67	0.44	0.020	1.03	1.61	0.08
Nd	0.540	3.07	2.83	8.45	1.98	0.0500	5.27	8.00	0.560
Sm	0.26	0.97	0.98	1.70	0.57	0.020	1.73	2.56	0.240
Eu	0.147	0.496	0.455	0.412	0.224	BDL	0.533	1.27	0.127
Gd	0.470	1.09	1.31	1.47	0.640	0.040	2.20	2.96	0.510
Tb	0.110	0.210	0.260	0.180	0.100	0.020	0.380	0.550	0.110
Dy	0.81	1.47	1.71	0.96	0.67	0.16	2.36	3.35	0.90
Ho	0.180	0.290	0.350	0.170	0.120	0.050	0.490	0.630	0.220
Er	0.540	0.900	1.05	0.460	0.350	0.200	1.42	1.64	0.650
Tm	0.087	0.142	0.160	0.061	0.047	0.036	0.199	0.223	0.104
Yb	0.560	0.970	1.00	0.380	0.330	0.260	1.21	1.42	0.75
Lu	0.094	0.150	0.155	0.058	0.051	0.044	0.176	0.219	0.134
Hf	0.20	0.40	0.50	0.30	0.30	0.10	0.80	1.30	0.50
Ta	BDL	0.020	0.040	0.230	0.010	BDL	0.070	0.110	0.180
Pb	BDL	BDL	BDL	BDL	BDL	BDL	BDL	BDL	BDL
Th	0.060	0.150	0.240	0.200	0.630	0.100	0.200	0.460	BDL
U	0.120	0.190	0.120	0.110	0.080	0.060	0.120	0.140	0.050

Table A4 (CONTINUED): Whole-rock chemistry of the ultramafic and mafic samples studied here. Major element concentrations are reported in wt% and trace element concentrations are reported in ppm. Elements with concentrations below detection limits are marked as BDL. (Low-Fe = low-Fe ultramafic rocks; High-Fe = High-Fe ultramafic rocks; M = Mafic metavolcanic rocks)

Sample	SG066	SG067	SG068	SG069	SG099	SG100	SG205	SG221
Lithology	Low-Fe	High-Fe	High-Fe	High-Fe	High-Fe	High-Fe	High-Fe	Low-Fe
Unit	Upernavik	Upernavik	Upernavik	Upernavik	Nulliak	Nulliak	Nulliak	Nulliak
SiO_2	46.32	48.42	45.94	46.67	43.35	46.65	45.42	45.93
TiO_2	0.20	0.76	0.79	0.81	0.39	0.55	0.41	0.13
Al_2O_3	8.83	5.34	7.07	6.87	3.49	4.98	3.80	7.24
FeO	8.79	11.68	12.64	12.40	15.12	13.22	11.81	7.66
MnO	0.12	0.20	0.25	0.18	0.18	0.17	0.19	0.14
MgO	29.41	20.05	20.31	21.51	31.21	23.37	31.29	36.25
CaO	5.10	11.96	10.90	9.82	4.17	8.14	4.68	1.67
Na_2O	0.18	0.18	0.21	0.22	0.20	0.40	0.46	0.10
K_2O	0.05	0.07	0.43	0.08	0.18	1.01	0.57	0.01
P_2O_5	0.01	0.05	0.05	0.06	0.02	0.03	0.04	0.02
LOI	7.92	3.88	4.08	3.97	6.99	3.65	8.01	9.59
Sc	BDL	BDL	BDL	BDL	BDL	BDL	BDL	BDL
V	120	177	187	190	101	153	83.0	95.0
Cr	3320	1810	1580	1420	2140	2190	1400	2730
Co	95.0	70.0	67.0	62.0	132	74.0	101	92.0
Ni	1660	670	860	580	1300	700	1870	1940
Cu	BDL	BDL	130	20.0	60.0	BDL	30.0	BDL
Ga	7.00	7.00	9.00	9.00	5.00	7.00	5.00	6.00
Ge	1.20	1.70	1.20	1.20	1.70	1.70	1.20	0.900
Rb	1.00	1.00	15.0	2.00	4.00	65.0	39.0	BDL
Sr	16.0	75.0	138	82.0	13.0	15.0	8.00	5.00
Y	6.70	13.4	14.4	14.2	6.20	10.9	7.00	3.50
Zr	8.00	41.0	43.0	45.0	22.0	27.0	23.0	5.00
Nb	BDL	1.90	1.00	1.00	1.30	1.60	0.30	BDL
Cs	0.700	0.100	3.90	0.000	0.500	52.4	1.60	0.300
Ba	5.00	5.00	123	16.00	43.0	131	23.0	BDL
La	0.33	2.85	3.05	3.51	1.88	3.54	1.96	0.17
Ce	0.73	7.71	8.27	8.99	4.75	8.99	5.16	0.400
Pr	0.13	1.15	1.31	1.37	0.66	1.27	0.75	0.07
Nd	0.620	6.24	6.35	6.50	3.19	6.26	3.86	0.30
Sm	0.24	2.01	2.10	2.01	1.03	1.78	1.09	0.150
Eu	0.118	0.825	1.03	0.775	0.268	0.657	0.363	0.088
Gd	0.480	2.40	2.54	2.49	1.09	2.03	1.27	0.25
Tb	0.110	0.390	0.420	0.430	0.190	0.330	0.230	0.060
Dy	0.92	2.40	2.59	2.67	1.16	1.95	1.29	0.48
Ho	0.220	0.480	0.520	0.510	0.220	0.390	0.250	0.120
Er	0.670	1.33	1.37	1.44	0.580	1.06	0.700	0.370
Tm	0.106	0.180	0.192	0.187	0.087	0.148	0.096	0.059
Yb	0.700	1.10	1.10	1.13	0.590	0.950	0.600	0.420
Lu	0.106	0.153	0.154	0.162	0.083	0.144	0.085	0.069
Hf	0.20	1.30	1.00	1.10	0.60	0.90	0.50	0.20
Ta	BDL	0.280	0.130	0.110	0.240	0.240	0.030	BDL
Pb	BDL	BDL	BDL	BDL	6.00	BDL	BDL	BDL
Th	BDL	0.320	0.450	0.430	0.290	0.520	0.380	BDL
U	0.000	0.120	0.130	0.150	0.130	0.290	0.180	0.030

Table A4 (CONTINUED): Whole-rock chemistry of the ultramafic and mafic samples studied here. Major element concentrations are reported in wt% and trace element concentrations are reported in ppm. Elements with concentrations below detection limits are marked as BDL. (Low-Fe = Low-Fe ultramafic rocks; High-Fe = High-Fe ultramafic rocks; M = Mafic metavolcanic rocks)

Sample	SG240	SG243	SG011	SG021	SG029A	SG035	SG044	SG046	SG051
Lithology	Low-Fe	Low-Fe	M	M	M	M	M	M	M
Unit	Upernavik	Upernavik	Nulliak	Nulliak	Nulliak	Nulliak	Nulliak	Nulliak	Nulliak
SiO_2	42.09	42.85	46.56	50.67	50.02	49.47	47.09	48.29	46.64
TiO_2	0.13	0.14	0.96	0.85	0.78	0.94	1.09	0.37	0.91
Al_2O_3	3.84	4.09	14.14	7.77	14.05	16.02	15.83	17.61	15.38
FeO	10.39	10.53	11.41	12.14	11.31	9.92	12.94	7.24	12.22
MnO	0.18	0.17	0.16	0.25	0.18	0.20	0.23	0.13	0.24
MgO	38.47	36.94	9.24	12.58	8.27	6.66	8.22	9.50	8.59
CaO	3.12	3.50	13.52	10.74	11.56	12.51	11.07	14.40	12.38
Na_2O	0.48	0.49	2.02	1.42	2.44	2.88	1.65	1.46	2.10
K_2O	0.14	0.09	0.67	2.15	0.08	0.21	0.37	0.19	0.17
P_2O_5	0.01	0.02	0.05	0.08	0.05	0.07	0.09	0.01	0.01
LOI	0.87	1.58	0.52	0.63	0.00	0.25	0.00	0.57	0.00
Sc	BDL	BDL	45.4	29.7	52.0	47.0	47.0	39.0	47.2
V	70.0	70.0	270	154	319	288	339	189	326
Cr	3090	2640	367	1282	240	150	200	840	362
Co	123	123	53.0	72.2	52.0	39.0	53.0	41.0	50.9
Ni	2520	2310	155	514	100	70.0	110	170	113
Cu	BDL	BDL	2.55	71.8	130	20.0	BDL	50.0	17.9
Ga	4.00	4.00	16.5	15.3	17.0	18.0	19.0	18.0	17.1
Ge	1.00	1.00	1.56	1.67	2.10	1.80	1.80	2.30	1.64
Rb	3.00	1.00	5.33	150.60	BDL	BDL	3.00	1.00	2.11
Sr	10.0	9.00	278	129	211	209	220	90.0	105
Y	3.00	3.70	19.5	17.8	18.9	20.7	25.7	10.6	24.7
Zr	5.00	6.00	37.3	45.3	27.0	44.0	52.0	11.0	40.2
Nb	BDL	BDL	1.52	6.53	1.80	2.00	2.40	3.90	2.28
Cs	BDL	0.200	0.029	2.98	BDL	BDL	BDL	BDL	0.065
Ba	8.00	5.00	27.1	339	15.0	37.0	70.0	17.0	21.8
La	0.69	0.58	2.71	9.64	2.05	2.97	4.50	1.66	1.96
Ce	1.60	1.46	7.08	29.5	6.88	9.31	12.9	4.35	6.26
Pr	0.22	0.21	1.09	4.71	1.18	1.48	2.04	0.65	1.10
Nd	0.92	1.00	5.77	21.4	6.35	7.44	9.76	3.03	5.87
Sm	0.31	0.32	1.99	5.07	2.10	2.59	3.07	1.09	2.24
Eu	0.119	0.117	0.715	0.679	0.806	0.829	0.986	0.366	0.809
Gd	0.37	0.51	2.64	4.62	2.82	3.17	3.84	1.53	3.19
Tb	0.080	0.090	0.489	0.643	0.490	0.570	0.730	0.290	0.625
Dy	0.49	0.61	3.26	3.48	3.51	3.76	5.06	1.91	4.27
Ho	0.110	0.120	0.714	0.657	0.740	0.810	1.07	0.410	0.925
Er	0.340	0.360	2.02	1.81	2.23	2.36	3.11	1.21	2.60
Tm	0.049	0.056	0.311	0.241	0.312	0.339	0.453	0.183	0.386
Yb	0.31	0.39	2.06	1.48	2.14	2.17	3.01	1.17	2.51
Lu	0.048	0.064	0.302	0.216	0.338	0.357	0.471	0.182	0.369
Hf	0.20	0.20	1.30	1.35	1.10	1.30	1.60	0.50	1.28
Ta	BDL	BDL	0.167	0.385	0.050	0.090	0.100	0.680	0.147
Pb	BDL	BDL	3.51	3.87	BDL	BDL	BDL	BDL	1.37
Th	0.130	0.110	0.305	0.229	BDL	BDL	0.280	BDL	0.028
U	0.080	0.090	0.201	0.092	0.000	0.020	0.030	0.020	0.011

Table A4 (CONTINUED): Whole-rock chemistry of the ultramafic and mafic samples studied here. Major element concentrations are reported in wt% and trace element concentrations are reported in ppm. Elements with concentrations below detection limits are marked as BDL. (Low-Fe = Low-Fe ultramafic rocks; High-Fe = High-Fe ultramafic rocks; M = Mafic metavolcanic rocks)

Sample	SG065	SG071	SG072	SG075	SG079	SG090	SG092	SG095	SG101
Lithology	Andesite	M	M	M	M	M	M	M	M
Unit	Upernavik	Upernavik	Upernavik	Upernavik	Upernavik	Nulliak	Nulliak	Nulliak	Nulliak
SiO_2	56.18	49.60	48.22	49.72	52.39	49.22	51.69	52.81	46.13
TiO_2	2.82	1.13	1.14	0.52	0.89	0.62	0.79	0.76	0.82
Al_2O_3	14.80	14.97	15.29	16.76	14.68	16.03	14.30	13.85	12.28
FeO	9.76	12.21	12.21	8.53	9.74	9.20	10.38	10.30	13.91
MnO	0.15	0.20	0.20	0.17	0.20	0.18	0.18	0.17	0.22
MgO	3.97	6.71	7.82	9.25	7.57	8.43	7.80	8.43	14.02
CaO	6.48	11.13	10.67	11.82	10.78	13.29	10.94	9.51	9.12
Na_2O	2.88	2.22	2.52	1.78	2.42	1.56	2.22	2.13	1.05
K_2O	1.55	0.38	0.49	0.47	0.20	0.38	0.50	0.82	0.84
P_2O_5	0.34	0.09	0.09	0.03	0.05	0.07	0.05	0.07	0.05
LOI	1.47	0.92	0.84	1.63	0.88	1.61	1.44	2.40	3.53
Sc	12.5	BDL	BDL	BDL	BDL	45.0	43.0	41	BDL
V	99.1	342	350	200	320	248	280	264	274
Cr	61.5	240	240	860	390	550	310	260	190
Co	30.2	49.0	52.0	52.0	51.0	41.0	44.0	43.0	80.0
Ni	56.7	130	150	200	110	130	90.0	80.0	380
Cu	10.5	20.0	20.0	30.0	30.0	10.0	50.0	20.0	BDL
Ga	25.4	17.0	17.0	13.0	15.0	16.0	16.0	16.0	14.0
Ge	1.55	1.20	1.30	1.70	1.40	2.40	2.30	2.40	1.80
Rb	72.6	7.00	8.00	15.0	5.00	5.00	6.00	26.0	36.0
Sr	531	111	93.0	126	125	75.0	123	103	25.0
Y	22.5	23.7	24.0	9.30	14.1	13.8	17.3	15.6	19.8
Zr	164	51.0	57.0	16.0	33.0	27.0	51.0	56.0	37.0
Nb	43.5	3.00	2.80	1.30	1.80	1.50	2.40	2.30	1.90
Cs	2.21	0.100	0.300	0.700	0.000	0.700	0.700	2.30	5.90
Ba	4.00	42.00	50.00	110	43.0	66.0	82.0	215	87.0
La	29.9	5.22	4.39	2.05	2.90	2.96	5.57	5.24	3.25
Ce	66.8	13.2	11.2	5.25	7.70	7.45	12.0	11.4	8.17
Pr	8.60	1.89	1.61	0.72	1.18	1.11	1.59	1.60	1.18
Nd	34.6	9.59	8.55	3.29	5.92	5.14	7.31	7.34	5.76
Sm	7.16	2.81	2.83	1.10	2.01	1.58	2.03	1.99	1.84
Eu	2.28	1.03	0.982	0.484	0.789	0.575	0.691	0.737	0.583
Gd	6.96	3.86	3.65	1.48	2.65	2.08	2.63	2.60	2.74
Tb	0.948	0.690	0.660	0.260	0.460	0.380	0.470	0.450	0.460
Dy	4.78	4.44	4.22	1.76	2.91	2.57	3.03	2.99	3.13
Ho	0.811	0.910	0.890	0.360	0.580	0.540	0.640	0.630	0.670
Er	2.03	2.61	2.59	0.990	1.66	1.62	1.85	1.81	2.01
Tm	0.241	0.391	0.392	0.151	0.231	0.236	0.278	0.270	0.294
Yb	1.40	2.52	2.49	1.02	1.51	1.48	1.84	1.71	1.94
Lu	0.194	0.379	0.394	0.155	0.236	0.231	0.284	0.279	0.292
Hf	4.42	1.70	1.70	0.60	1.20	0.80	1.30	1.50	1.20
Ta	2.46	0.280	0.270	0.130	0.170	0.070	0.180	0.160	0.320
Pb	6.59	BDL	BDL	BDL	BDL	12.0	9.00	5.00	BDL
Th	3.13	0.280	0.370	0.080	0.270	0.070	0.970	0.490	0.300
U	1.442	0.160	0.140	0.030	0.090	0.080	0.310	0.200	0.260

Table A4 (CONTINUED): Whole rock chemistry of the ultramafic and mafic samples analysed for this study. Major element concentrations are reported in wt% and trace element concentrations are reported in ppm. Elements with concentration below the detection limit are marked as BDL. (Low-Fe = Low-Fe ultramafic rocks; High-Fe = High-Fe ultramafic rocks; M = Mafic metavolcanic rocks)

Sample	SG109B	SG110	SG112	SG123	SG126	SG128	SG129	SG130
Lithology	M	M	M	M	M	M	M	M
Unit	Nulliak	Nulliak	Nulliak	Upernavik	Upernavik	Upernavik	Upernavik	Upernavik
SiO_2	48.65	47.45	49.10	48.40	46.27	47.91	48.19	47.93
TiO_2	0.69	0.38	0.73	0.39	1.00	0.66	0.81	0.66
Al_2O_3	15.73	17.01	15.17	17.57	16.65	15.66	14.98	15.39
FeO	9.17	8.75	11.07	8.46	12.38	10.18	10.50	10.10
MnO	0.21	0.15	0.20	0.17	0.22	0.16	0.18	0.17
MgO	10.04	10.89	8.27	9.31	8.58	10.51	9.92	9.43
CaO	12.62	12.53	11.16	12.21	11.23	11.67	11.52	12.95
Na_2O	1.56	1.51	2.61	1.17	1.76	1.83	2.23	1.99
K_2O	0.26	0.33	0.42	1.35	0.45	0.23	0.45	0.19
P_2O_5	0.05	0.02	0.04	0.03	0.07	0.05	0.05	0.06
LOI	1.09	1.16	0.73	2.58	0.47	0.40	0.76	0.36
Sc	BDL	BDL	BDL	26.0	41.4	29.0	33.0	31.0
V	260	136	216	153	281	198	267	215
Cr	170	550	240	400	378	440	440	390
Co	44.0	56.0	52.0	53.0	58.7	55.0	55.0	51.0
Ni	90.0	280	180	240	173	310	270	260
Cu	80.0	BDL	110	BDL	98.1	20.0	20.0	50.0
Ga	16.0	13.0	13.0	13.0	20.2	16.0	19.0	16.0
Ge	2.10	1.00	1.30	2.30	1.65	1.50	1.80	1.70
Rb	7.00	4.00	6.00	25.0	2.39	1.00	3.00	2.00
Sr	96.0	96.0	130	97.0	66.1	93.0	86.0	126
Y	18.2	8.80	12.6	7.90	21.2	13.1	15.5	14.8
Zr	32.0	15.0	21.0	21.0	33.8	37.0	42.0	37.0
Nb	1.70	1.00	1.40	0.90	2.23	1.80	1.70	1.60
Cs	0.700	0.200	0.400	0.100	0.041	BDL	BDL	BDL
Ba	22.0	37.0	130	149	41.0	24.0	43.0	38.0
La	1.80	1.53	2.99	2.55	9.53	3.50	2.53	3.86
Ce	5.75	4.08	7.58	5.25	21.3	9.32	7.21	9.50
Pr	0.90	0.61	1.11	0.66	2.73	1.44	1.12	1.44
Nd	4.89	2.78	5.37	2.99	11.2	6.98	5.57	6.61
Sm	1.85	0.980	1.81	0.93	2.90	1.95	1.85	1.96
Eu	0.564	0.459	0.752	0.474	0.818	0.701	0.676	0.742
Gd	2.46	1.37	2.11	1.22	3.13	2.38	2.58	2.49
Tb	0.440	0.250	0.400	0.220	0.530	0.400	0.460	0.450
Dy	2.94	1.60	2.50	1.40	3.57	2.54	3.02	2.82
Ho	0.600	0.320	0.480	0.300	0.786	0.520	0.620	0.580
Er	1.72	0.930	1.31	0.920	2.25	1.50	1.78	1.69
Tm	0.259	0.140	0.183	0.133	0.346	0.223	0.260	0.248
Yb	1.80	0.950	1.20	0.850	2.20	1.37	1.62	1.52
Lu	0.280	0.153	0.199	0.135	0.318	0.219	0.244	0.237
Hf	1.10	0.50	0.70	0.60	1.21	1.20	1.30	1.10
Ta	0.240	0.090	0.110	0.040	0.154	0.080	0.060	0.060
Pb	5.00	BDL	17.0	BDL	2.78	BDL	BDL	BDL
Th	BDL	BDL	0.150	1.16	1.32	0.110	BDL	0.160
U	0.020	0.000	0.050	0.620	0.269	0.030	0.030	0.060

Table A5: Petrological descriptions of the Saglek dikes

Saglek dikes				
Sample	**Mineral abundances**	**Alteration minerals**	**Textures**	**Notes**
BR-82-119B	50% amphiboles (hornblende + actinolite) + 20% plagioclase + 10% garnet + 5% feldspar + 5% chlorite + 5% sulphides and oxides	moderate to strong alteration, moderate alteration of plagioclase into sericite	subeuhedral amphibole and plagioclase grains	sutured contacts, reaction rims around amphiboles
BR-83-122	40% amphibole (hornblende) + 20% quartz + 20% plagioclase + 15% clinopyroxene + 5% oxides and sulphides	weak alteration of pyroxene	Stubby plagioclase	possible cumulate texture : amphiboles around plagioclase
BR-83-46B	40% amphibole (hornblende) + 25% plagioclase + 15% feldspar + 15% quartz + 5% iron oxides	weak to no apparent alteration	Tabular plagioclase	clear cleavage of amphibole, reaction rims around amphibole grains
SG-225	20% biotite + 40% amphibole (Hbd) + 20% plagioclase + 15% quartz + some trace sulphides (pyrite)	weak alteration of plagioclase (very rare)		weak foliation, presence of reaction rims around amphibole rims, elongated biotite
SG-226	40% amphibole (hornblende + actinolite) + 35% plagioclase + 20% clinopyroxene + 5% biotite + trace oxides	strong alteration of pyroxene	euhedral to sub-euhedral amphibole and plagioclase grains	euhedral to subeuhedral grains, weak foliation, clear cleavage present in hornblende grains, reaction rims around the amphibole, actinolite present around the pyroxene grains
SG-231	50% amphibole (hornblende + actinolite) + 40% plagioclase + 5% clinopyroxene + 5% biotite + trace oxides	moderate to strong plagioclase alteration (sericite), strong alteration of pyroxene	subeuhedral amphibole and plagioclase grains	Weak foliation, clear cleavage in hornblende, reaction rims around amphibole grains, pyroxene grains displaying some twinning

Saglek dikes				
Sample	**Mineral abundances**	**Alteration minerals**	**Textures**	**Notes**
SG-232	35% amphiboles (Hornblende) + 35% plagioclase + 20% clinopyroxene + 10 % orthopyroxene + trace oxides	small alteration veinlet	Sub-euhedral amphibole and plagioclase grains, pyroxene displaying exsolution textures	OPX displaying clear cleavage, some poikilitic textures
SG-237	50% amphibole (actinolite + hornblende) + 35% plagioclase + trace biotite + trace oxides + 5% spinel	Moderate to strong alteration of plag (sericite)	Euhedral to sub-euhedral amphibole and plagioclase grains	amphibole grains displaying clear cleavage, presence of reaction rims around the amphiboles, actinolite present as very fine grain
SG-250	45% Amphibole (hornblende and actinolite) + 10% quartz + 35% plagioclase + 5% clinopyroxene + trace olivine (<1%) + some chlorite (1-2%) + disseminated sulphides (<5%) (Bornite and pyrite)	Moderate to strong sericite alteration of feldspars and quartz grains.	euhedral to sub-euhedral amphibole and plagioclase grains	Some amphiboles have very high birefringent rims (CPX), presence of rounded qtz grains within the amphibole grains (Poikilitic), weak foliation
SG-251	50% Amphibole (Hornblende and actinolite), 5% quartz, 20% plagioclase, 10% clinopyroxene, 10% OPX, (<1%), trace chlorite (<1%), Trace olivine (<1%), Disseminated sulphides and oxides (5%) (chromite, pyrite, pyrrhotite)	moderate sericite alteration, moderate alteration of amph, pyroxene	euhedral to sub-euhedral amphibole grains, anhedral plagioclase grains,	Chlorite are long and elongated. Some rounded quartz grains present in the amphiboles (poikilitic); some irregular contact boundaries; amphiboles are the secondary mineral to crystallise, filling the voids between the quartz and plagioclase grains. Amphiboles have display clear 60/120 cleavage. Weak foliation

Saglek dikes				
Sample	**Mineral abundances**	**Alteration minerals**	**Textures**	**Notes**
SG-253	45% Amphibole (hornblende + actinolite) + 30% plagioclase + 15% clinopyroxene + trace olivine (<1%) + trace oxides and sulphides (<5%) (bornite, pyrite)	Moderate to strong sericite alteration. Some alteration of the pyroxene. Moderate alt of pyroxene, plag with spotty alt	euhedral to sub-euhedral amphibole grains, sub-euhedral plagioclase grains	Some contact boundaries are irregular. Weak foliation. Reaction rims around amphibole grains
SG-256	40% amphibole (Hornblende + actinolite) + 25% clinopyroxene + 20% plagioclase + 10% orthopyroxene + trace olivine (1-2%) + some sulphides and oxides (5%) (Bornite)	moderate to strong sericite alteration. Alteration of the pyroxene	euhedral to sub-euhedral amphibole grains, sub-euhedral plagioclase grains	Some poikilitic textures. Weak foliation. Some amphibole with reaction rims
SG-257	40% Amphibole (hornblende + actinolite) + 10% quartz + 35% plagioclase + 10% clinopyroxene + trace chlorite (5%)+ trace biotite (<5%) + Trace sulphides and oxides (<1%) (Bornite, Pyrite)	Moderate to strong sericite alteration	sub-euhedral amphibole and plagioclase grains	Weak foliation (deformation), some irregular grain boundaries (qtz), some poikilitic texture, amphibole grains are subeuhedral
SG-263	55% amphibole (hornblende + actinolite)+ 5% quartz, 30% plagioclase + 10% clinopyroxene + trace olivine (<1%) + some oxides and sulphides (<1%)	weak to moderate sericite alteration	Porphyritic (amphibole grains in finer matrix), euhedral to sub-euhedral amphibole grains	Weak foliation, some poikilitic textures, plagioclase is the secondary mineral, occurring between the amphibole grains. Some amphibole with reaction rims.
SG-289	45% amphibole (hornblende + actinolite) + 35% plagioclase + 10% clinopyroxene + 5% orthopyroxene + 5% quartz + some kspar + some oxides	Broken up/ altered pyroxene grains (most grains)	Equigranular, grains are generally subeuhedral	Some reaction rims around the pyroxene (rare), foliation present but weak

Table A6: Petrological descriptions of the undeformed mafic dikes

Mafic dikes				
Sample	**Mineral Abundances**	**Alteration minerals**	**Textures**	**Notes**
SG-001	40% plagioclase + 30% clinopyroxene + 25% amphibole (hornblende) + 5% oxides + trace sulphides + trace quartz	moderate alteration of pyroxene	Stubby plagioclase grains	some sutured contacts between grains, presence of amphibole between grains (actinolite)
SG-036	45% plagioclase + 35% clinopyroxene + 10% quartz + 5% hornblende + 3% iron oxides + 2% sulphides	moderate alteration of plagioclase and quartz (sericite)	Acicular plagioclase grains, sub-ophitic texture	presence of carlsbad twinning in plagioclase, amphibole around the pyroxene gains (actinolite)
SG-040	45% plagioclase + 35% clinopyroxene + 10% quartz + 5% amphibole (hornblende) + 5% iron oxides	weak to moderate alteration of plagioclase (sericite)	Acicular plagioclase grains, sub-ophitic texture	presence of carlsbad twinning in plagioclase grains, some amphibole around pyroxene grains (actinolite)
SG-050	55% plagioclase + 25% clinopyroxene + 10% amphibole (hornblende + actinolite), 5% oxides + 5% quartz + trace sulphides	moderate alteration of pyroxene, weak to moderate alteration of plagioclase (sericite)	Stubby plagioclase grains, subophitic texture	some amphibole around the pyroxene grains (actinolite)
SG-052	60% amphibole (hornblende) + 30% plagioclase + 5% oxides and sulphides	strong alteration of pyroxene, strongly deformed contacts (sutured)	Elongated plagioclase grains	Some amphibole around pyroxene grains (Actinolite), sutured contacts, highly birefringent inclusions in plagioclase
SG-058	60% plagioclase + 25% clinopyroxene + 10% amphibole (hornblende), 5% oxides and sulphides	weak to moderate alteration of plagioclase (sericite), moderate to strong alteration of pyroxene	Stubby plagioclase grains, subophitic texture	carlsbad twinning, some amphibole around the pyroxene grains
SG-059	50% plagioclase + 30% amphibole (hornblende) + 5% chlorite + 5% oxides and sulphides	strong alteration of pyroxene, chlorite alteration	elongated plagioclase grains	amphibole around pyroxene grains (actinolite)

Mafic dikes				
Sample	**Mineral Abundances**	**Alteration minerals**	**Textures**	**Notes**
SG-094	50% clinopyroxene + 35% plagioclase + 10% amphibole (hornblende + actinolite) + 5% iron oxides + trace sulphides	weak sericite alteration of plagioclase	elongated plagioclase grains, ophitic texture	amphibole around pyroxene grains (actinolite)
SG-098	45% plagioclase + 30% clinopyroxene + 10% amphibole (hornblende) + trace chlorite + trace quartz + trace sulphides and oxides	moderate alteration of pyroxene		sutured contacts
SG-120	45% amphibole (hornblende), 25% quartz + 10% plagioclase + 5% (muscovite + biotite) + trace oxides and sulphides + trace calcite	strong alteration	Porphyritic texture	pyroxene phenocryst in finer matrix, phenocrysts are altered, presence of calcite of possible fracture, weakly foliated, myrmekite textures, presence of sigma structures
SG-121	45% plagioclase + 35% clinopyroxene + 15% amphibole (hornblende + actinolite) + 5% quartz + 5% iron oxides + trace biotite	weak alteration of pyroxene	Elongated plagioclase grains, subophitic textures	myrmekite texture, carlsbad twinning, serpentinised 0.1 mm veinlet cross-cutting, light coloured amph in ppl, actinolite around the grains
SG-211	40% plagioclase + 30% clinopyroxene + 20% orthopyroxene + some sulphides and oxides (10%)(magnetite, illmenite, pyrite, chalcopyrite)	moderate to strong alteration of pyroxene into amphiboles	Equigranular, elongated plagioclase	plagioclase between the pyroxene grains
SG-212	45% Clinopyroxene + 30% plagioclase + 20% orthopyroxene + some opaques (5%) (magnetite, illmenite, pyrite, chalcopyrite)	moderate sericite alteration, moderate to strong alteration of pyroxene, some granophyric texture	Equigranular	Amphibole surrounding the pyroxene (rims), some amphibole present as grains as well. Some carlsbad twinning in the pyroxene. Presence of high relief minerals as elongated needles in pyroxene and plag, some granophyric textures, some presence of radial pyroxenes

Mafic dikes				
Sample	**Mineral Abundances**	**Alteration minerals**	**Textures**	**Notes**
SG-213	40% clinopyroxene + 30% plagioclase + 20% orthopyroxene + amphibole 5% + some oxides (5%) (magnetite, chromite, pyrite, pyrrhotite)	weak to strong sericite alteration, moderate to strong alteration of pyroxene	Equigranular	amphibole occur as grains but also on rims of pyroxenes (alteration product), high relief inclusion in pyroxene, pyroxene exhibiting twinning, some granophyric textures
SG-214	45% clinopyroxene + 25% plagioclase + 20% orthopyroxene + some oxides (5%) (Magnetite, chromite, pyrite)+ 5% trace chlorite (<1%)	moderate sericite alteration, moderate to strong alteration of pyroxene	Equigranular	amphibole occurs mainly as grains but also along the pyroxene rims, high relief inclusions in pyroxenes, some granophyric textures, some radial pyroxenes
SG-215	25% clinopyroxene + 5% amphibole (hornblende) as grains + 45% plagioclase + 15% orthopyroxene + some opaques (5-10%) (magnetite, illmenite, pyrite, chalcopyrite, pyrrhotite) + trace chlorite (1%)	moderate to strong sericite alteration, moderate to strong alteration of pyroxene.	Equigranular	amphibole occurs on the rims and some as grains, carlsbad twinning in the pyroxene, some irregular contact boundaries, some radial pyroxene, myrmekite, some elongated high relief inclusions in pyroxenes
SG-217	50% plagioclase + 25% clinopyroxene + 15% orthopyroxene + trace amphibole (hornblende) as grains + disseminated sulphides (1%) + 5-10% chromite and magnetite	weak to moderate sericite alteration, moderate alteration of pyroxene,	Elongated plagioclase grains	some radial pyroxene and plagioclase, amphibole occurs on pyroxene rims
SG-218	50% plagioclase + 30% clinopyroxene + <5% amphibole (hornblende) + 15% orthopyroxene + trace biotite (<1%) + rare olivine + 10% oxides and sulphides (chromite, magnetite, bornite, pyrrhotite)	weak to moderate sericite alteration, weak to moderate alteration of pyroxene	elongated plagioclase grains	amphibole occurs around the pyroxene and rarely as grains, possible cumulate texture

Mafic dikes				
Sample	**Mineral Abundances**	**Alteration minerals**	**Textures**	**Notes**
SG-219	50% plagioclase + 30% clinopyroxene + <5% amphibole + 15% orthopyroxene + 5% oxides + sulphides (Magnetite, pyrite, pyrrhotite, chalcopyrite)	weak sericite alteration, weak to moderate alteration of pyroxene	subeuhedral to euhedral grains	amphibole occurs on the rims of the pyroxenes, myrmekite textures, possible cumulate texture
SG-220	30% clinopyroxene + 45% plagioclase + 15% orthopyroxene + 10% sulphides + oxides (spinel, bornite, pyrite, pyrrhotite)	moderate alteration of pyroxene, weak to moderate sericite alteration,	sub euhedral to euhedral grains	amphibole occurs as rims and some grains, radial pyroxene and plagioclase, possible cumulate texture
SG-222	30% clinopyroxene + 45% plagioclase + 20% orthopyroxene + 5% oxides (magnetite, chromite) disseminated sulphides (bornite) + some chlorite (<1%),	weak to moderate sericite alteration, moderate alteration of pyroxenes		Amphibole occurs on rims of pyroxenes as well as grains, presence of chloritized veins, myrmekite textures, some twinning in pyroxene, some granophyric textures
SG-223	50% plagioclase + 30% clinopyroxene + 20% orthopyroxene + 5% oxide and sulphides (magnetite, pyrite) + trace amphibole as grains (<5%)	weak sericite alteration, weak to moderate alteration of pyroxenes	Coarse plagioclase grains, that have crystallised first, followed by the crystallisation of the pyroxene grains	Most amphibole occur as grains, carlsbad twinning the pyroxene, some irregular contact boundaries between the pyroxenes grains
SG-246	35% clinopyroxene + 55% plagioclase + 5% orthopyroxene + 5% disseminated sulphides (pyrite, chalcopyrite)	strong alteration of pyroxene	fine grained (<5mm)	amphibole occur as grains and as rims around the pyroxene, some carlsbad twinning in the px, reaction rims around the pyroxene
SG-248	<1% amphibole (hornblende) + 45% plagioclase + 35% clinopyroxene + 10% orthopyroxene + 5% sulphides + oxides (magnetite, pyrite, pyrrhotite) + trace chlorite (<1%)	weak to moderate sericite alteration, moderate pyroxene alteration	Pyroxene crystallised first, followed by elongated plagioclase grains	some irregular contact boundary between pyroxene, some granophyric texture, amphibole occurs on the rims of the pyroxene, some myrmekite texture

Mafic dikes				
Sample	**Mineral Abundances**	**Alteration minerals**	**Textures**	**Notes**
SG-249	60% plagioclase + 20% clinopyroxene + 15% orthopyroxene + 5% sulphides + oxides (fine disseminated pyrite)	moderate to strong alteration of pyroxene, moderate sericite alteration	fine grained (<5%), pyroxene have crystallised first followed by plagioclase grains, needle like plagioclase grains	radial plagioclase grains
SG-261	45% plagioclase + 30% clinopyroxene + 15% orthopyroxene + 10% sulphides + oxides (pyrite, magnetite)	moderate to strong alteration of pyroxene	equigranular	some granophyric texture, possible cumulate texture
SG-262	50% plagioclase + 30% clinopyroxene + 10% orthopyroxene + trace chlorite (<1%) + 10% sulphides and oxides	weak sericite alteration, Strong alteration of pyroxene	equigranular	some granophyric texture, some veinlets of chlorite, amphibole as rims, high relief inclusions in pyroxene grains
SG-268	45% plagioclase + 35% clinopyroxene + 10% orthopyroxene + 10% sulphides and oxides (pyrite, chalcopyrite, magnetite, chromite)	moderate pyroxene alteration, weak to moderate sericite alteration		some granophyric texture, some contact boundaries between pyroxenes are irregular, amphibole occur on rims of pyroxene and alteration, possible cumulate texture
SG-269	55% plagioclase + 35% clinopyroxene + 15% orthopyroxene + trace chlorite (<1%) + <1% sulphides and oxides (pyrite, bornite)	strong sericite alteration, moderate to strong alteration of pyroxene.	Porphyritic texture, plagioclase are present as fine needles	Sericitised phenocryst and clinopyroxene grains in finer plagioclase dominated matrix
SG-285	40% plagioclase + 30% clinopyroxene + 20 orthopyroxene + 10% sulphides and oxides (ilmenite, magnetite, pyrite) + some olivine (<5%)	weak to moderate alteration of pyroxene, very weak sericite alteration		amphibole are rimming the opaques, irregular contact boundaries between feldspar grains and between pyroxenes. Some myrmekite textures

Table A7: Whole-rock chemistry of the Saglek dikes and the undeformed mafic dikes analysed for this study. Major element concentrations are reported in wt% and trace element concentrations are reported in ppm. Elements with concentration below the detection limit are marked as BDL. (SD = Saglek dikes; MD = Undeformed mafic dikes)

Sample	BR-82-119b	BR-83-122	BR-83-46b	SG225	SG226	SG231	SG232	SG237
Lithology	SD	SD	SD	SD	SD	SD	SD	SD
SiO_2	45.78	49.65	51.21	48.07	48.88	51.53	50.46	49.51
TiO_2	2.77	1.11	1.22	1.16	1.12	0.81	0.84	1.11
Al_2O_3	12.40	13.91	14.76	15.00	14.93	14.11	14.10	14.97
FeO	19.03	13.87	12.25	13.56	13.61	11.60	12.45	12.38
MnO	0.31	0.21	0.20	0.22	0.21	0.20	0.20	0.19
MgO	6.01	6.68	6.28	6.60	6.64	7.10	8.05	6.63
CaO	10.65	10.50	9.66	8.83	8.17	9.54	8.93	8.88
Na_2O	1.58	2.86	3.41	3.62	3.95	2.76	2.80	4.01
K_2O	1.28	1.14	0.91	1.33	0.88	0.97	0.70	0.84
P_2O_5	0.18	0.08	0.11	0.10	0.10	0.07	0.08	0.10
LOI	0.23	0.49	0.32	1.01	0.85	0.62	0.37	0.63
Sc	55.5	48.3	42.1	BDL	38.1	47.4	48.6	37.8
V	575	335	326	281	274	302	307	269
Cr	111	183	177	180	179	198	229	181
Co	49.9	55.4	50.0	52.0	52.8	44.7	48.2	54.0
Ni	42.1	84.7	101	110	104	52.1	58.4	110
Cu	48.4	149	124	80.0	45.9	62.4	11.3	37.5
Ga	21.7	18.1	19.9	19.0	18.8	14.9	15.7	19.1
Ge	2.67	2.00	1.76	1.80	1.74	1.46	1.63	1.69
Rb	15.5	7.75	7.27	50.0	68.0	14.3	11.0	20.0
Sr	99.8	152	192	133	147	58.7	57.2	135
Y	44.8	26.5	33.2	25.8	25.5	21.1	21.9	24.8
Zr	55.3	38.0	95.8	81.0	69.9	52.8	36.6	74.4
Nb	5.89	3.94	4.91	2.40	3.13	2.23	2.30	3.09
Cs	0.070	0.007	0.033	3.70	7.50	0.171	0.462	0.368
Ba	116	151	34.0	12.0	22.3	141	116	15.4
La	6.49	33.8	8.98	4.79	4.87	4.96	4.46	3.95
Ce	18.2	62.3	19.9	12.5	12.7	11.4	11.2	11.3
Pr	2.92	7.78	2.84	1.92	1.96	1.60	1.62	1.83
Nd	15.0	26.0	13.1	9.56	9.54	7.43	7.60	9.10
Sm	4.96	4.42	3.85	2.99	2.98	2.19	2.27	2.94
Eu	1.64	1.26	1.20	0.910	0.858	0.676	0.772	0.819
Gd	6.32	4.82	4.90	3.80	3.68	2.83	2.98	3.57
Tb	1.16	0.731	0.869	0.710	0.641	0.528	0.540	0.625
Dy	7.70	4.58	5.66	4.43	4.38	3.48	3.61	4.13
Ho	1.66	0.972	1.23	0.890	0.943	0.771	0.807	0.912
Er	4.70	2.77	3.49	2.56	2.67	2.21	2.33	2.61
Tm	0.696	0.409	0.519	0.383	0.391	0.324	0.333	0.388
Yb	4.41	2.68	3.34	2.42	2.51	2.15	2.22	2.45
Lu	0.654	0.386	0.488	0.365	0.383	0.315	0.313	0.365
Hf	2.18	1.53	2.86	2.00	2.14	1.59	1.32	2.17
Ta	0.384	0.252	0.344	0.170	0.221	0.185	0.166	0.237
Pb	6.57	5.09	5.49	16.0	18.3	7.52	2.47	22.4
Th	0.171	0.787	0.923	0.690	0.624	0.596	0.062	0.687
U	0.058	0.077	0.312	0.750	0.173	0.585	0.028	0.327

Table A7 (CONTINUED): Whole-rock chemistry of the Saglek dikes and the undeformed mafic dikes analysed for this study. Major element concentrations are reported in wt% and trace element concentrations are reported in ppm. Elements with concentration below the detection limit are marked as BDL. (SD = Saglek dikes; MD = Undeformed mafic dikes)

Sample	SG250	SG251	SG253	SG256	SG257	SG263	SG289	SG001	SG036
Lithology	SD	SD	SD	SD	SD	SD	SD	MD	MD
SiO_2	55.16	48.79	49.25	49.09	57.19	49.41	47.64	50.96	50.42
TiO_2	0.67	1.74	1.45	0.98	0.76	0.88	0.55	1.88	0.84
Al_2O_3	14.25	13.54	13.46	14.02	11.34	14.71	18.77	13.41	13.93
FeO	9.29	15.86	14.77	12.76	10.14	12.39	8.52	13.73	11.66
MnO	0.17	0.25	0.25	0.21	0.18	0.21	0.13	0.23	0.21
MgO	6.45	4.93	5.50	6.51	7.77	7.44	7.86	5.27	7.44
CaO	7.86	8.73	9.56	10.38	7.74	10.77	12.87	9.72	12.30
Na_2O	3.20	2.94	2.42	3.35	2.78	2.11	2.27	2.56	1.67
K_2O	1.76	1.29	1.60	1.21	0.87	0.64	0.37	0.53	0.17
P_2O_5	0.16	0.17	0.11	0.08	0.09	0.06	0.07	0.18	0.07
LOI	1.16	0.71	1.06	0.86	1.16	1.00	1.01	0.99	0.66
Sc	20.4	36.4	37.7	41.8	16.8	39.2	33.4	BDL	50.0
V	114	317	324	260	108	236	181	375	294
Cr	315	94.7	112	141	646	191	520	70	180
Co	30.4	45.3	46.1	47.7	45.7	48.5	45.2	48.0	54.0
Ni	114	60.4	53.0	59.0	264	78.5	163	60.0	90.0
Cu	39.1	90.0	108	105	39.4	59.3	186	280	160
Ga	13.6	19.1	16.5	15.9	14.8	15.4	15.9	20.0	15.0
Ge	0.99	1.44	1.23	1.02	1.22	1.08	1.12	1.20	1.80
Rb	42.1	18.3	26.1	22.0	32.1	26.7	10.2	36.0	4.00
Sr	188	146	94.7	116	248	84.5	112	233	97.0
Y	17.1	33.4	25.4	20.5	14.0	18.1	11.5	28.2	19.2
Zr	81.1	75.8	40.1	31.5	124	21.4	24.6	109	45.0
Nb	3.68	5.67	4.06	2.18	8.34	1.90	1.38	10.4	1.70
Cs	0.427	0.369	0.345	0.243	1.27	0.795	0.105	3.80	BDL
Ba	447	128	174	42.5	127	49.3	45.7	116	55.0
La	15.3	8.87	5.12	3.53	21.0	2.81	2.22	19.2	2.95
Ce	34.0	22.5	13.5	8.84	46.4	7.70	5.42	43.4	7.93
Pr	4.49	3.26	2.14	1.42	6.11	1.23	0.78	5.58	1.22
Nd	17.9	15.2	10.4	6.94	23.4	6.04	3.83	23.3	5.99
Sm	3.36	4.20	3.09	2.12	4.08	1.86	1.26	5.54	1.95
Eu	0.867	1.30	1.01	0.788	0.942	0.653	0.522	1.67	0.734
Gd	3.24	5.29	3.88	2.99	3.75	2.56	1.53	5.81	2.67
Tb	0.528	0.952	0.703	0.539	0.511	0.444	0.285	0.950	0.500
Dy	2.79	5.88	4.51	3.48	2.84	2.98	1.96	5.75	3.25
Ho	0.599	1.206	0.948	0.705	0.551	0.650	0.434	1.11	0.680
Er	1.65	3.33	2.65	2.10	1.29	1.90	1.24	3.00	2.12
Tm	0.241	0.495	0.396	0.319	0.205	0.287	0.183	0.424	0.319
Yb	1.67	3.45	2.62	2.13	1.32	1.90	1.18	2.78	2.10
Lu	0.226	0.458	0.361	0.295	0.164	0.265	0.186	0.423	0.325
Hf	2.23	2.45	1.39	1.15	3.49	0.93	0.76	3.10	1.20
Ta	0.223	0.348	0.274	0.154	0.566	0.146	0.097	0.940	0.160
Pb	1.26	2.00	1.78	2.58	3.99	1.12	5.63	15.0	BDL
Th	1.15	0.705	0.544	0.318	3.568	0.223	0.370	2.19	0.380
U	0.385	0.191	0.333	0.096	0.597	0.103	0.225	0.560	0.110

Table A7 (CONTINUED): Whole-rock chemistry of the Saglek dikes and the undeformed mafic dikes analysed for this study. Major element concentrations are reported in wt% and trace element concentrations are reported in ppm. Elements with concentration below the detection limit are marked as BDL. (SD = Saglek dikes; MD = Undeformed mafic dikes)

Sample	SG040	SG050	SG052	SG058	SG059	SG094	SG098	SG118	SG120
Lithology	MD	MD	MD	MD	MD	MD	MD	MD	MD
SiO_2	50.54	50.92	51.52	50.68	49.43	50.38	51.41	49.93	49.21
TiO_2	0.91	1.40	1.54	1.32	1.86	1.44	1.86	1.26	1.27
Al_2O_3	13.82	13.32	12.98	13.28	14.41	12.94	13.97	13.29	14.52
FeO	11.55	13.74	14.40	13.70	13.39	13.66	11.79	13.59	13.22
MnO	0.21	0.23	0.24	0.23	0.21	0.24	0.21	0.23	0.24
MgO	7.73	6.13	5.43	6.20	6.56	6.64	5.98	6.81	6.59
CaO	12.09	10.33	9.43	10.82	9.50	10.76	11.14	10.97	10.36
Na_2O	1.68	2.00	2.34	1.97	2.50	1.75	1.99	2.02	2.41
K_2O	0.11	0.30	0.37	0.18	0.24	0.55	0.21	0.29	0.60
P_2O_5	0.06	0.11	0.15	0.09	0.40	0.11	0.14	0.10	0.11
LOI	0.47	0.17	0.43	0.00	0.52	1.09	1.98	0.42	1.80
Sc	BDL	BDL	BDL	47.0	BDL	BDL	BDL	50.4	BDL
V	319	400	402	349	327	414	323	363	364
Cr	170	90.0	90.0	90.0	170	130	90.0	122	180
Co	54.0	54.0	52.0	53.0	54.0	54.0	42.0	54.7	57.0
Ni	90.0	60.0	50.0	70.0	70.0	90.0	70.0	71.7	90.0
Cu	150	130	120	140	30.0	180	220	122	150
Ga	15.0	17.0	18.0	17.0	20.0	17.0	18.0	16.8	17.0
Ge	1.30	1.30	1.40	1.70	1.00	1.50	1.20	1.78	1.40
Rb	2.00	11.0	6.00	5.00	3.00	30.0	4.00	8.19	17.0
Sr	89.0	104	158	107	305	122	219	104	119
Y	19.7	29.2	33.8	27.5	34.4	28.2	23.2	26.9	31.5
Zr	36.0	68.0	99.0	84.0	115.00	63.0	92.0	70.1	51.0
Nb	2.40	4.10	4.80	3.40	5.60	3.40	8.80	3.32	2.60
Cs	0.100	0.300	0.000	0.100	0.100	3.90	0.500	0.235	0.300
Ba	43.0	83.0	121	59.0	247	111	97.0	83.8	99.0
La	3.65	6.72	15.9	5.80	26.8	6.58	15.9	5.39	4.19
Ce	9.21	16.7	36.5	14.8	61.8	15.9	36.8	13.5	11.4
Pr	1.36	2.39	4.81	2.23	8.18	2.23	4.73	1.98	1.72
Nd	6.57	11.3	20.4	10.3	35.6	11.0	20.3	9.48	8.62
Sm	2.07	3.48	4.96	3.28	7.34	3.36	4.99	2.85	3.02
Eu	0.794	1.15	1.52	1.09	2.35	1.16	1.63	1.01	1.03
Gd	2.76	4.29	5.52	4.01	6.96	4.19	5.11	3.64	4.14
Tb	0.500	0.790	0.950	0.760	1.110	0.770	0.800	0.667	0.800
Dy	3.38	5.01	6.14	5.06	6.45	5.12	4.74	4.45	5.60
Ho	0.730	1.04	1.27	1.04	1.29	1.04	0.910	0.988	1.21
Er	2.07	3.02	3.71	2.93	3.63	3.00	2.51	2.81	3.59
Tm	0.307	0.459	0.546	0.431	0.534	0.447	0.356	0.426	0.550
Yb	2.05	3.08	3.55	2.91	3.41	2.86	2.14	2.78	3.74
Lu	0.326	0.459	0.522	0.473	0.527	0.436	0.301	0.407	0.596
Hf	1.10	2.00	2.90	2.10	3.20	1.90	2.70	2.06	1.60
Ta	0.260	0.390	0.370	0.270	0.420	0.300	0.770	0.222	0.190
Pb	BDL	BDL	BDL	BDL	7.00	BDL	BDL	1.36	BDL
Th	0.380	0.710	0.940	0.740	0.590	0.560	1.65	0.560	0.080
U	0.090	0.170	0.180	0.180	0.120	0.230	0.440	0.154	0.080

Table A7 (CONTINUED): Whole-rock chemistry of the Saglek dikes and the undeformed mafic dikes analysed for this study. Major element concentrations are reported in wt% and trace element concentrations are reported in ppm. Elements with concentration below the detection limit are marked as BDL. (SD = Saglek dikes; MD = Undeformed mafic dikes)

Sample	SG121	SG211	SG212	SG213	SG214	SG215	SG217	SG218	SG219
Lithology	MD	MD	MD	MD	MD	MD	MD	MD	MD
SiO_2	51.06	49.99	50.26	49.76	49.93	50.57	50.49	50.46	50.63
TiO_2	1.45	1.23	1.53	1.56	1.60	1.40	1.25	1.21	1.11
Al_2O_3	13.39	13.51	13.22	13.46	14.04	13.54	13.17	13.14	13.13
FeO	12.86	13.45	13.51	13.13	13.12	13.29	13.88	13.44	13.32
MnO	0.22	0.22	0.22	0.22	0.22	0.22	0.23	0.22	0.22
MgO	6.60	6.84	6.27	6.44	6.23	6.33	6.57	6.84	6.95
CaO	10.15	10.67	10.66	10.86	9.79	10.04	10.45	10.91	10.87
Na_2O	2.10	1.77	1.87	2.19	2.43	2.14	1.86	1.78	1.84
K_2O	0.58	0.71	0.79	0.74	0.96	0.82	0.45	0.40	0.36
P_2O_5	0.16	0.11	0.17	0.19	0.23	0.17	0.11	0.10	0.08
LOI	1.22	1.37	1.74	2.06	1.57	1.22	0.73	0.97	0.70
Sc	BDL	49.5	45.2	42.0	37.3	42.2	43.7	45.8	46.1
V	331	347	334	306	260	292	318	322	304
Cr	100	116	71.6	89.3	69.1	83.1	59.9	78.9	69.9
Co	51.0	52.8	49.9	46.9	46.9	46.6	50.5	50.3	51.7
Ni	70.0	65.1	54.5	59.1	58.2	58.3	56.5	59.6	60.3
Cu	110	121	109	105	84.5	99.6	129	115	121
Ga	17.0	16.4	16.2	16.1	16.1	16.1	14.8	14.2	14.2
Ge	1.30	1.52	1.29	1.36	1.49	1.49	1.27	1.15	1.33
Rb	29.0	43.5	48.1	37.1	46.2	43.0	24.0	20.6	18.1
Sr	128	121	134	148	164	125	95.5	97.5	99.5
Y	26.3	26.3	28.1	26.3	26.5	24.5	24.5	23.5	23.0
Zr	74.0	73.1	94.1	108	115	89.8	71.0	65.5	62.8
Nb	4.70	3.72	5.41	6.79	8.11	5.52	3.27	3.17	3.06
Cs	0.900	2.14	1.70	1.52	2.02	1.47	0.718	0.839	0.543
Ba	147	86.5	153	172	261	181	79.4	76.2	76.8
La	9.94	5.59	8.83	10.3	12.2	9.15	5.00	4.71	4.68
Ce	22.7	13.5	20.6	23.7	28.1	21.1	12.4	11.8	11.7
Pr	3.05	2.01	2.91	3.25	3.92	2.98	1.88	1.75	1.78
Nd	13.9	9.41	13.2	14.3	16.7	12.8	8.82	8.53	8.34
Sm	3.62	2.75	3.30	3.34	3.76	3.17	2.48	2.38	2.25
Eu	1.26	0.979	1.21	1.21	1.37	1.09	0.923	0.859	0.867
Gd	4.31	3.62	4.24	4.19	4.68	3.71	3.46	3.15	3.29
Tb	0.750	0.699	0.772	0.734	0.764	0.673	0.647	0.607	0.632
Dy	4.82	4.57	4.79	4.58	4.67	4.28	4.23	4.07	3.74
Ho	1.00	0.992	1.05	0.984	1.03	0.920	0.927	0.891	0.838
Er	2.89	2.84	2.96	2.75	2.86	2.73	2.68	2.48	2.49
Tm	0.428	0.417	0.441	0.427	0.433	0.397	0.403	0.381	0.364
Yb	2.75	2.90	2.85	2.73	2.77	2.60	2.68	2.52	2.34
Lu	0.424	0.388	0.387	0.375	0.391	0.378	0.343	0.357	0.345
Hf	2.10	2.18	2.67	2.82	3.14	2.54	2.12	2.04	1.81
Ta	0.350	0.369	0.385	0.490	0.468	0.399	0.271	0.247	0.189
Pb	BDL	1.82	1.64	BDL	1.63	1.27	0.90	1.02	0.669
Th	0.680	0.676	0.773	0.803	0.860	0.736	0.744	0.720	0.655
U	0.170	0.171	0.223	0.183	0.201	0.196	0.179	0.159	0.147

Table A7 (CONTINUED): Whole-rock chemistry of the Saglek dikes and the undeformed mafic dikes analysed for this study. Major element concentrations are reported in wt% and trace element concentrations are reported in ppm. Elements with concentration below the detection limit are marked as BDL. (SD = Saglek dikes; MD = Undeformed mafic dikes)

Sample	SG220	SG222	SG249	SG261	SG262	SG268	SG269
Lithology	MD	MD	MD	MD	MD	MD	MD
SiO_2	50.41	51.32	50.19	50.63	50.43	50.43	50.47
TiO_2	1.25	0.96	1.29	1.27	1.33	1.22	0.95
Al_2O_3	13.25	13.50	13.20	13.25	13.34	13.35	13.76
FeO	13.96	12.36	13.62	13.34	13.77	13.62	12.07
MnO	0.23	0.22	0.22	0.21	0.23	0.23	0.21
MgO	6.45	6.78	6.77	6.75	6.36	6.45	7.31
CaO	10.55	10.88	10.83	10.38	10.71	10.66	11.58
Na_2O	1.76	1.87	1.92	1.90	1.70	1.99	1.82
K_2O	0.49	0.66	0.34	0.66	0.48	0.43	0.41
P_2O_5	0.10	0.08	0.10	0.11	0.11	0.11	0.08
LOI	0.83	1.06	0.51	1.31	1.44	0.59	0.39
Sc	44.6	43.3	43.0	45.0	43.0	43.9	43.5
V	325	272	329	334	343	316	278
Cr	58.2	40.1	125	123	91.9	85.5	133
Co	51.6	49.2	48.1	50.0	48.0	50.4	48.1
Ni	53.5	44.8	61.7	68.6	61.1	61.9	72.2
Cu	119	111	103	109	114	105	129
Ga	15.1	14.6	14.7	15.4	15.1	15.3	13.9
Ge	1.40	1.12	1.06	1.29	1.29	1.25	1.06
Rb	30.0	32.6	18.5	51.5	37.3	22.0	26.7
Sr	97.9	97.5	98.0	138	136	111	96.3
Y	25.1	19.8	24.2	25.3	25.4	25.7	18.1
Zr	69.9	57.4	70.9	75.4	72.6	72.2	49.1
Nb	3.02	2.95	3.28	3.48	3.37	3.37	2.66
Cs	1.29	1.31	1.35	2.38	1.78	0.574	0.352
Ba	71.0	108	55.2	90.6	70.2	89.8	64.5
La	5.07	4.73	5.22	5.79	5.72	5.45	3.77
Ce	12.7	11.2	13.2	14.7	14.1	13.1	9.34
Pr	1.90	1.66	2.05	2.14	2.13	2.05	1.44
Nd	9.21	7.28	9.55	10.1	10.2	9.67	6.80
Sm	2.68	2.05	2.65	2.94	2.81	2.60	1.94
Eu	0.938	0.718	0.964	1.00	1.00	0.947	0.762
Gd	3.54	2.65	3.48	3.58	3.85	3.61	2.66
Tb	0.656	0.504	0.646	0.671	0.665	0.660	0.479
Dy	4.25	3.36	4.12	4.32	4.34	4.04	3.15
Ho	0.923	0.746	0.906	0.913	0.929	0.875	0.685
Er	2.67	1.99	2.58	2.70	2.71	2.60	1.87
Tm	0.374	0.311	0.369	0.396	0.387	0.393	0.275
Yb	2.81	2.22	2.55	2.80	2.74	2.69	1.92
Lu	0.373	0.298	0.352	0.362	0.357	0.372	0.279
Hf	2.16	1.74	2.11	2.24	2.31	2.11	1.49
Ta	0.199	0.242	0.252	0.240	0.242	0.232	0.185
Pb	0.918	0.861	0.923	1.08	1.18	2.28	0.607
Th	0.752	0.721	0.599	0.644	0.617	0.575	0.479
U	0.158	0.173	0.148	0.151	0.142	0.160	0.101